

Active small-scale space debris removal by a space-based laser

MSc Thesis Aerospace Engineering

Liam Pieters

4967259

Delft University of Technology



Active small-scale space debris removal by a space-based laser

MSc Thesis Aerospace Engineering

by

Liam Pieters
4967259

in partial fulfillment of the requirements for the degree of

Master of Science

in Aerospace Engineering

at Delft University of Technology,

to be defended publicly on Friday November 6, 2020 at 14:00 PM.

Student number: 4967259
Project duration: Mar 1, 2019 – Oct 1, 2020
Supervisor: Ir. R. Noomen
Thesis committee: Dr. Ir. W. van der Wal, TU Delft
Ir. J. Sinke, TU Delft

This thesis is confidential.

Acknowledgements

The following document is a report for the completion of the MSc Aerospace Engineering at TU Delft. For more than 3 years the problem of uncontrolled objects in space have fascinated me greatly. Solving the problem using the ablative effects of a space-based laser has particularly appealed to me from the very first moment I learned about this technique. It is not only a most elegant removal method, it is also the only one suitable for removing debris objects with sizes between 1 and 10 cm. This report is the culmination of all the knowledge that I have gathered on the subject in those 3 years. Working on such a far-fetched concept has stimulated me every day and conducting research on the matter was such a pleasure that I am strongly convinced that I want to pursue a career in this field. I would like to give special thanks to my supervisor Ron Noomen for all the great feedback and the abundance of positive reinforcement during our weekly meetings. Ron truly got the best out of me and made me realise that I was capable of much more than I initially thought.

*Liam Pieters
4967259
Delft, October 2020*

Abstract

Space debris objects with sizes between 1 and 10 cm form the greatest risks for creating new collisions with active spacecraft as they are too small to track and too large to be shielded against. This research has simulated the performance of a space-based laser system on the removal of these small-scale debris objects. The selected system is placed in a Sun-synchronous orbit and consists of a high power 20 kW laser that shoots 600 J energy pulses with a repetition frequency of 33.33 Hz. The system detects and tracks the objects in-situ using a 1.5 m telescope from 800 km distance. From a distance of about 500 km, the laser fluence on the targets is sufficiently high to trigger ablation on the material surface. This decelerates the debris object and lowers its lifetime. The laser is tested on a randomly generated debris population of 5 000 objects. The results show that after 10 days of simulation, the lifetime of 334 objects are effectively lowered below 25 years and 614 objects are lowered below one month. At longer simulation time the efficiency decreases since less and less objects are left to target. Extrapolating the results, the laser could on an annual basis lower the lifetime of more than 36 000 objects below 1 month and 18 000 objects below 25 years, which is very promising. The results show that a space-based laser system is highly efficient as an Active Debris Removal (ADR) technique for debris objects between 1 and 10 cm.

Contents

Abstract	v
1 Introduction	5
2 Relevance and justification for research	7
3 Space debris environment	11
3.1 Fragmentation debris	13
3.2 Non-fragmentation debris	15
3.3 Spatial and material density of debris	15
3.4 Lifetime of LEO debris	21
4 Theoretical framework	23
4.1 Debris dynamics	23
4.2 Geometries	27
4.3 Laser physics	29
4.4 Laser parameter constraints	34
4.5 Target acquisition	38
5 Interaction with one debris object	41
5.1 Methodology	41
5.1.1 Creating the environment	41
5.1.2 Propagation of laser and debris orbit until encounter	45
5.1.3 Propagation of the laser and debris interaction	48
5.2 Coplanar interactions	52
5.3 Non-coplanar interactions	57
6 Laser simulation with debris population	65
6.1 Methodology	65
6.1.1 Creating the debris population	66
6.1.2 Propagating the laser and the debris population	66
6.1.3 Propagating the interaction of the laser and debris target	68
6.2 Debris population distribution	70
6.3 Simulation result on debris population	71
6.3.1 Laser performance over time	71
6.3.2 Atmospheric sensitivity	75
6.3.3 Evolution of total debris population	77
6.3.4 Predicting results on longer time scale	79
6.3.5 Laser performance per debris parameter	81
7 Validation and verification	89
8 Conclusions and recommendations	95
A Project outline	97
Bibliography	99

List of Symbols

Roman

a_{las}	Debris acceleration due laser [m/s ²]
a	Semi-major axis [m]
A	Debris area [m ²]
C_m	Material coefficient [N/MW]
C_d	Drag coefficient
C_r	Reflection coefficient
d_{rel}	Relative position [m]
D	Diameter telescope [m]
e	Eccentricity
E_{pulse}	Laser pulse energy [J]
f	Laser pulse frequency [Hz]
F_{thrust}	Laser thrust [N]
i	Inclination [rad]
I	Intensity of laser [W/m ²]
L_{rel}	Relative distance [m]
L_{time}	Lifetime of orbital object [s]
M^2	Laser beam quality
\hat{n}	Direction of normal vector
p_l	Laser pressure [Pa]
P_l	Laser power [W]
\hat{r}	Direction of radial vector
r_a	Apogee [m]
r_p	Perigee [m]
R	Radius Earth [m]
v_{rel}	Relative velocity [m/s]
w	Beam width [m]

Greek

α	Mirror redirection fraction
β	angle between d_{rel} and v_{rel} [rad]
$\hat{\theta}$	Direction of tangential vector
λ	Laser wavelength [m]
μ	Gravitational parameter [m ³ /s ²]
ν	True anomaly [rad]
ρ	Density [kg/m ³]
τ	Laser pulse time [s]
ϕ	Azimuth angle [rad]
Φ	Fluence of material [J/m ²]
ω	Argument of periapsis [rad]
Ω	Right Ascension of Ascending Node [rad]

List of Abbreviations

ADR	Active Debris Removal
AMR	Area-to-Mass Ratio
CAM	Collision Avoidance Manoeuvre
CW	Continuous Wave
FOV	Field Of View
IADC	Inter Agency Space Debris Coordination Committee
LEO	Low Earth Orbit
GEO	Geostationary Orbit
RAAN	Right Ascension of Ascending Node
RK4	Runge Kutta 4
SBR	Signal-to-Background Ratio
SRM	Solid Rocket Motor
SRP	Solar Radiation Pressure
SSB	Solar System Barycenter
SSN	Space Surveillance Network
SSO	Sun Synchronous Orbit
Tudat	TU Delft Astrodynamical Toolbox

1

Introduction

If all broken ships and boats that have ever roamed Earth's oceans would have remained floating on the surface as debris instead of sinking to the bottom, this would have had big implications for sea travel nowadays. Ships would have to make many manoeuvres deviating from their nominal course to prevent collisions with this debris. Mankind finds itself exactly in this scenario, but the corresponding venue is Earth's orbits. Whereas sea vessels sink to the bottom of an ocean when broken down, spacecraft remain orbiting Earth, posing a great risk to active satellites and other space objects. The launch of Sputnik in 1958 initiated a prosperous era for space exploration, but until recently there were never any guidelines for the removal of the material being launched into orbit [1]. Due to this lack of infrastructure for the prevention or disposal of space waste, every space mission launch since Sputnik contributed to a growing number of uncontrolled space objects. This has resulted in the current situation where more than 5 million kg of uncontrollable objects orbit Earth, severely threatening the safety of ongoing space missions [2]. One of the most densely populated regions is the Low Earth Orbit (LEO), ranging from about 200 to 1000 km [3]. Due to decelerating effects by the atmosphere, objects below 700 km tend to slowly spiral downwards into the atmosphere and burn up. However, objects at higher altitudes will remain in space for an indefinite period of time. The growing number of space debris is increasingly becoming one of the hardest challenges for modern spaceflight.

Space debris has a plethora of different sources and is found in the size range between 1 μm and 100 m [3]. The smallest fragments, the amount of which is deduced from the impacts on surfaces of returned satellites, are the result of Solid Rocket Motor (SRM) exhausts, motor coolant or deteriorating surfaces of satellites such as paint flakes or shielding material. However, despite their large velocity, the kinetic energy of these minuscule particles is low enough to protect active satellites from damage using multi-layered shields. A far larger threat is debris with sizes between 1 cm and 100 m [4]. These are the product of in-orbit fragmentation events, such as collisions between two objects or explosions. The largest of these events was the collision between the U.S. Iridium-33 satellite and the Russian Kosmos-2251 satellite in 2009, which produced more than 2000 new debris fragments in LEO [5]. The kinetic energy of these generated fragments is large enough to puncture satellite walls or even have them break up entirely. Subsequently these fragments themselves can cause new fragments resulting in a cascading rundown where each fragmentation event increases the probability of a next event, potentially transforming Earth's orbits into an impenetrable cloud of uncontrolled

objects. In 1978, such a hypothetical catastrophic scenario has already been predicted by Donald Kessler, who coined the name 'the Kessler syndrome' [6].

The methods of preventing these fragmentation cascades are generally split in three equally important safety measures: passivation, mitigation and removal. First, passivation implies that inactive spacecraft or satellites that have reached the end of their mission lifetime have to be depleted from any remaining propellant or energy. Any excess energy in batteries or propellant stored in tanks could cause spacecraft to explode due to a build-up in pressure, resulting in large break-up events [7]. Secondly, mitigation means that an object launched into LEO will have to spiral back into the atmosphere within at least 25 years after its mission lifetime has been completed. Finally, removal means that platforms for Active Debris Removal (ADR) will have to be employed to counteract the possibility of any Kessler cascades in Earth's orbit. Each year a number of inactive satellites will have to be removed to decrease the probability of fragmentation events [8]. A successful stabilization of Earth's environment will only occur if significant progress is achieved for all three safety measures.

Technically, ADR is the most challenging. Many concepts have been designed for debris removal such as capturing with nets, harpoons or robotic arms [9]. Other concepts use magnets to attach a de-orbit kit to the piece of debris. However, these methods are mainly directed at removing large debris fragments such as a defunct satellites. Few concepts have been designed for the removal of small-scale space debris - between 1 and 10 cm. This is an interesting size range because debris fragments in this range have sufficient kinetic energy to cause a satellite break-up whilst being too small to be monitored by radar observations [10]. In 2020, there are at least 900 000 fragments in this size range: for the safety of future space missions it is crucial that these objects are taken care of [11]. In another concept, the debris is decelerated by the ablative effects of a laser, either ground-based or space-based, to make it spiral into the atmosphere and burn up [12]. Since the ground-based system would still need a debris catalogue to know where to shoot the laser, only the space-based laser remains to target debris objects below 10 cm. This is the focus of this research report: 'Could a space-based laser system successfully be used as an ADR method in the LEO region for debris fragments in the size range of 1-10 cm?'

To answer this research question, this report will first explain the scientific and social relevance for this research in Chapter 2 to justify the employment of an in-orbit laser system. Chapter 3 will describe the dynamic environment of the LEO region, listing all various sources of space debris and their characteristics. Chapter 4 describes a theoretical framework about debris fragment dynamics and the physics of in-orbit laser ablation. It will also show why specific, certain values for the laser parameters were chosen to test the interaction. Chapter 5 will show the methodology and results of the interaction of the laser with a single debris object under different geometries. Chapter 6 will show the methodology and results of the simulation of the laser interaction with a complete debris population. Chapter 7 will compare the results with literature to validate and verify the results. Conclusions and recommendations are given in Chapter 8. The original project outline is attached in the appendix.

2

Relevance and justification for research

If people continue to launch missions as 'business-as-usual', Earth orbits will not only become polluted but could even turn into a series of impenetrable shields, making future space missions impossible [8]. This section will expand on the three different measures that will have to be applied to counteract this scenario.

- **Passivation.** One of the biggest sources of space debris is the remaining propellant in spent rocket stages or charged batteries in satellites at the end of their lifetime. The extreme environment in space causes severe changes in temperature and pressure in spacecraft which over time can make a non-empty propellant tank explode. Figure 2.1 shows that 33% of the fragmentation events of the last ten years comes from excess propulsion and 5% is due to remaining electrical energy in the spacecraft [11].

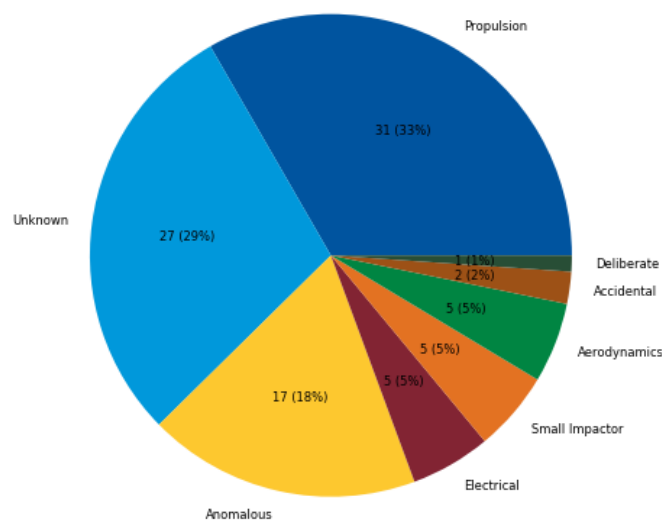


Figure 2.1: Causes of fragmentation events over the last ten years [11].

Through passivation, spacecraft are depleted of causes that might induce fragmentation events. Excess propellant can be used to steer the satellite back into Earth's atmosphere and a simple electrical light empties the batteries after its mission has ended [7].

- **Mitigation.** In 1999, The United Nations Committee on the Peaceful Uses of Outer Space prepared a technical report on the problems of space debris which claimed that man-made debris has a small probability of harming spacecraft [13]. However, the use of space has grown significantly and after the detrimental in-orbit break-up of the Chinese FengYun-1C satellite in 2007 [14], a new report by the Inter-Agency Space Debris Coordination Committee (IADC) provided guidelines on how to ensure the safety of space: the so-called Space Debris Mitigation Guidelines which state that further launches should minimize the generation of new debris fragments and that spacecraft in LEO should re-enter and burn up in the atmosphere within 25 years after completion of their mission [1].
- **Active Debris Removal.** Even in a hypothetical scenario where from this moment on no further release of debris objects will occur, new debris fragments will still be generated due to the large number of debris present in most popular orbits [8].

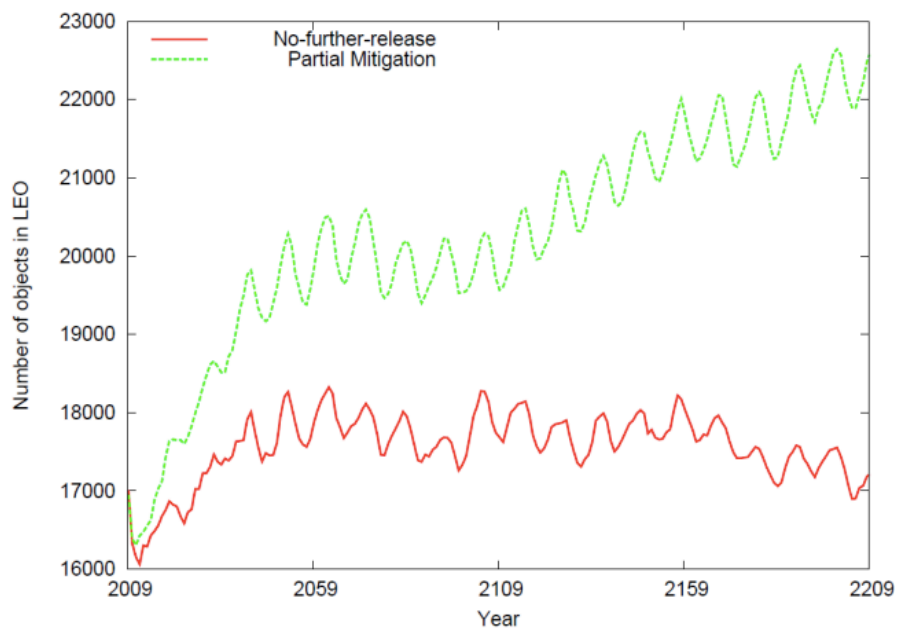


Figure 2.2: Evolution of LEO debris objects in a no-further release scenario and where 90% of mitigation rules are followed [8].

Figure 2.2 shows that even when the mitigation guidelines are successfully followed 90% of the time, the number of objects will still increase significantly over time. This implies that pieces of debris have to be removed from Earth orbits to stabilize the space environment.

It is important to note that passivation, mitigation and removal will have to be applied simultaneously to clean the space environment properly. If a successful ADR platform gets installed, but no mitigation guidelines are adhered to, Earth orbits will stay polluted [8]. However important passivation and mitigation, ADR will be the focus of this report. ADR is defined as the systematic removal of pieces of debris from Earth orbits. A distinction has to be made between the removal of large debris objects (>1 m) and small debris objects (<10 cm). The large objects are considered the main source of new debris fragments, while the small debris objects present the main risk [15]. This means that new debris objects will originate from the large debris objects while the fragmentation event was caused by a small debris object. Solutions will have to be found at both ends of the debris size spectrum.

Removal of large debris fragments

Currently there are several concepts on how to remove large pieces of debris. The premise of these concepts is to get near enough to the object so the removal technique can attach itself to the object, after which both the removal spacecraft and the debris object are sent on a trajectory to spiral into the atmosphere to burn up. For example, the removeDebris project researches the performance of catching a debris object with a net [16]. The manoeuvring would be difficult since any thrust might burn the rope between the net and the object. Other projects want to catch debris with robotic arms or harpoons. [17]. Another concept is to attach a de-orbit kit to debris objects that would steer them back into the atmosphere. However, the efficiency of these techniques is low. First, every launched removal spacecraft will only be able to de-orbit one debris object. Secondly, attaching the removal craft is most challenging: the removal vehicle will have to spin around the object and match its attitude to successfully connect to the debris. All these extra manoeuvres require large amounts of propellant [17]. To successfully stabilize the number of objects in LEO, 5-10 large objects per year should be removed [8]. Though inefficient, these methods are currently the only options that could succeed in removing the requested number of objects.

Removal of small-scale debris fragments

Even if every single large piece of space debris were removed from orbit, active satellites are still at risk of collision with the numerous small fragments that orbit in LEO. Specially challenging are debris fragments with sizes between 1 and 10 cm that can cause a break-up of a satellite in a collision, and are too small to track from Earth [18]. The methods briefly described above cannot be applied to these fragments, since they are too numerous to sacrifice a spacecraft to de-orbit them one by one [9]. To actively remove these fragments, the solution should not rely on contact with the debris and should be able to target many objects consecutively. One concept that satisfies these demands is to inject a cloud of particles into LEO that would act as an artificial atmosphere and would reduce the lifetime of debris objects by deceleration [19]. However, this would also affect active satellites in LEO and would be difficult and costly to realise. Another concept is using an ion-thruster satellite that would rendezvous with the debris fragment and decelerate it by exerting an ion thrust on the target [17]. However, it would require an unfeasible amount of propellant to perform a rendezvous with all separate fragments one by one. One more solution that could decelerate targets from LEO would be using a laser system [12]. A ground-based laser system will not be able to target the debris, since objects below 10 cm are too small and are invisible for the laser. The only option that remains is to use a space-based laser system which can detect objects in-situ by a telescope and target them as they move towards the laser [15, 20]. The high-power laser can then ablate the material surface and exert a thrust on the object resulting in a change of velocity. For certain geometries, this change in velocity is sufficient to de-orbit the debris fragment within half a revolution around Earth. For other, less optimal geometries, the laser can still reduce the lifetime of the object. Since the small-scale debris is the main risk for causing new fragmentation events and a space-based laser is the only feasible and efficient method to remove small objects, the relevance for ADR by laser ablation is getting increasingly higher.

Status ADR by laser ablation

The concept of removing LEO debris objects using a space-based laser was first presented by Schall [21] in 1991. The main subsystems were already present in this concept: the paper describes an orbital system equipped with a laser, optics and a subsystem for the detection and tracking of the target. In the following years, a NASA headquarters study named 'the

Orion project' researched the possibility of cleaning LEO debris by ablation of a ground-based laser [22]. In a follow-up research by Phipps *et al.* [12], the performance of a ground-based laser was compared to a space-based laser. One of the conclusions was that at least for debris objects with sizes between 1 and 10 cm, the space-based laser is the favored option since the ground-based laser has a detection limit. Since then, different versions of a space-based laser have been developed. A study by Soulard *et al.* [23] in 2014 showed that a kW powered ICAN laser with kHz repetition frequency would be able to de-orbit debris objects with sizes between 1 and 10 cm in one interaction. The L'ADROIT concept by Phipps [10] in 2014 showed that a 20-40 kW UV laser in an elliptical orbit would also be able to do so, as well as raise or lower large objects in LEO by many consecutive interactions. A follow-up research in 2015 showed that such a system could also be applied to nudge LEO debris objects out of a collision course [20]. The conclusions from these three papers are all theoretical: first, an average flux of debris objects is assumed which results in an estimation for a target access rate dN/dt . Next, it is shown that the laser could in theory achieve ablation on an object. Then, the performance of the laser is given by how many debris objects it encounters assuming every encountered debris object is identical and every interaction results in a de-orbited target. This report intends to contribute to the literature of space-based lasers by simulating how a space-based laser performs on a randomly created debris population that represents real LEO debris objects. Instead of assuming that every debris object is instantly de-orbited, every debris encounter will be treated individually, taking into account at what angle and from what altitude the object is targeted. By computing the achieved reduction in lifetime per targeted object, this report will try to show how good a laser system will function when operational and what the long-term effects on the space environment will be.

3

Space debris environment

Space debris is the collective name for the numerous uncontrolled fragments that occupy Earth orbits [3]. There are many different events that lead to the production of these uncontrolled objects, resulting in the current debris population with widely divergent characteristics. The objects differ in material density, shape and size, owing to their origins. In general, a division can be made between debris resulting from fragmentation events and those from non-fragmentation events. The first are often substantial pieces of shrapnel consisting of alloys with unclear defined shapes [3]. These fragments are the result of break-up events such as anti-satellite tests, explosions or collisions. The latter are more accurately described as small debris objects of known material composition and sometimes even regular shapes. Debris from non-fragmentation events does not result from a break-up, but is a by-product from the satellite mission. These include motor ejecta, motor coolant or the results of continuous degradation of satellite surfaces due to the harsh environment in space [3].

Figure 3.1 shows the evolution of the number of tracked space objects since the launch of Sputnik in 1957 [11]. Since 1957, there have been 5560 successful rocket launches, depositing about 9600 satellites into orbit. About 5500 of these are still in orbit, displayed by the red bottom part in Figure 3.1. Of these 5500 satellites, only 2300 are still functioning [11]. The defunct satellites either have no more propellant to carry out their mission or have lost communication with ground stations. From 1985 to 2007 the number of objects has doubled from 5000 to 10000. This number doubled again between 2007 to 2018, partly due to the constant rise in number of launches providing new debris objects like payload and rocket bodies. Most debris is due to fragmentation of rockets and payloads, the yellow and green bars in Figure 3.1. The sudden increase in object count in 2007 and 2009 are due the two most detrimental in-orbit fragmentation events.

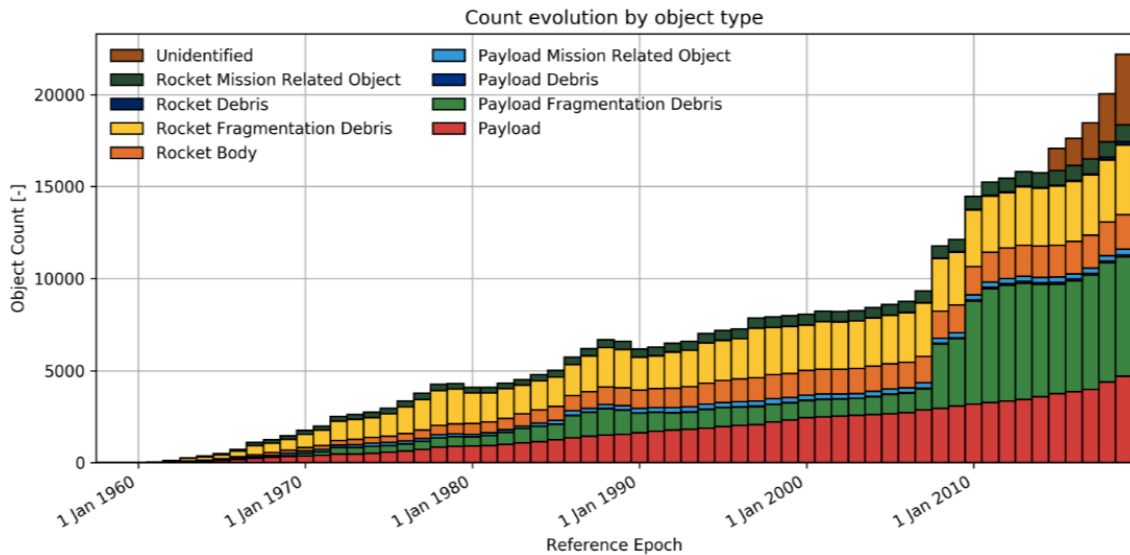


Figure 3.1: Tracked space debris population since the launch of Sputnik [11].

It is important to note that Figure 3.1 only shows the set of debris that can be tracked by the USAF Space Surveillance Network and is stored in their catalogue [11]. The probability of collisions between objects in the catalogue is constantly monitored. When two objects find themselves on a collision course and the probability of the collision P_{col} exceeds a safety threshold of 10^{-4} , a Collision Avoidance Maneuver (CAM) is performed to prevent the event [4]. Figure 3.2 shows how many CAMs a satellite with a cross-sectional area of 2.5 m^2 in polar orbit has to make to stay below a certain collision probability level. To maintain the safety probability threshold of 10^{-4} , the satellite will have to make at least 3 maneuvers per year.

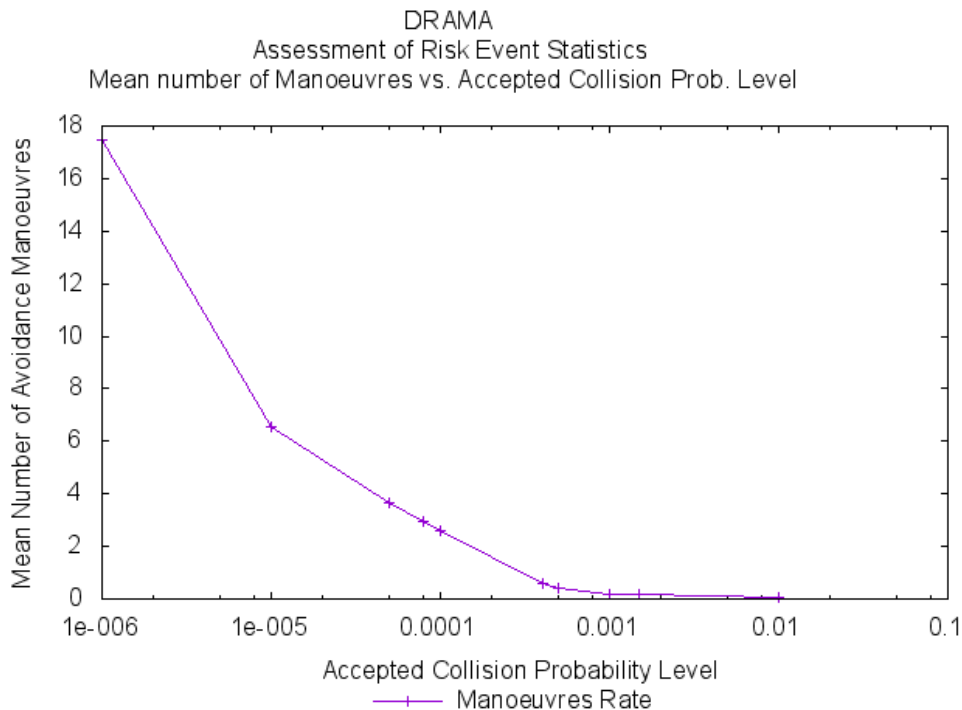


Figure 3.2: Number of maneuvers a satellite with 2.5 m^2 cross-sectional area in polar orbit has to perform to avoid collisions. Made with ESA's DRAMA tool.

Since the current technological limits for tracking of debris lies between 5-10 cm for LEO debris and about 1 m for geostationary (GEO) debris, this implies that Figure 3.1 only shows a part of the true debris population [18]. Estimations from impacts on satellites show that the number of untracked debris objects far exceeds the number of tracked objects. Statistical models predict that there are more than 900 000 objects between 1-10 cm in space, of which more than 500 000 reside in LEO [11]. Objects between 1 mm and 1 cm are even more numerous: a total of more than 128 million is estimated. The latter form no real danger since satellites can be built to endure these impacts. However, the debris fragments between 1 and 10 cm have too much kinetic energy and will almost certainly cause a break-up when a collision takes place [20]. Because they are not tracked and thus can not be prematurely avoided when on a collision course, this 1-10 cm debris forms the greatest danger to the safety of active satellites.

Below a brief overview is given of all the possible sources of space debris and the resulting current debris population in LEO. The spatial and material density of the LEO debris will be discussed and from this, three objects will be chosen on which the initial performance of the laser will be tested.

3.1. Fragmentation debris

Fragmentation events have the most polluting effect on the space environment because they produce debris in the range between 1 mm and 10 m. Because these pieces can be so large, fragmented debris accounts for the majority of the mass distribution in space [2]. Since Sputnik in 1957, more than 250 fragmentation events have taken place in space. Figure 3.3 shows the number of debris objects resulting from these events.

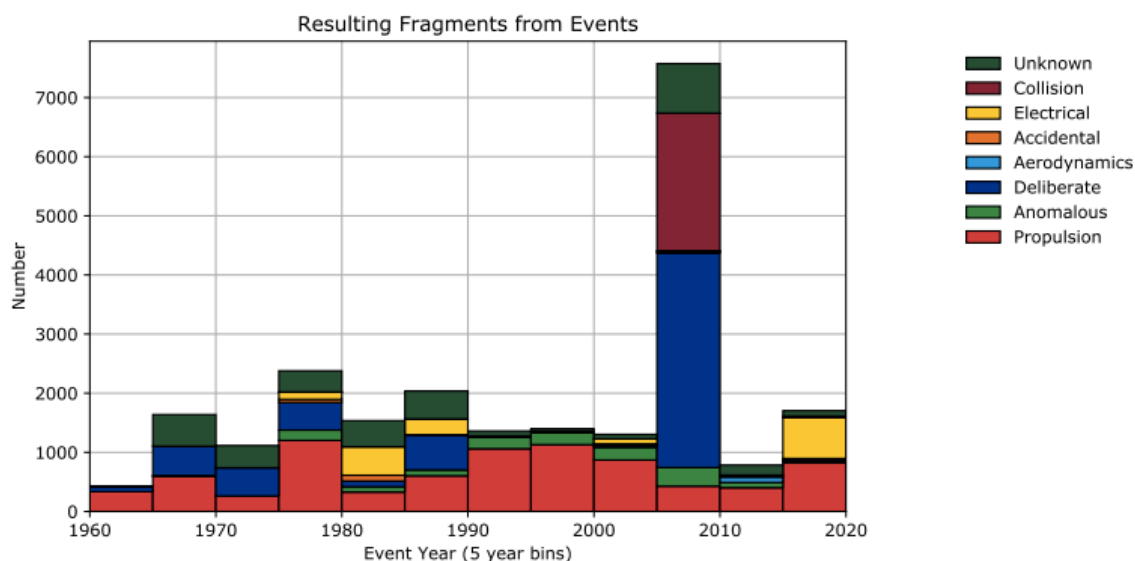


Figure 3.3: Debris resulting from fragmentation events in space by source [11].

Debris can be created by fragmentation in several ways. The most detrimental are in-orbit collision events, where two spacecraft crash into each other. This typically occurs when one or both of the involved spacecraft is defunct, thus without the possibility for a CAM. Collisions between two satellites do not occur frequently. The most devastating event was the in-orbit collision between two satellites, contributing to the sudden increase in objects in between 2005 and 2010 in Figure 3.3. Other fragmentation events are caused by break-ups from undepleted spacecraft. The third category of fragmentation events occurs when satellites are removed intentionally by anti-satellite missiles launched towards a satellite to destroy it, should the

satellite present a risk when entering the atmosphere. When this is performed on a satellite in a densely populated orbit, this can have catastrophic results. These various fragmentation events will be briefly discussed below.

In-orbit collisions

The US Space Surveillance Network (SSN) monitors more than 20 000 space objects [3]. Because LEO is getting so densely populated, two satellites may find themselves orbiting on a collision course. If the probability of a collision is too high, the US SSN sends out an alarm to the two satellite agencies. Currently the LEO space environment is so dense that satellites have to perform 1 CAM per month on average [4]. However, if one or both of the satellites involved is defunct and thus uncontrollable, collisions can occur with devastating effects. This is what happened on the 10th of February 2009 with the active U.S. satellite Iridium-33 and the defunct Russian satellite Cosmos-2551, collectively weighing over 1500 kg [24]. The collision took place at a densely populated altitude of 780 km and created over 2000 shrapnel fragments (Figure 3.3). At impact, the debris fragments were shot in all directions between 200 to 1600 km altitude. Most of the debris stayed at 800 km altitude and formed a cloud of debris orbiting Earth [24]. Due to slight changes in initial conditions of the individual debris particles, the cloud disperses in a short period of time. Figure 3.4 shows how much the debris cloud had already dispersed six weeks after the collision [24].

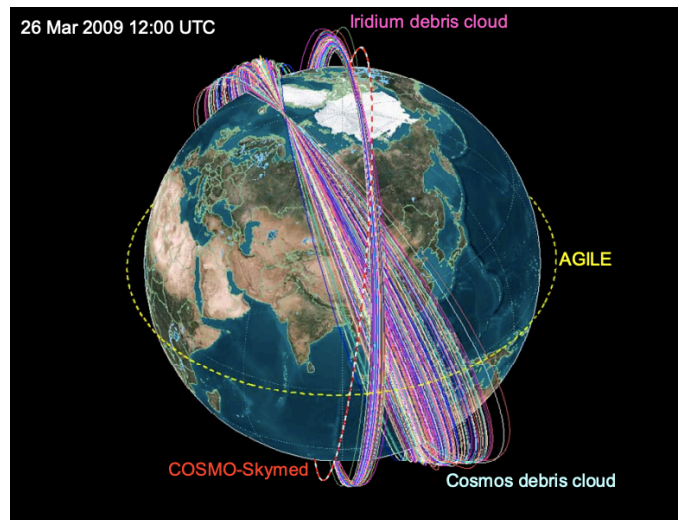


Figure 3.4: Debris cloud 1,5 month after Cosmos-Iridium collision [24].

Explosions

An estimated 750 000 objects above 1 cm are created by explosions of satellites and spent rocket stages, which is most of all small-scale debris objects [25]. The explosions are caused by spacecraft undepleted of their propellant or battery charge. Large temperature differences lead to a build-up in pressure until the rocket tank explodes. Also, interactions of the tank walls and the propellant over time may cause an explosion [3]. Next to these risks, leftover propellant or charge will also dramatically increase the damage in a collision. The two most destructive explosions were that of the rocket body of the European Ariane 1 in 1986 and the propulsion system of the American Pegasus in 1996, together injecting more than 1100 debris objects into orbit [3].

Anti-satellite test

Satellites can pose a potential danger to human safety when re-entering the atmosphere. If the satellite is too large or massive, substantial pieces can reach Earth's surface. To prevent such events, space agencies can launch an anti-satellite missile directly at a satellite to destroy it in-orbit. This technology has been successfully tested by the U.S., Indian and Chinese space agencies; the downside is that each launch created thousands of new debris objects [14]. On the one hand, the U.S. and Indian anti-satellite test were performed at such a low altitude that almost all of the created debris fragments spiralled into the atmosphere within a short time. On the other hand, the Chinese anti-satellite test has been declared as the most catastrophic fragmentation event to date, contributing a large part to the increase in debris fragments between 2005 and 2010 in Figure 3.3. In January 2007 a missile was launched at the Chinese Fengyun-1C satellite orbiting at 860 km altitude. The impact created a cloud of over 2600 debris fragments, increasing the debris population by 25% [14]. On top of destroying a potentially dangerous re-entering satellite, this technology also grants space agencies the possibility to eliminate enemy spacecraft; a scenario that fortunately has not yet occurred.

3.2. Non-fragmentation debris

New space missions cause a continuous release of smaller debris objects, next to the occasional generation of large debris through fragmentation events [3].

Solid Rocket Motor firings

In the 1980's, Solid Rocket Motors (SRM's) were frequently used to launch payload into LEO, and SRM's were sometimes even integrated into the satellite itself [26]. SRM's are unfavourable compared to liquid motors since they require added aluminium powder to ensure a steady combustion. This aluminium is found to produce debris in multiple ways. First, it reacts with oxygen to form Al_2O_3 dust, which is ejected and stays in orbit. Secondly, the aluminium can also concentrate and accumulate in cavities in the rocket tank to form 'slag'. Whereas the dust particles are harmless and will reach a maximum diameter of 50 μm , the aluminium slag can reach a diameter of 3 cm, which could form a danger [27]. It is estimated that about 3 000 kg of aluminium slag distributed over approximately 160 000 objects still reside in space [2].

Motor coolant

Another source of space debris is the motor coolant used for the RORSAT mission, a collection of Russian Earth observation satellites active between 1970 and 1988 [3]. It was wrongly assumed that an orbit at 900 km would suffice as a graveyard orbit for satellites that were orbiting at 250 km. During the transfers to the higher orbit, substantial amounts of Sodium-Potassium (NaK), meant to cool the motors, was ejected and formed debris particles between 0.1 mm and 5.5 cm [28]. While the RORSAT missions have only cumulatively resulted in 50 kg of NaK space debris, the total number of their separate droplets is more than 500 000, making it an important source of debris. There are some more sources of debris, such as Westford needles or debris from surface degradation [3]. Since these reach maximally 100 μm in size, they lie outside of the space debris range relevant to this report and will not be discussed.

3.3. Spatial and material density of debris

Many different orbits around Earth are being used for spaceflight, each with its own advantages and disadvantages for space missions. GEO satellites orbit the Earth exactly once a day, so a constant communication with a ground station can be attained. Figure 3.5 shows the mission type of each object in GEO, dominated by launches of communication satellites providing

telephone, radio, television and internet services.

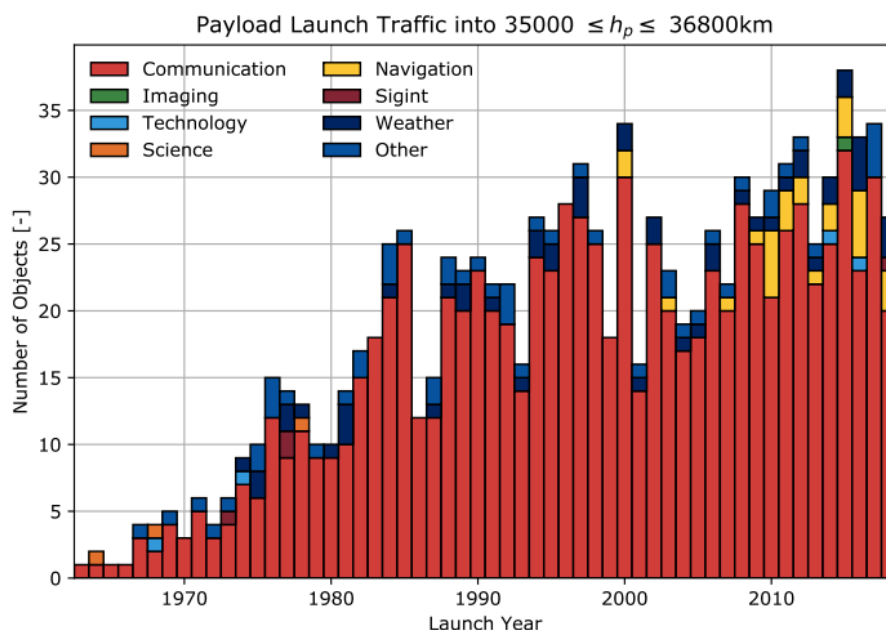


Figure 3.5: Type of mission of objects in GEO [11].

LEO satellites are closer to Earth than GEO satellites and are preferred for Earth observation missions. Figure 3.6 shows the mission types in LEO. Because of the short distance to Earth, the field of view of a LEO satellite is limited and it can only communicate with a ground station at a specific time each day. Space agencies and commercial companies have solved this problem by launching constellations of small satellites instead of one large satellite, a solution that is rapidly increasing the number of LEO objects, as can be seen over the last 5 years (Figure 3.6) [11].

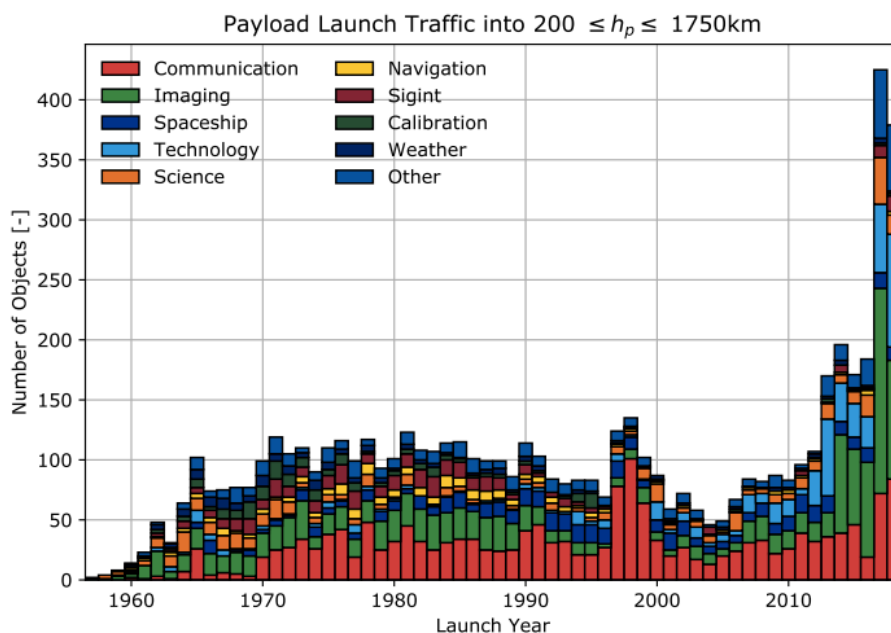
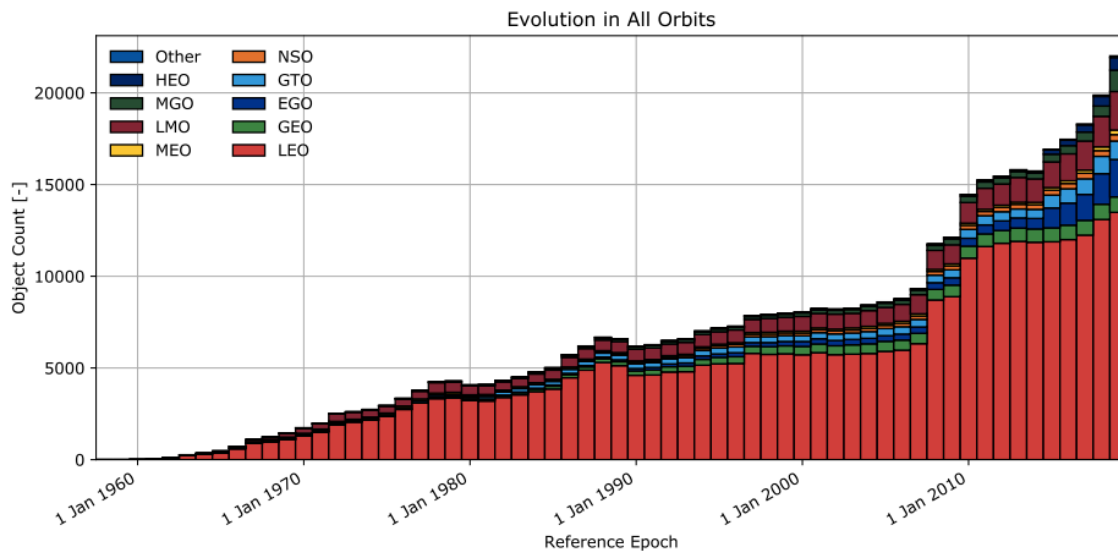


Figure 3.6: Type of mission of objects in LEO [11].

Figure 3.7 shows the evolution of the number of debris objects in different orbital regions.

The demand for communication, imaging and technology satellites has made LEO the most densely populated orbit with over 14 000 tracked objects. LEO contains more objects than all the debris in other orbit regions together [2].



(a) Evolution of number of objects.

Figure 3.7: Evolution of debris objects in different orbital regions [11].

Figure 3.8 shows the distribution of the number of objects within LEO. It can be seen that many objects reside in orbits with an inclination around 90° and altitude between 500 and 1000 km [11]. These orbits are called polar orbits and are particularly useful for earth observation missions, since satellites in polar orbits cross the equator at a different location each orbit and cover all of Earth surface in one day [29]. A special type of polar orbit, the Sun-Synchronous Orbit (SSO), can even be adjusted to make a satellite cross a specific Earth location at the same time each day, for example the Amazon jungle every day at noon [29]. A satellite in SSO will typically have an altitude between 600 and 800 km and an inclination of $i = 96^\circ \pm 4^\circ$. Objects orbiting in SSO have an orbital precession $\Delta\Omega$ of nearly $1^\circ/\text{day}$. This means that after one year, the satellite will be in the exact same orbit as where it started and a constant angle is maintained with respect to the Sun. Satellites in SSO can even be set to always orbit in dawn or dusk, so that the satellite is never shadowed by the Earth and receives the most sunlight as possible. This is a feature that is especially in high demand with satellites powered by solar panels.

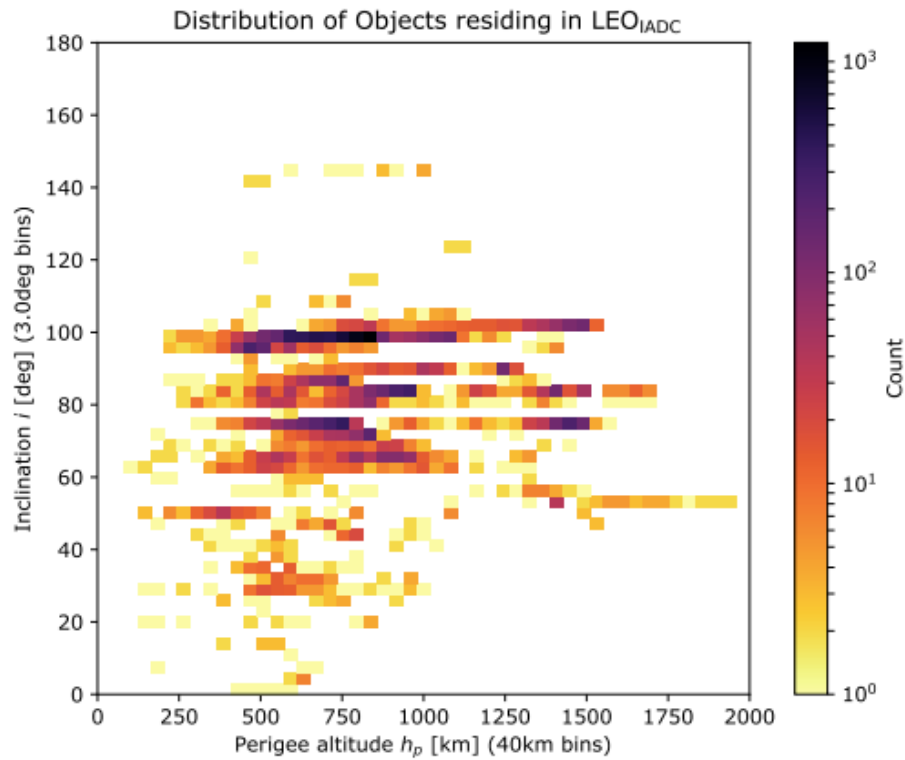


Figure 3.8: Distribution of objects in LEO [11].

Material size range

The performance of a laser ablation system depends on the material that it ablates [30]. Since the laser system is to interact with objects with sizes between 1 and 10 cm, Figure 3.9 shows that fragments from three different sources will be targeted: SRM slag, NaK droplets and fragmentation debris.

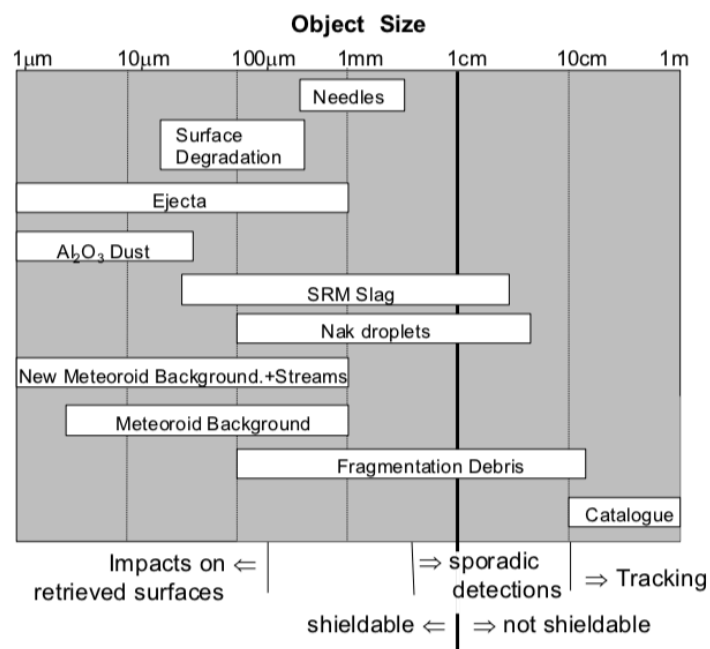


Figure 3.9: Size range of different sources [3].

The densities of SRM slag and NaK droplets are easily attained, since the composition is known and particles will not have any cavities since the shape of the frozen liquid droplets in space can be assumed spherical [27]. The densities of the three debris sources are listed in Table 3.1. The density of debris from fragmented spacecraft is harder to determine. Spacecraft predominantly exists of aluminium and carbon [31]. It would be false, however, to say that a spacecraft would have the density of aluminium $\rho_{alu} = 2.7 \text{ g/cm}^3$ or that of carbon $\rho_{carbon} = 2.3 \text{ g/cm}^3$. This is mostly because satellites are not one massive object and contain many cavities inside. In general, the density of spacecraft is estimated to be $\rho_{sc} = 0.03 \text{ g/cm}^3$ [31]. The fragmented debris from these spacecraft on the other hand, will have a higher density, since the cavities have most likely disappeared in a break-up. The density of fragmented space debris is estimated at $\rho_{frag} = 0.2 \text{ g/cm}^3$. Since fragmentation events have caused the most of 1-10 cm debris, the objects that the laser will be tested on should at least have a density equal or higher than this value to accurately represent fragmentation debris. The shape of the fragmented debris is irregular and will be assumed spherical in this report.

Table 3.1: Material density of debris between 1 and 10 cm.

Source	SRM slag	Motor coolant	Fragmentation events
Material	Al_2O_3	NaK	Al / C
Density [g/cm^3]	3.5	0.86	0.2
Shape	spherical	spherical	(assumed spherical)

Area-to-Mass Ratio

Another parameter that influences the performance of the laser is the Area-to-Mass Ratio (AMR). Since mass increases with $m \propto r_{object}^3$, while the area increases with $A \propto r_{object}^2$, it can be stated that in general large objects have low AMR and small objects have high AMR [29]. The AMR distribution can be plotted for all tracked objects in LEO using the ESA DISCOS database (Figure 3.10). It can be seen that the average AMR is about $0.01 \text{ m}^2/\text{kg}$.

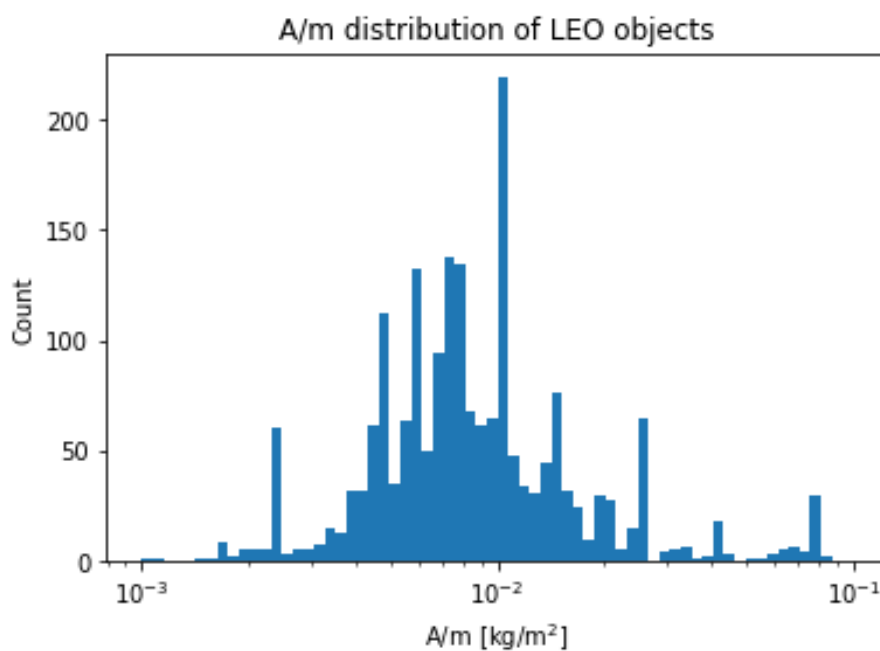


Figure 3.10: AMR distribution of tracked objects in LEO. From the ESA DISCOS database.

However, this average value holds only for the tracked objects that by definition are larger than 10 cm. A corresponding AMR value for smaller debris was found by [32] after measuring the resulting debris shrapnel from artificially created collision tests. Data points were also included from an ESA Ariane explosion test, which is a good simulation of an in-orbit fragmentation event. Figure 3.11 shows that debris fragments with characteristic size between 0.01 m and 0.1 m have AMR values between 0.04 and 0.5 m²/kg, which is higher than what Figure 3.10 would suggest.

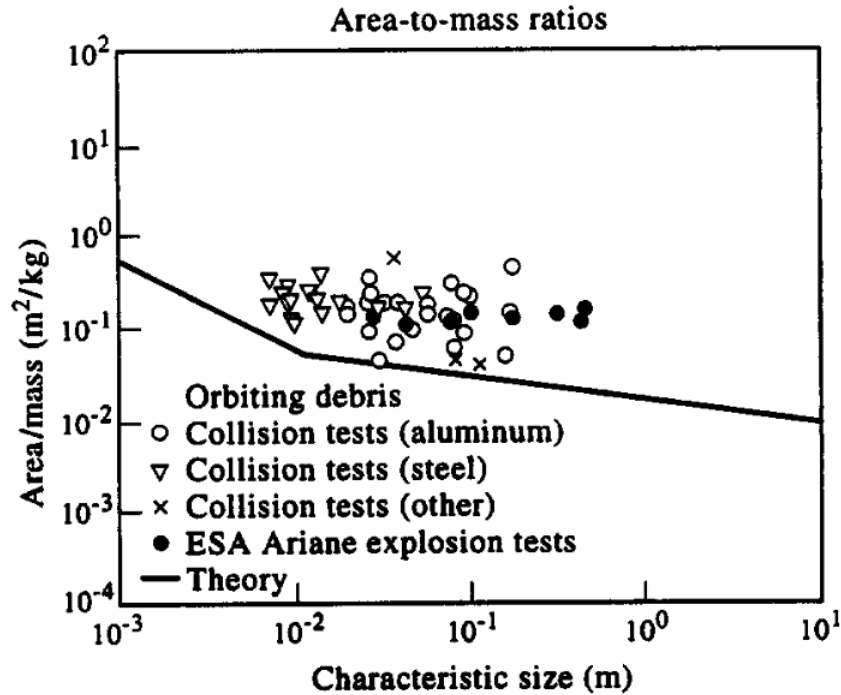


Figure 3.11: AMR distribution of debris fragments resulting from artificial explosion [32].

Table 3.2 shows the properties of three potential targets a laser system could encounter. The AMR values are selected using Figure 3.11: the AMR of the 1 cm and the 10 cm object will be 0.16 and 0.04 respectively. The area and the volume of the objects are computed assuming a spherical shape of the debris. A corresponding mass for the objects is calculated using the area and the AMR values. The resulting densities of the objects are computed from the mass and the volume. The 1 cm object has a density $\rho_{1cm} = 0.952$ [g/cm³] and the 10 cm a density $\rho_{10cm} = 0.380$ [g/cm³]. These densities are all higher than the estimated density for fragmentation debris, which means the created objects are not unrealistic. A value of $C_D = 2.2$ is assumed for the drag coefficient of the objects [29]. The reflection coefficient for all objects is estimated at $C_r = 1.1$ [33].

Table 3.2: Three debris objects to test laser performance on.

	1 cm	5 cm	10 cm
AMR [m ² /kg]	0.16	0.07	0.04
Area [m ²]	7.85 · 10 ⁻⁵	1.96 · 10 ⁻³	7.85 · 10 ⁻³
Volume [m ³]	5.25 · 10 ⁻⁷	6.54 · 10 ⁻⁵	5.25 · 10 ⁻⁴
Mass [kg]	0.5 · 10 ⁻³	30 · 10 ⁻³	200 · 10 ⁻³
ρ_{debris} [g/cm ³]	0.952	0.458	0.380

3.4. Lifetime of LEO debris

The particles in Earth’s atmosphere interact with objects in LEO. These interactions induce slight breaking effects on spacecraft and debris, which reduces the orbital energy and slowly but steadily make the objects spiral into the atmosphere where they burn up. The rate at objects spiral back to Earth depends on two parameters: the orbiting altitude and the AMR [34]. The density of the atmosphere determines how many atmospheric particles hit the surface of the spacecraft while orbiting. Since the density decreases with increasing altitude, particles at higher altitude get decelerated less by the atmosphere than particles at low altitude. The AMR affects the lifetime in two ways: the area of the spacecraft determines how many atmospheric particles it encounters and the mass determines how much these particles will decelerate the spacecraft [29]. Figure 3.12 shows the lifetime in seconds and years of three different objects of 1, 10 and 100 cm [22].

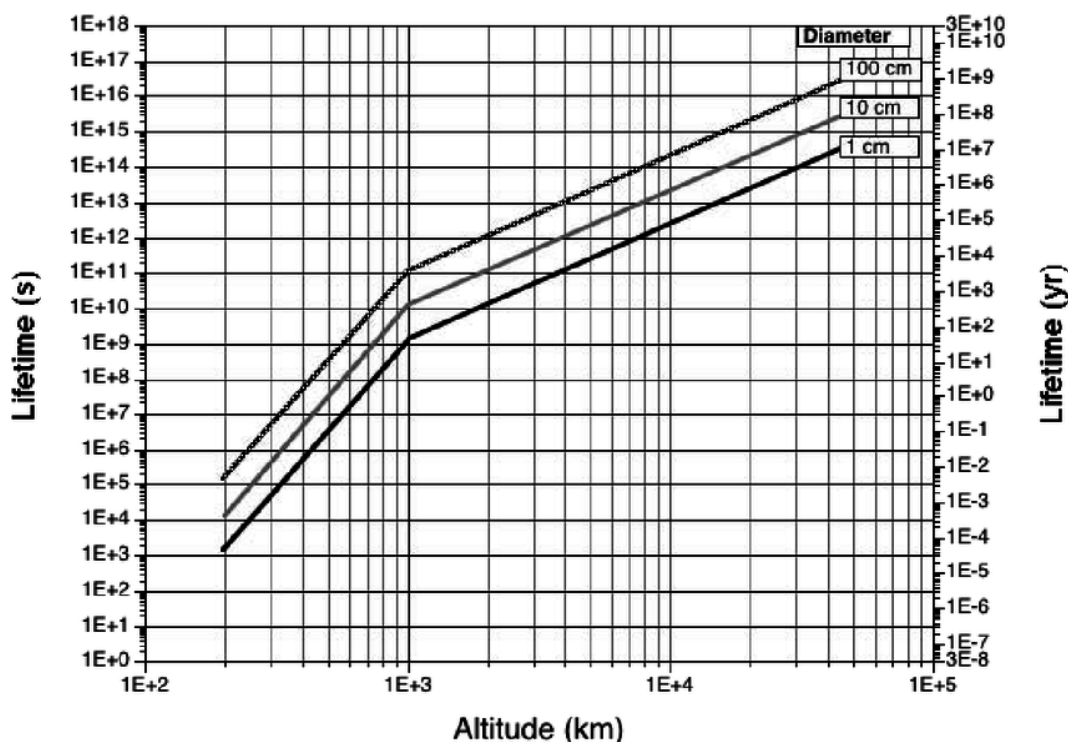


Figure 3.12: Lifetime of three spherical debris fragments with size 1, 10 and 100 cm. The density of each object is $\rho = 0.2 \text{ g/cm}^3$ [22].

At low altitudes, debris will spiral into the atmosphere in a short time. At 500 km, a 1 cm

object spirals into the atmosphere in nearly a month, whereas the 100 cm object will take about a year. At around 1000 km, the atmospheric interaction is too little to cause significant breaking and objects orbit indefinitely: a 10 cm debris takes over 300 years to spiral into the atmosphere. IADC guidelines state that spacecraft have to re-enter Earth's atmosphere within 25 years after the nominal mission lifetime [1]. Figure 3.12 shows that a 1 cm object naturally re-enters within 25 years from an altitude of about 900 km and a 10 cm object from about 700 km. Debris above these altitudes do not adhere to the safety guidelines, at least not by means of a natural mechanism. This research report aims to find out if a laser system would be able to lower the lifetime of these objects below the IADC mitigation guidelines.

4

Theoretical framework

The understanding of the mechanism of laser ablation requires some theoretical background. First, the basic mechanism of lowering an object as a result of a Δv will be explained. Next, the geometries from which the laser could target debris will be discussed. Through the Lagrange Planetary Equations, it will be shown how Δv 's in different directions affect the debris orbit and what geometries result in the highest Δv . Then, the necessary background will be given on laser physics, which will predominantly be about how the laser will transfer momentum to a debris object through the effects of ablation. Finally, the technical constraints on the laser parameters will be discussed.

4.1. Debris dynamics

An object orbiting around Earth is assumed, only influenced by Earth's fully symmetrical gravitational field. The equation of motion for such an object is the following (Equation 4.1) [34].

$$\ddot{\vec{r}} = -\frac{\mu}{r^3} \cdot \vec{r} \quad (4.1)$$

with $\mu = GM_{Earth}$ being the gravitational constant of Earth. The velocity of this object can be found using the vis-viva equation, which describes the orbital velocity of objects in any arbitrary orbit (Equation 4.2).

$$v^2 = \frac{2\mu}{r} - \frac{\mu}{a} \quad (4.2)$$

where v is the orbital velocity of the object and a is the semi-major axis of the orbit. A special case is the circular orbit where the radius of the orbit r equals the semi-major axis and Equation 4.2 becomes the expression for the orbital speed of an object in a circular orbit.

$$v^2 = \frac{\mu}{r} \quad (4.3)$$

When a Δv is exerted on an object in a circular orbit, the object is injected into an elliptical transfer orbit (Figure 4.1) [35].

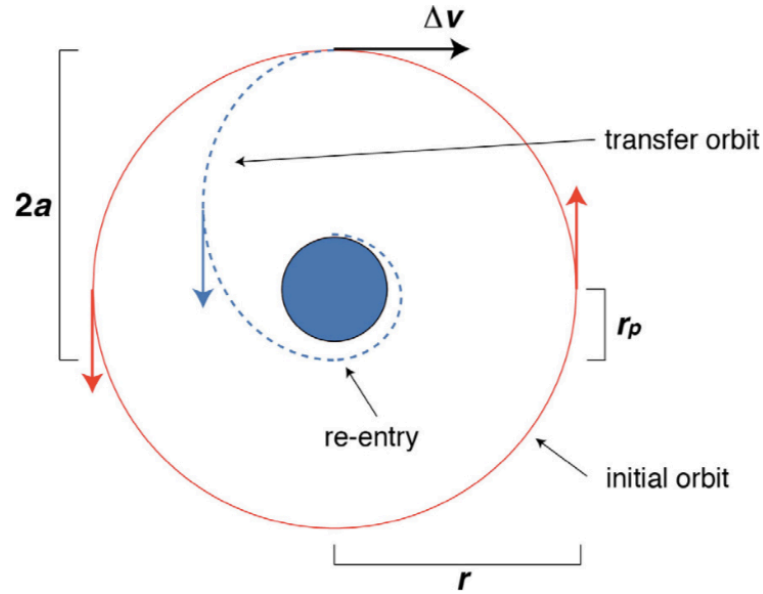


Figure 4.1: Transfer orbit after exerted Δv [35].

The velocity of the original circular orbit is given in Equation 4.3. After the produced Δv the object will travel along an elliptical orbit with semi-major axis $a = \frac{1}{2}(r_a + r_p)$ and a velocity defined by Equation 4.2. The lower the perigee of the elliptical orbit, the more the object gets decelerated by interactions with particles in Earth's atmosphere. From about a height of 200 km, the density of the atmosphere is high enough to decelerate the object such that it spirals into the atmosphere and burns up [29]. The Δv required to end up at this altitude can be computed by taking the difference between the elliptical velocity at apogee and the circular velocity at that point, which is constant throughout the orbit [34].

$$\Delta v = v_{circ} - v_{apo,ellips} = \sqrt{\frac{\mu}{r_a}} - \sqrt{\frac{2\mu}{r_a} - \frac{2\mu}{r_a + r_p}} \quad (4.4)$$

$$\Delta v = v_c \left[1 - \sqrt{2 - \frac{2r_a}{r_a + r_p}} \right] = v_c \left[1 - \sqrt{\frac{2r_p}{r_a + r_p}} \right] \quad (4.5)$$

$$\Delta v = v_c \left[1 - \sqrt{\frac{2r_p}{\Delta r + 2r_p}} \right] = v_c \left[1 - \sqrt{\frac{1}{\frac{\Delta r}{2r_p} + 1}} \right] \quad (4.6)$$

$$\Delta v = v_c \left[1 - \left(1 - \frac{\Delta r}{4r_p} \right) \right] = v_c \frac{\Delta r}{4r_p} \quad (4.7)$$

where the first-order Taylor expansion $\sqrt{\frac{1}{x+1}} = 1 - \frac{x}{2}$ is used to rewrite Equation 4.6 to Equation 4.7. The parameter $\Delta r = r_a - r_p$ is defined as the difference between the apogee and the perigee of the elliptical transfer orbit. Equation 4.6 is illustrated in Figure 4.2 which shows the Δv required to lower LEO debris to a perigee of 200 km where it will burn up. A debris object at 500 km requires around $\Delta v \approx 90$ m/s to de-orbit within half a revolution, but a debris object at 1000 km needs about $\Delta v \approx 220$ m/s.

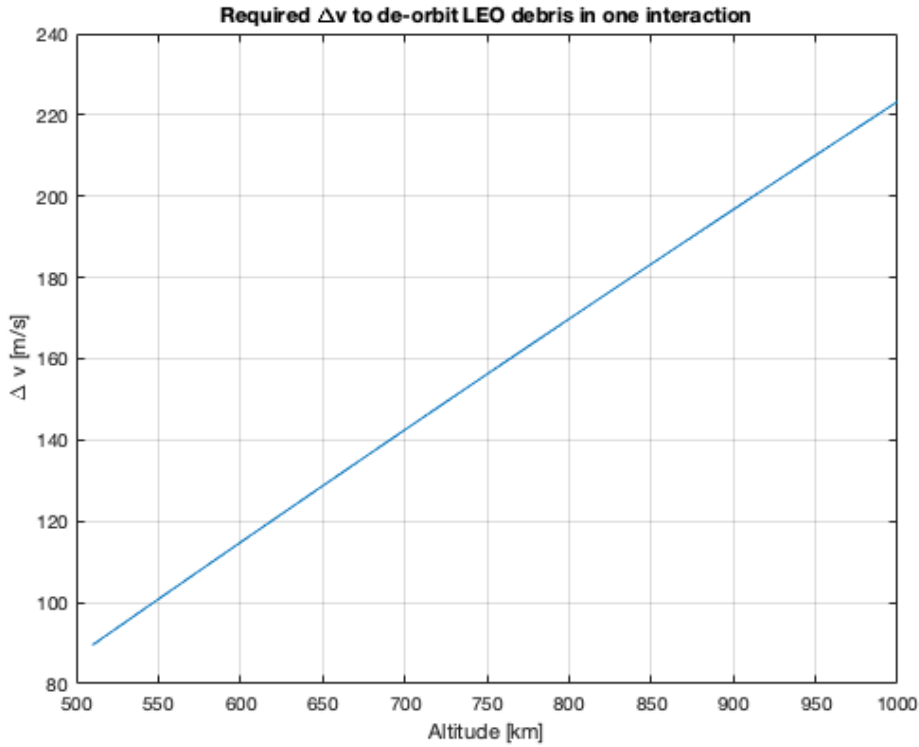


Figure 4.2: Required impulsive shot to lower LEO debris to perigee at 200 km.

Lifetime before and after the interaction

A Δv in the right direction will lower the orbital energy of the debris object and will cause it to lower its perigee [34]. Lower Δv 's than depicted in Figure 4.2 may not de-orbit the object within one revolution, but may still reduce the object's lifetime significantly. Section 3.4 showed the lifetime of objects orbiting Earth, and that objects higher than a certain altitude will orbit Earth indefinitely. If the lifetime of these objects can be lowered below the IADC guideline of 25 years, this would be beneficial for the safety of the LEO environment. The lifetime of a circular orbiting object is estimated as follows [29]:

$$T_{life} \approx -\frac{T_{period} \cdot H}{\Delta a_{rev}} = \frac{T_{period} \cdot H}{2\pi C_D \left(\frac{A}{m}\right) \rho a^2} \quad (4.8)$$

where Δa_{rev} is the loss in semi-major axis per revolution, T_{period} is the time to complete one revolution at semi-major axis a and H is the density scale height of the atmosphere, defined as the distance over which the density of the atmosphere drops by a value of $1/e$ [29]. Equation 4.8 holds two other parameters: the drag coefficient of the object C_D and the AMR introduced in Section 3.3. The lifetime of any object is thus inversely proportional to its A/m value. Since Section 3.4 showed that in general small objects have higher AMR values, this means that small objects take longer to spiral into the atmosphere than large objects at the same initial altitude. When a Δv is generated on a debris target, it is sent onto an elliptical orbit and its lifetime changes. However, Equation 4.8 only holds for circular orbits that have a constant atmospheric density throughout the orbit. This is not the case for elliptical orbits where a debris particle experience much more drag at low altitudes than at high altitudes [29]. An estimation is made that the average density throughout the orbit can be assumed to be the

density at an effective circular orbit with the following semi-major axis [36]:

$$a_{eff} = r_{perigee} + 900 \cdot (e)^{0.6} \quad (4.9)$$

where e is the orbit eccentricity. However, this assumption only holds for low elliptical orbits below $e < 0.1$. The most elliptical orbit that the laser would be able to generate would be when a debris at 1000 km altitude would be sent onto an elliptical orbit with $r_{peri} = 200$ km, since any perigee lower than this would be considered a de-orbit. The corresponding eccentricity for this orbit would be:

$$e = \frac{r_{apo} - r_{peri}}{r_{apo} + r_{peri}} = \frac{800}{7378 + 6578} = 0.06 \quad (4.10)$$

Since this maximum eccentricity is below 0.1, the assumption can be safely made. The results of the lifetime computation before and after the interaction are shown below, see Figure 4.3.

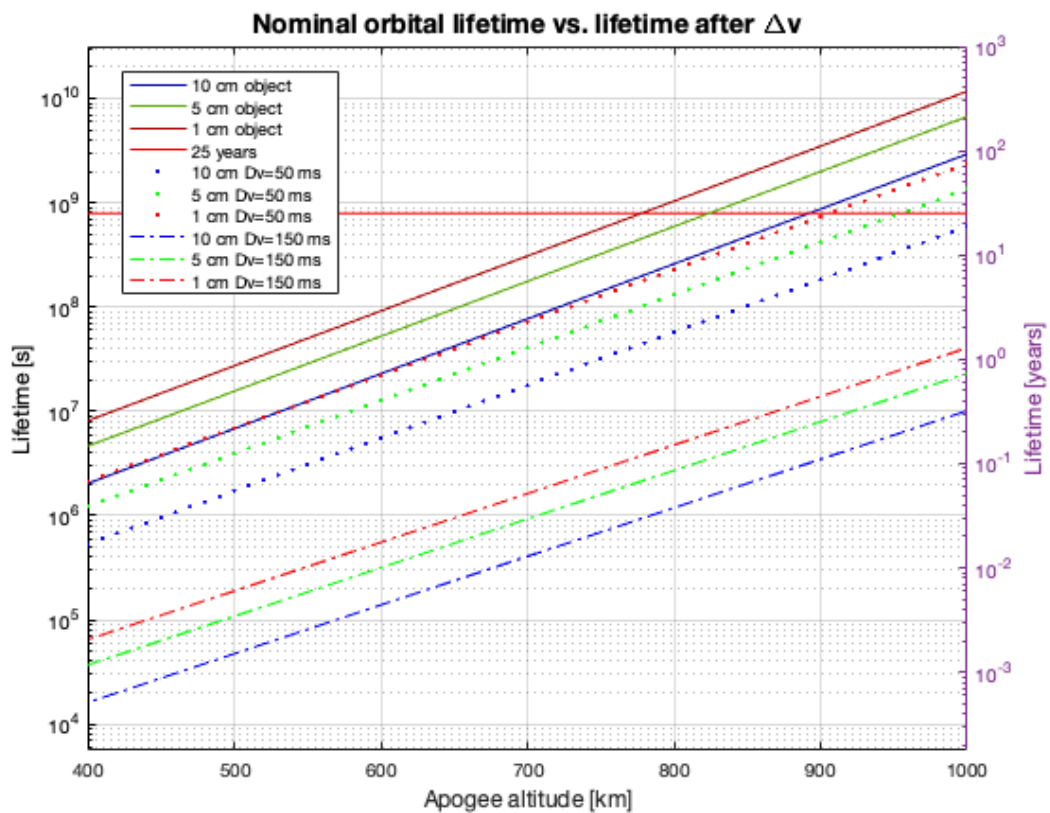


Figure 4.3: Reduction of lifetime for given Δv 's on LEO debris objects.

Three objects with different diameters and AMR values are shown in Figure 4.3. The top three lines show the nominal lifetime of the objects without any Δv . The two set of lines below (dotted and dashed) correspond to the reduced lifetime after a change in velocity of respectively $\Delta v = 50$ and 150 m/s. The lifetimes are calculated using Equation 4.8 assuming an exponential atmospheric model with $\rho_0 = 2.91 \cdot 10^{-10}$ and a scale height of $H = 82.0$ km. More on the exponential atmospheric model in Section 5.1.1. The lifetimes of the elliptical orbits after a Δv are computed following Equation 4.9. In Figure 4.3, the red horizontal line shows the 25 year guideline. The altitude at which this guideline is naturally followed is approximately 890 km for a 1 cm object (AMR = $0.16 \text{ m}^2/\text{kg}$), 825 km for a 5 cm object (AMR = $0.7 \text{ m}^2/\text{kg}$) and 775 km for a 10 cm object (AMR = $0.04 \text{ m}^2/\text{kg}$). At higher altitudes than

these values, the objects will have to be lowered artificially. A 10 cm object takes more than 300 years to spiral into the atmosphere naturally, while a 1 cm object does so in about 100 years. It can be noted that a velocity change of 50m/s already reduces the lifetime of the 1 cm object at 1000 km below 25 years. The 5 and 10 cm object get reduced to below 25 years from an altitude of 950 and 900 km respectively. A higher Δv of 150 m/s, the bottom set of three lines, will lower all objects far below the 25 year guideline: the lifetime of the 10 cm object at 1000 km is reduced to approximately 1 year and the 1 cm object at 1000 km is reduced to about 10 days. The figure further shows that the laser ablation system should at least be able to perform velocity changes of $\Delta v = 50\text{m/s}$. Important to note is that the Δv 's should be applied in the anti-velocity direction so that the orbital velocity of the debris is reduced. The effects of the direction of the velocity change will be discussed in the next section.

4.2. Geometries

Section 3.3 showed that the LEO debris population occupies more than one orbit. To target a large fraction of objects, the laser ablation system will have to be able to interact with objects orbiting at higher and lower altitudes than the laser system itself. This will result in interactions with many different geometries and thus different directions of generated Δv . Any imparted Δv can be split up in three direction components of a Local Vertical Local Horizontal (LVLH) reference frame: a radial component Δv_r , a tangential component Δv_θ and a normal component Δv_n that complements the orthogonal reference system which has its origin in the centre of the spacecraft (Figure 4.4) [29].

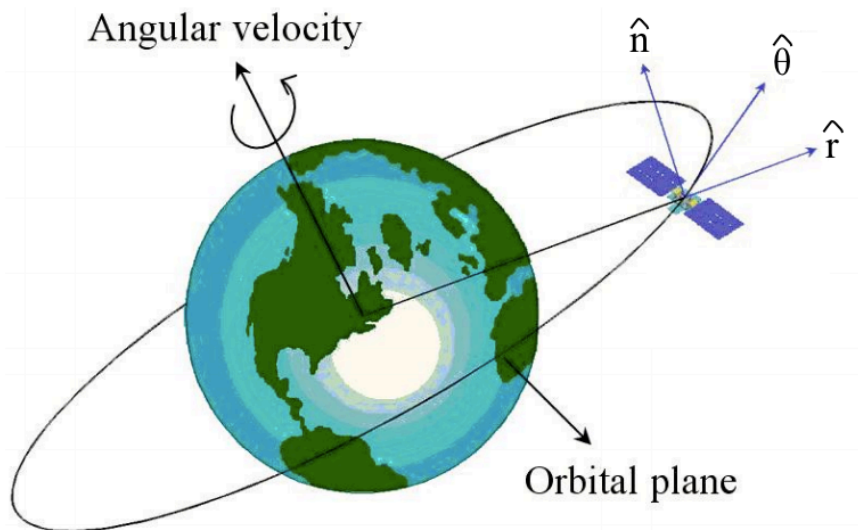


Figure 4.4: Schematic of three components of LVLH frame [37].

In a similar fashion, the orbital velocity of an orbiting object can be decomposed into these three components (Equation 4.11). A change in any direction will change the orbital velocity of the object. A special type of orbit is the circular orbit where the object has no radial and normal velocity component throughout the orbit [34]. The tangential velocity then automatically equals the orbital velocity.

$$v_{orb} = \sqrt{v_\theta^2 + v_r^2 + v_n^2} \quad (4.11)$$

The optimal direction to generate Δv to decelerate an orbiting object is the exact opposite direction of its orbital velocity [34]. In reality this could only be accomplished if the object is hit in a 'head-on' interaction. Since many interactions between the laser and the debris objects can be expected to have a difference in altitude and even a difference in azimuth target angle, Δv 's will be produced in the radial and normal direction as well. The Lagrange planetary equations can be used to inspect the effect that these Δv 's have on the orbital elements of the debris object (Equations 4.12 - 4.17) [34]. The changes in orbital elements can then be used to check the effects on the reduction of lifetime of the debris.

$$\Delta a = \frac{2}{n_0 \sqrt{1 - e_0^2}} [\Delta v_r e_0 \sin(v_0) + \Delta v_\theta (1 + e_0 \cos(v_0))] \quad (4.12)$$

$$\Delta e = \frac{\sqrt{1 - e_0^2}}{n_0 a_0} [\Delta v_r \sin(v_0) + \Delta v_\theta (\cos(E_0) + \cos(v_0))] \quad (4.13)$$

$$\Delta i = \frac{r_0 \cos(\omega_0 + v_0)}{n_0 a_0^2 \sqrt{1 - e_0^2}} \Delta v_n \quad (4.14)$$

$$\Delta \omega = \frac{\sqrt{1 - e_0^2}}{n_0 a_0} [-\Delta v_r \cos(v_0) + \Delta v_\theta \frac{2 + e_0 \cos(v)}{1 + e_0 \cos(v_0)} \cos(v_0)] - \cos(i_0) \Delta \Omega \quad (4.15)$$

$$\Delta \Omega = \frac{r_0 \sin(\omega_0 + v_0)}{n_0 a_0^2 \sqrt{1 - e_0^2} \sin(i_0)} \Delta v_n \quad (4.16)$$

$$\Delta M = n_0 - \frac{1 - e_0^2}{n_0 a_0 e_0} \left[\Delta v_r \left(\frac{2e_0 r_0}{p_0} - \cos(v_0) \right) + \Delta v_\theta \left(1 + \frac{r_0}{p_0} \right) \sin(v_0) \right] \quad (4.17)$$

Equations 4.12 and 4.13 result in the following change in perigee and apogee [38]:

$$\Delta r_p = (1 - e_0) \Delta a - a_0 \cdot \Delta e \quad (4.18)$$

$$\Delta r_a = (1 + e_0) \Delta a + a_0 \cdot \Delta e \quad (4.19)$$

First, it can be noted that a Δv_n in the normal direction only affects the inclination i , argument of periapsis ω and the Right Ascension of the Ascending Node (RAAN) Ω . Since these parameters only change the direction of the trajectory of the orbit, it can be concluded that any Δv_n will not affect the lifetime of the targeted debris object. The only orbital parameters that will alter the lifetime of the debris are the semi-major axis and the eccentricity, because both determine the change in perigee and apogee (Equations 4.18 and 4.19) [29]. The semi-major axis and eccentricity are only influenced by a velocity change applied in the radial or tangential direction (Equations 4.12 and 4.13). A positive Δv_θ , which is co-aligned with the velocity direction, will always increase the semi-major axis which will lead to an extension of the objects lifetime. In the same way, a negative Δv_θ , opposite to the velocity vector, will always decrease the semi-major axis and thus lower the lifetime. A statement about a change in velocity in the radial direction is made less easily, since the outcome depends strongly on the current position the spacecraft is in, denoted by the true anomaly v . This is because the direction of the radial velocity component changes in an eccentric orbit. At perigee ($v = 0^\circ$) or apogee ($v = 180^\circ$) of the orbit, the radial velocity component is zero and neither a positive or negative Δv_r will have a large effect. If the shot is applied between $v = 0^\circ$ and $v = 180^\circ$, the object is moving away from the perigee and the radial velocity will point away from the Earth [34]. Then, a positive Δv_r will only increase this radial velocity and thus the total velocity, which will result in an increased semi-major axis and eccentricity. A negative Δv_r will point opposite of the radial component and cause a decrease in velocity. The exact opposite holds

when the shot is applied between $\nu = 180^\circ$ and $\nu = 360^\circ$. The object is now moving towards perigee, meaning that the radial component is directed towards Earth. A negative Δv will now increase this radial component and thus increase the total orbital velocity and lifetime of the object. In this geometry, a positive Δv will now decrease the velocity since it is pointed opposite to the radial velocity component.

Two possible geometries are depicted in two dimensions below (Figures 4.5-a and b). In both scenarios a Δv is generated on the object in the tangential and radial direction. In both cases it is uncertain if the Δv_r will affect the lifetime of the object in a positive or negative way. However, the main goal of the laser will be to lower substantial amounts of the orbital velocity of debris objects and since the Δv in the tangential direction will dominate the Δv in the radial direction given the geometries where a debris flies towards the laser, the sign of the Δv_r will not be decisive for the final result. This is quantified in Figure 5.11.

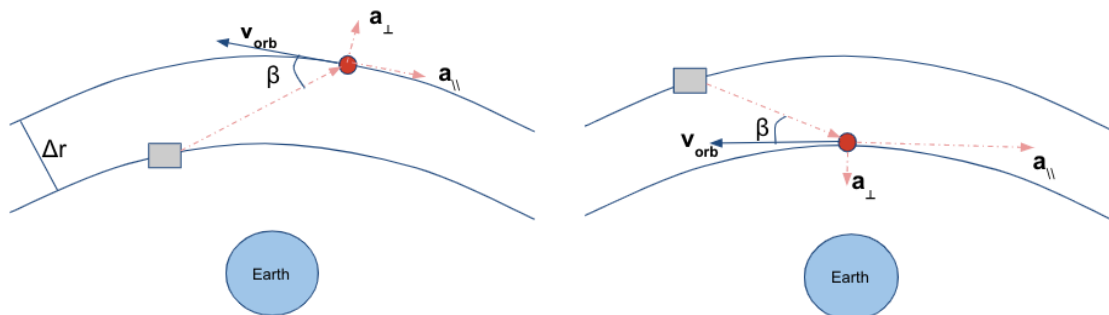


Figure 4.5: Geometry of laser (grey box) targeting debris (red circle) from **(a)** lower altitude (left) and **(b)** higher altitude (right).

4.3. Laser physics

Because lasers have various parameters that affect the applicability and performance of the system, there are many considerations to be made when designing a space-based laser.

Continuous wave vs. Pulsed laser

Using a laser, momentum can be transferred to a target in two different ways: by means of a Continuous Wave (CW) laser that delivers an unbroken signal of laser energy to the target, or a pulsed laser that sends short bursts of high-intensity laser pulses (Figure 4.6).

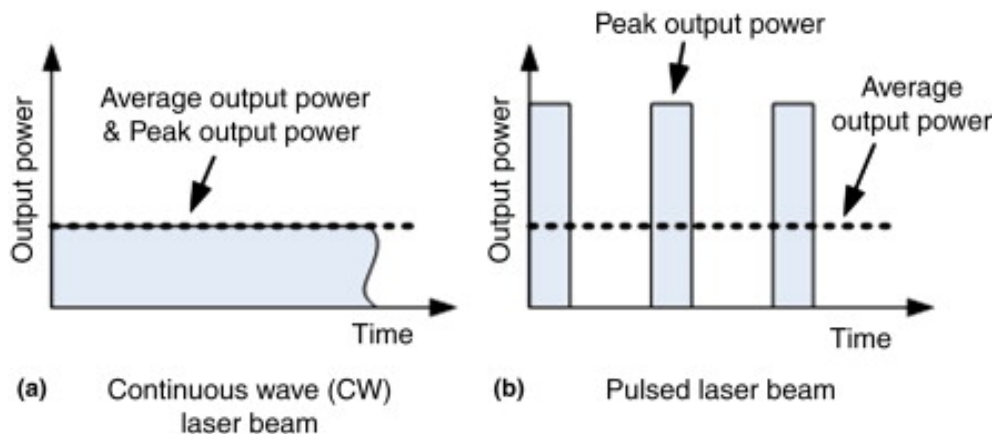


Figure 4.6: The Continuous Wave (CW) laser vs. the pulsed laser [39].

While both laser mechanisms use the same amount of average power, the peak intensity of a pulsed laser is much higher [10]. The intensity of both lasers is computed as follows.

$$I = \frac{P}{\frac{1}{2}\pi w(L)^2} = \frac{E/\tau}{\frac{1}{2}\pi w(L)^2} \quad (4.20)$$

where P is the total power of the laser, E is the laser pulse energy, τ is the pulse duration and $w(L)$ is the laser beam width, which is the radius from the center at which the beam intensity drops below a value of $1/e^2$. The definition of the beam width is depicted in Figure 4.7, which shows that the beam intensity profile decreases radially outwards.

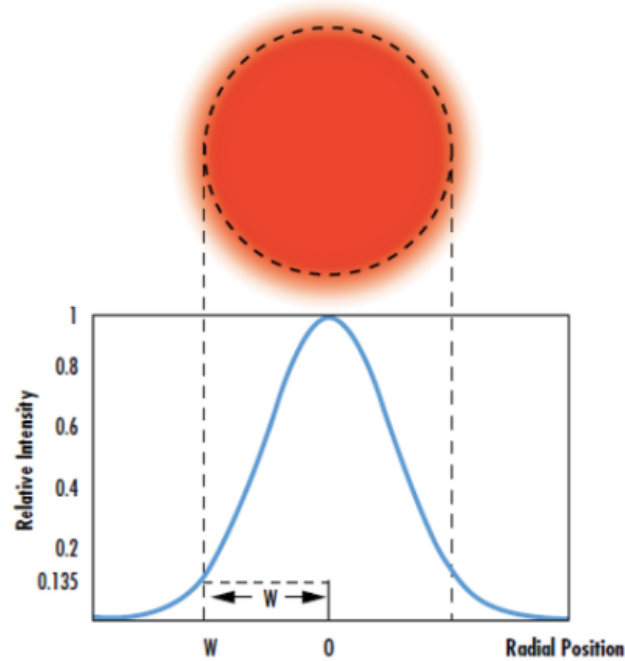


Figure 4.7: The beam radius profile of a Gaussian beam [40].

The beam width is an important factor since it defines the radius of the area over which the laser power gets distributed at a propagation distance L . It is defined as follows (Equation 4.21) [35]:

$$w(L) = \frac{aM^2\lambda L}{2\pi D_{eff}} \quad (4.21)$$

where a is a constant that takes laser diffraction into account, M^2 is the beam quality of the laser and λ is the laser wavelength. D_{eff} is the effective diameter of the beam and is defined as $D_{eff} = \alpha D_{mirror}$, with α being a fraction of the total diameter of the mirror that redirects the laser. The width of both the CW and the pulsed laser beam can be computed at large distances using this beam width. Table 4.1 shows the difference in performance of both methods. If both lasers would have the same beam width, the pulsed laser can generate peak intensities many orders of magnitude larger than a CW laser by decreasing the pulse duration to small time lengths ($\tau \approx 100$ ns). A smaller pulse leads to a higher peak intensity. The average intensity of the pulsed laser on the other hand depends on the pulse frequency f .

Table 4.1: Comparison of CW laser system and Pulsed laser system providing the same order of average intensity

Parameter	CW laser	Pulsed laser
λ (nm)	1064	1064
Beam width w (cm)	1 cm	1 cm
Power (kW) / Pulse energy (J)	1 kW	20 J
Pulse time (ns)	-	200
Frequency (Hz)	-	10
Total interaction time (s)	10	10
Peak intensity (W/m ²)	$6.36 \cdot 10^6$	$6.36 \cdot 10^{11}$
Average intensity (W/m ²)	$6.36 \cdot 10^6$	$1.27 \cdot 10^6$

The pulsed laser is able to deliver much more promising results with a far lower power requirement, which is specifically interesting for a system in space that relies on a limited power supply. The pulsed laser beam will be adopted for the laser system in this report.

Ablation threshold

The laser beam will focus on targets and direct the energy pulses to the debris fragment's surface. The total energy per area that the laser delivers on the target is called the fluence Φ and is defined as follows [30].

$$\Phi = \frac{E}{\frac{1}{2}\pi w(L)^2} = I\tau \quad (4.22)$$

The ablation threshold of a material depends on the pulse duration of the laser and the incident fluence. Longer pulse durations require higher values for the fluence to still initiate ablation. There exists an optimal pulse duration relating to a minimal fluence that would still cause ablation [20]. This relation is plotted below (Figure 4.8). The experiment included laser wavelengths between 100 nm and 10.6 μm and tested the effects on metals like gold, iron, lithium and aluminium. For pulses longer than $\tau = 10^{-9}$ s, the data points are best fitted by the relation $\Phi = 4.8 \cdot 10^8 \sqrt{\tau}$. However, below $\tau = 10^{-10}$ s the incident fluence does not seem to decrease. A pulse duration of 100 ps thus requires the lowest amount of energy per area to still achieve ablation on the material surface and it will not be necessary to maintain pulse durations lower than this value. For the tested metals this corresponds to an optimal fluence Φ between 1 and 10 $\cdot \text{kJ/m}^2$.

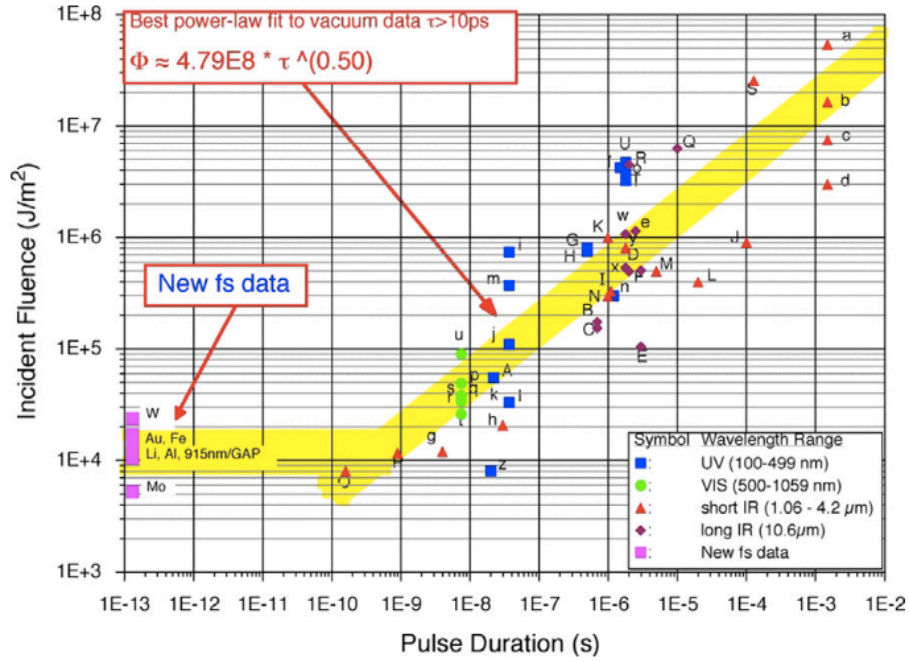


Figure 4.8: Ablation threshold for values of fluence and pulse duration [20].

Ablation is a material-specific process, so the material that the laser targets also influences the ablation threshold. The material coefficient C_m relates how much received laser power is converted to force, and thus how much the target can get decelerated from a given energy pulse. It is defined as follows [10].

$$C_m = \frac{C_{m,0}}{(I\lambda\tau)^{1/4}} \quad (4.23)$$

where $C_{m,0}$ is the coefficient that differs per material, for aluminium this value is $C_{m,0}$ 420 N/Wm. Equation 4.23 shows that C_m is inversely related to the laser intensity, wavelength and pulse duration. Since the laser interaction should ideally result in a high conversion from power to force, the wavelength should be minimized. Examples of the most common options for space-based laser ablation are the CO₂ laser that transmits infrared light at $\lambda = 10.6 \mu\text{m}$, the ICAN laser operating in the infrared at $\lambda = 1.064 \mu\text{m}$ and the crystal Neodymium:Yttrium Aluminum Garnet (Nd:YAG) that also operates at $\lambda = 1.064 \mu\text{m}$ [10, 23]. However, the frequency of the latter can be tripled to get a third harmonic Nd:YAG laser that operates in the UV spectrum at $\lambda = 355 \text{ nm}$. Next to the fact that smaller wavelengths are favored because it leads to higher material coefficients, materials also absorb them more efficiently than at higher wavelengths. Besides, Equation 4.21 shows that a smaller wavelength leads to a smaller beam width which translates to a higher fluence on the target. Since a Nd:YAG is a highly efficient laser and the laser wavelength can be brought to such a low value, this laser would be the optimal candidate for in-orbit ablation. The relation in Equation 4.23 is also illustrated in Figure 4.9 [20].

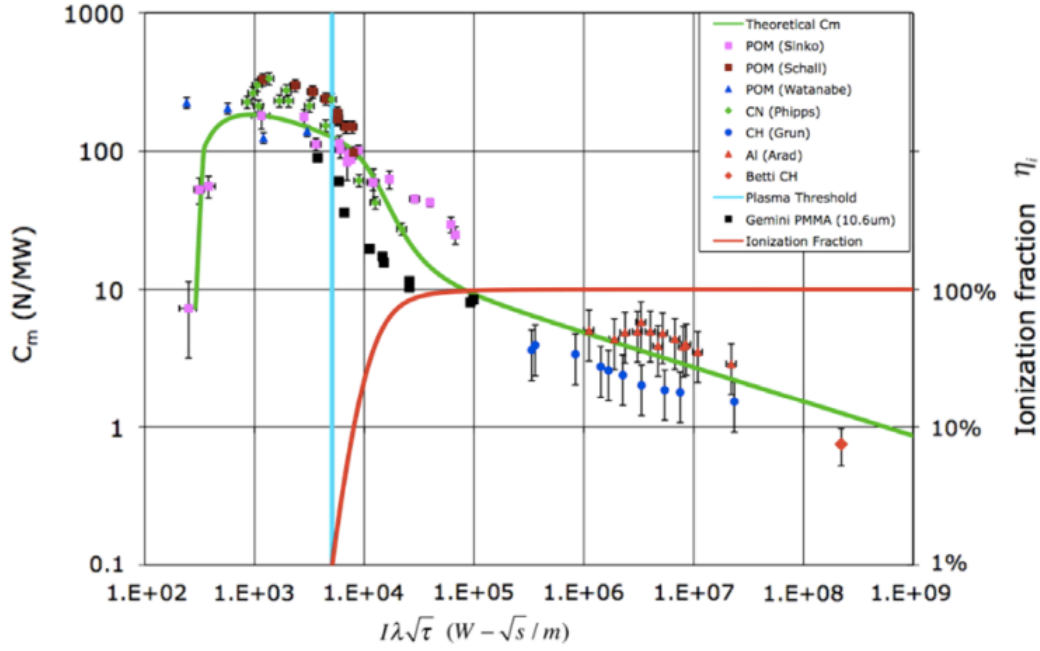


Figure 4.9: Material coefficient versus intensity, wavelength and pulse duration [20].

Here, data points from multiple experiments are combined and show a good agreement with the theoretical expectations for C_m , which is that the material coefficient increases up to a certain optimal value after which it gradually decreases. This is because any intensity larger than the ablation threshold causes energy to go into ionization instead of ablation, depicted by the red line in Figure 4.9. It is preferred to operate in the regime left of the blue line, after which the ionization starts to occur. For aluminium, the specific material coefficient lies around $C_{m,0} = 420$ N/MW, resulting in $C_{m,alu} = 128$ N/MW for a wavelength of $\lambda = 355$ nm with $\tau = 10^{-10}$ s.

Laser thrust

Since the material coefficient is defined as the amount of power that is converted to force by the laser beam, it can be used to get an expression for the thrust that is produced by the laser interaction (Equation 4.25) [41].

$$C_m = \frac{F_{thrust}}{P_{laser}} = \frac{F_{thrust}}{\Phi \cdot A_{target} \cdot f} \quad (4.24)$$

$$F_{thrust} = \Phi \cdot A_{target} \cdot C_m \cdot f \quad (4.25)$$

where the relation $P = \Phi \cdot A \cdot f$ was used in Equation 4.24, implying that the total power equals the laser pulse energy on the debris area times the pulse frequency. The area A_{target} is defined as the area on which laser energy gets absorbed. For large targets this would be defined by the area of the laser beam that hits the target, but as this report focuses on targeting small objects between 1 and 10 cm, the laser beam will not be smaller than the debris surface and the affected area can be assumed to be the area of the debris object. From Equation 4.25, the produced acceleration (or rather deceleration) on the debris fragment can be computed as follows:

$$a_{debris} = \frac{F_{thrust}}{m} = \Phi \cdot \frac{A}{m} \cdot C_m \cdot f \quad (4.26)$$

with m the mass of the debris target. Equation 4.26 verifies that objects with higher AMR get accelerated more than objects with low AMR. However, it should be noted that a_{debris}

only reaches high values when Φ has passed the ablation threshold. If the absorbed energy per area on the target is insufficient to initiate ablation, the acceleration will only be given by photon pressure, given as follows [42].

$$a_{photon} = \frac{p_{photon} \cdot A_{target}}{m} = \frac{A}{m} \cdot \frac{C_r}{c} \quad (4.27)$$

$$a_{photon} = \frac{A}{m} \cdot C_r \cdot 3.33 \cdot 10^{-3} \mu\text{m/s}^2 \quad (4.28)$$

where the photon pressure is defined as $p = 1/c$ with c the speed of light and the factor C_r defines whether the surface material is translucent ($C_r = 0$) or reflecting ($C_r = 2$). Noting that the acceleration generated from the Solar Radiation Pressure (SRP) is the following [29]:

$$a_{srp} = \frac{A}{m} \cdot C_r \cdot 4.7 \mu\text{m/s}^2 \quad (4.29)$$

it can be concluded that the laser photon pressure will have little effect on the trajectory of the debris fragment. The laser system should thus be able to achieve ablation on large distances to properly decelerate debris objects. The next section will discuss the necessary parameter range for this to be possible.

4.4. Laser parameter constraints

The material of the encountered objects will get ablated if the fluence on the object's surface crosses the ablation threshold, which for aluminium lies at $\Phi = 8.5 \text{ kJ/m}^2$ [10]. To get an expression for the delivered fluence at propagation distance L from the laser, Equation 4.22 can be rewritten to express the beam width as function of the fluence:

$$w(L)^2 = \frac{2E_{pulse}}{\pi \cdot \Phi} \quad (4.30)$$

After substituting the expression for the beam width found in Equation 4.21 in Equation 4.30 and rewriting this leads to the following expression for the effective laser fluence:

$$\Phi_{eff} = \frac{4 \cdot E_{pulse} \cdot D_{eff}^2 \cdot T_{eff}}{\pi \cdot M^2 \cdot \alpha^2 \cdot \lambda^2 \cdot L^2} \quad (4.31)$$

in which the relation $\Phi_{eff} = \Phi \cdot T_{eff}$ has been adopted where T_{eff} is a factor that takes some aspects into account that may result in a lower system performance. These include apodization, the process of focusing the optical signal, and atmospheric corrections, which will be small at high altitudes but not zero [20]. For space-based laser use, this factor is set on $T_{eff} = 0.9$ [43]. The simulation will use Equation 4.31 to check at what distance L ablation is achieved and then use Equation 4.25 to compute the generated thrust, so correct values need to be found for each of the listed laser parameters.

Laser power

The amount of energy per second that has to be generated by the laser leaves a large mark on the design of the system. Since the laser is placed in orbit, the power supply will be limited. This basically leaves three options for the generation of power: a nuclear reactor, Radioisotope Thermoelectric Generators (RTG's) or solar panels. The first option, a nuclear reactor would be able to generate a large amount of power (25 kW) [44]. However, the idea of a nuclear reactor flying in LEO is very unattractive and given the risk of re-entering Earth or the potential harm done if the system breaks up in space, this option is discarded. An

RTG produces power by transforming the heat that is radiated from a radioactive material into electricity [29]. Although it is true that RTG's take up much less space than solar panels, RTG's maximally produce a power output of a few kW, which is insufficient for the laser system. This means that the laser system will have to rely on solar panels for the generation of power. A solar panel is able to generate around $P/A = 0.27 \text{ kW/m}^2$ [45]. A moderate total power requirement for the firing of the laser system would be around $P = 20 \text{ kW}$. An extra $P_{\text{electronics}} = 7 \text{ kW}$ will be reserved for the electrical system that will regulate the laser heating, steering and other electrical requirements. This places the total power at an estimated $P = 27 \text{ kW}$, resulting in a solar array area of 100 m^2 . Knowing that ENVISAT had a solar array of 70 m^2 and the four solar panels on the ISS sum up to an area of 2500 m^2 , the required area for the laser satellite should be attainable [46].

The average laser power has the following relation to the energy pulse and the pulse frequency:

$$P_{\text{laser}} = E_{\text{pulse}} \cdot f \quad (4.32)$$

which means that the laser power $P = 20 \text{ kW}$ can be achieved by different combinations of pulse energy and pulse frequency. The optimal combination can be found by plotting the resulting Δv from Equation 4.26 against energy pulse E_{pulse} . Figure 4.10 shows the results for interactions with three objects with different AMR listed in Section 3.4.

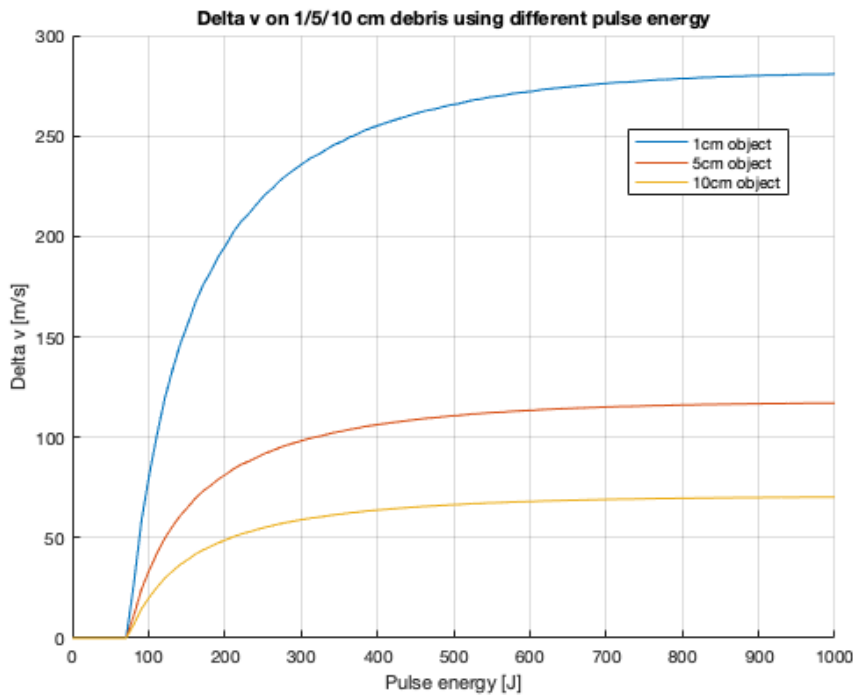


Figure 4.10: Resulting velocity from interactions using different pulse energy and frequency.

Each pulse energy on the x-axis corresponds to a pulse frequency of $f = P/E_{\text{pulse}}$, such that the total required power P equals 20 kW . It can be seen that a pulse energy below $E_{\text{pulse}} < 80 \text{ J}$ does not produce any Δv on the objects. This is explained by the fact that using a small energy pulse, Equation 4.31 shows that the ablation threshold is passed at a distance too close to the laser to still be effective. More on this effect in Section 5.1.3. Moreover, Figure 4.10 shows that a higher pulse energy leads to a higher velocity change, but the lines

seem to converge. It can be seen that any pulse energy E_{pulse} higher than 600 J does not result in much gain in Δv . The corresponding pulse frequency f is 33.33 Hz.

Laser beam

The other parameters in Equation 4.31 that have to be discussed are the laser beam characteristics. To start with, a visualisation of the laser beam quality M^2 is given in Figure 4.11.

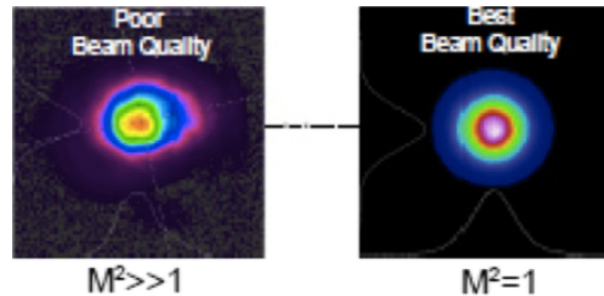


Figure 4.11: Laser beam quality. Right picture shows perfect beam quality [23].

The right picture shows a laser beam on a target with a perfect beam quality $M^2 = 1$. The beam is a Gaussian and is circularly symmetrical. This causes the laser energy to be spread over the smallest possible area and thus results in a high fluence. The picture on the left shows a 'poor' beam quality, where the intensity of the laser is not centered and is distributed over a larger area, requiring more energy to achieve ablation. Due to diffraction, a perfect M^2 will not be attainable in reality. The current state-of-the-art of laser propagation allows for a beam quality of $M^2 = 2$ [20]. Both pictures in Figure 4.11 show a decrease of intensity radially outwards. This is described by the beam quality factor a . For a Gaussian beam, this beam quality factor is defined as $a = 4/\pi = 1.27$ [20].

The laser will have to be able to create a small spot size at large distances, which starts by defining the diameter of the mirror that will focus the laser beam. The parameter D_{eff} denotes the beam diameter that is effectively launched from the laser station and is defined as $D_{eff} = \alpha D_{mirror}$. Equation 4.31 shows that a larger effective diameter is quadratically proportional to the produced fluence and thus has a strong impact. A reasonable value for the diameter fraction is $\alpha = 0.9$. The effective diameter is chosen as $D_{eff} = 1.5$ m, which would require a focusing mirror diameter of $D_{mirror} = 1.67$ m. This mirror diameter is relatively small and certainly attainable. The summary of all the laser parameters are given in Table 4.2.

Table 4.2: Chosen parameters for the laser system.

Parameter	Chosen value
P_{laser} [kW]	20
E_{pulse} [J]	600
f_{pulse} [Hz]	33.33
D_{eff} [m]	1.5
λ [nm]	335
$C_{m,alu}$ [N/MW]	128
A_{solar} [m ²]	100
T_{eff}	0.9
M^2	2.0
a	1.27

Figure 4.12 shows the fluence of the laser at different propagation distances when using the laser parameters in Table 4.2. The red line shows the ablation threshold ($\Phi = 8.5 \text{ kJ/m}^2$). The fluence increases quadratically with the distance. With an energy pulse of $E_{pulse} = 600 \text{ J}$, the ablation threshold is reached at a distance $L = 500 \text{ km}$.

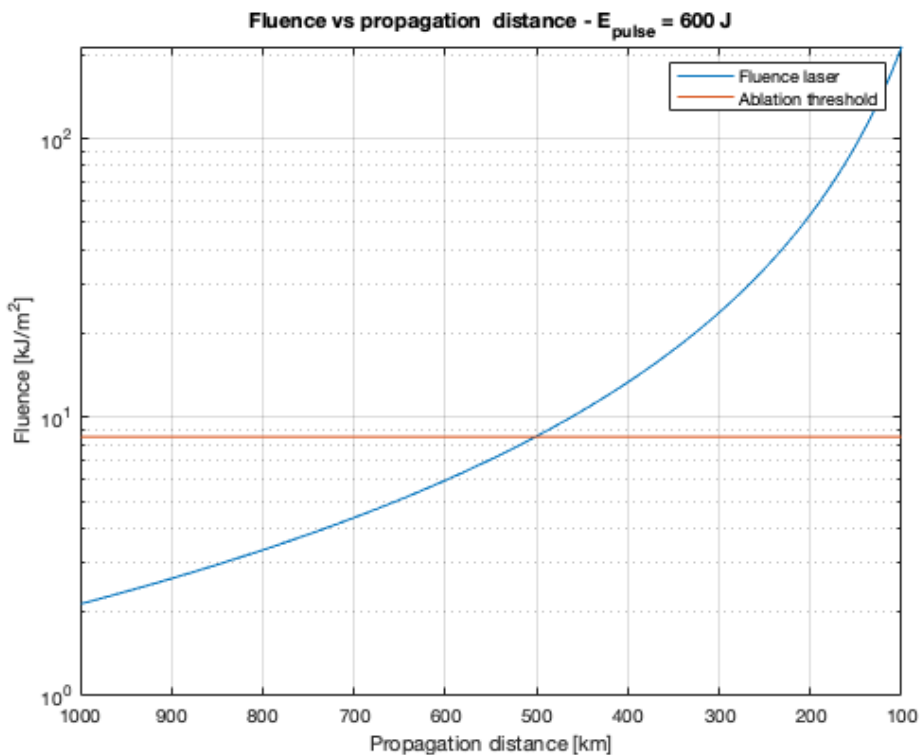


Figure 4.12: Laser fluence over propagation distance for parameters listed in Table 4.2.

Figure 4.13 shows the acceleration the laser would produce on three objects with different

AMR. The fluence on the targets is the same as in Figure 4.12. The acceleration is computed as in Equation 4.26.

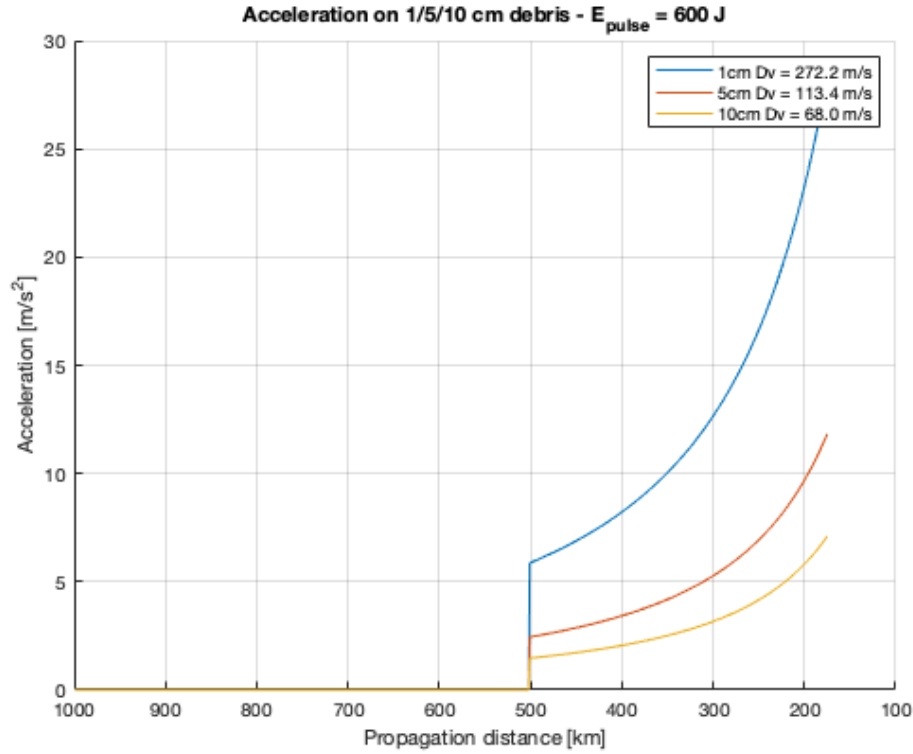


Figure 4.13: Acceleration on three objects listed in Table 4.2.

The total generated velocity changes are listed for each of the interactions as well. The velocities are computed as follows:

$$\Delta v = \int_{t_{end}}^{t_o} a_{debris}(L) \cdot dt = \int_{L_{end}}^{L_o} a_{debris}(L) \cdot \left(\frac{dL}{v_{rel}}\right) \quad (4.33)$$

with a_{debris} defined in Equation 4.26. The plot is cut-off at a distance $L = 175$ km to show that the laser can not perform ablation at distances too close to the system. This is because the closer the objects get to the laser, the faster the laser has to rotate to still track the objects. When the laser passes a threshold of a certain angular rate, the ablation will be stopped. This will be discussed in more detail in Section 5.1.3. Some geometries will lead to a limit higher than $L = 175$ km and some will lead to a lower limit, this value is taken as a dummy value to not show misleading values for Δv . Figure 4.13 shows that the acceleration on the objects starts at $L = 500$ km, agreeing with the passing of the ablation threshold in Figure 4.12. Further away than 500 km the fluence is not sufficient to achieve ablation on the material surface and the acceleration is just a result of the photon pressure, which is negligible in comparison to ablative pressure. The plot further shows that promising Δv 's can be reached on the three objects from an ablation regime from 500 to 175 km using the parameters in Table 4.2.

4.5. Target acquisition

The detection and tracking of debris objects is one of the most innovative and characteristic aspects of the laser system. In-situ debris detection removes the dependency on an object catalogue. This makes an orbital laser system specifically interesting for the removal of debris

fragments between 1 and 10 cm as they can not be monitored and stored in a catalogue. The detection telescope will leave its mark on the laser system performance: the limit at which small debris objects can be detected will determine from what distance the laser can start the interaction with the target. This section will briefly discuss the mechanism and design of the telescope subsystem of the laser.

Tracking system

There are two different options available for the tracking of debris objects in-situ: an optical tracking system and a radar system. Results from a space-based radar system show that a debris object of size 10 cm could only be detected from a distance of between 40 and 120 km, depending on their relative velocities [47]. Figure 4.13 shows that at these values are much too low. The optical tracking system delivers much more interesting results. An example is given in Figure 4.14.

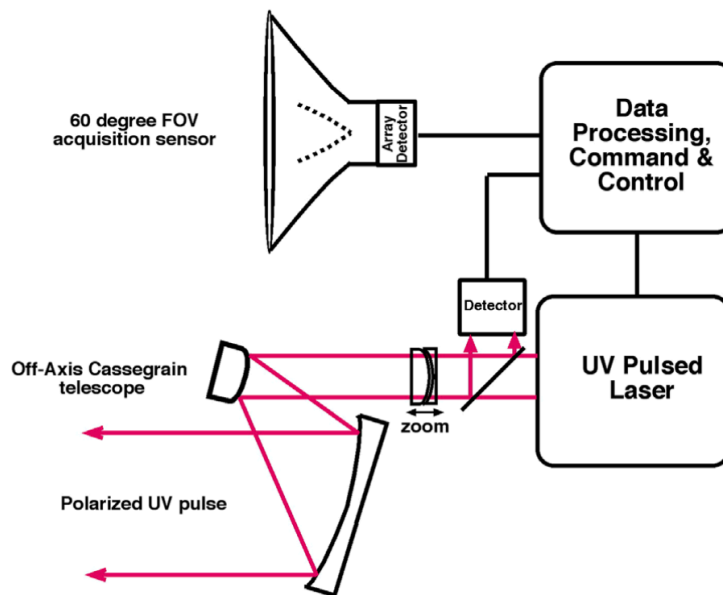


Figure 4.14: Laser system with optical tracking telescope [20].

The system consists of two different telescopes. A large 60° Field-of-View (FOV) telescope will acquire targets using the detection of sunlight reflection of the surface material [20]. Every array-pixel detects the electrons produced by a photoelectric effect resulting from the incoming reflected photons. A photoelectron number of $N_{pe} = 10$ per array pixel combined with a sufficient Signal-to-Background Ratio (SBR) will trigger a detection of a potential target. Table 4.3 shows that a debris object of 1 cm reflects enough photons to be detected at a distance of 900 km using a telescope with $D = 1.5$ m and $FOV = 60^\circ$ [10].

Table 4.3: Photoelectron number and SBR for debris objects at 900 km distance using [10].

Debris diameter [m]	N_{pe} /pixel	SBR
0.05	$6.5 \cdot 10^3$	55.1
0.01	$2.45 \cdot 10^2$	2.21

Once the large telescope triggers a detection, the second telescope will actively track the tar-

get and send laser pulses. These pulses will be in UV as discussed in Section 4.3. This second small telescope will also detect the returning photons that are reflected from the laser beam hitting the target. Since these reflected laser pulses are much more intense than the reflected sunlight, the resulting N_{pe} and SBR of the object will be much higher during the active tracking (Table 4.4). The SBR for a 5 cm debris object during active tracking at 900 km is increased by a factor $\sim 10^5$, which is why the relatively low SBR during passive daylight acquisition is tolerated. When the passive sensor detects a candidate object which turns out to be false signal, the active tracking system will abort the interaction and the system will start scanning for a new target. This makes sure no debris will be accelerated in the wrong direction and no active satellites will accidentally be targeted [10].

Table 4.4: Received photons and SBR for debris objects at 900 km distance during active tracking [10].

Debris diameter [m]	Photons received per pulse	SBR
0.1	$9.85 \cdot 10^2$	$3.31 \cdot 10^7$
0.05	$2.39 \cdot 10^2$	$8.28 \cdot 10^6$
0.015	$2.16 \cdot 10^1$	$7.45 \cdot 10^5$

The design of the telescope has implications on the performance of the laser in three ways. First, the FOV of the telescope will determine the maximum azimuth angle at which debris objects can be encountered. A 60° FOV is currently the state-of-the-art and will be used in the final simulation, in particular in Section 5.3 [20]. Secondly, the detection limit determines from what distance the laser can start the interaction. Tables 4.3 and 4.4 show that a 1 cm debris could already be detected at 900 km. For the simulation in this report, a detection limit of $L_{detect} = 800$ km will be maintained. Finally, the telescope design relies on the reflection of sunlight on the debris material. To optimize this signal, a maximally lit object against a black background is favored. This demand would favor a dawn/dusk SSO for the laser system, so that the objects are lit and the telescope can detect the objects against a black background.

5

Interaction with one debris object

Before the laser can be tested on a complete debris population, the performance of the laser should be tested a single object first. This will show that the code is properly functioning and will indicate the range of geometries from which the laser can generate sufficient Δv 's to reduce the lifetime of an object. This chapter will first discuss the methodology of the code, showing how the interaction between the laser and the debris object will be simulated. All implemented termination conditions of the code will be explained in detail. Then the results will be given for interactions from different geometries. The so-called head-on collision will be discussed, where the laser encounters a debris object that is orbiting at the same altitude and traveling towards the laser with an azimuth angle $\Delta\phi = 0^\circ$. Next, the scenario will be discussed where the laser targets a debris object orbiting at altitudes above and below the laser with a zero azimuth difference. Then, the scenarios with non-zero azimuth angle are discussed, meaning that the debris will impact from an angle instead of straight forward. Finally, the geometries where the debris object has an altitude difference and an azimuth difference with respect to the laser orbit are simulated.

5.1. Methodology

The laser and debris object are simulated in the TU Delft Astrodynamical Toolbox (Tudat), a C++ program environment [48]. In summary, the program will first create the environment and specify the objects that will be propagated. Then both the laser and debris object will be propagated one integration step at a time. At every timestep, the program will check if the debris is within range of the laser and if it is moving towards it. If so, the propagation stops and a second propagation will start with a smaller stepsize to accurately model the interaction between the objects. The interaction will be stopped when the laser has to rotate too fast to track the debris object or if the target debris has passed the laser. The flowchart of the program is shown in Figure 5.7. This section will explain in detail what happens in each element.

5.1.1. Creating the environment

The program starts by defining the total time for which the simulation will run and during which the environment has to be created. The total simulation time is set to one week. The debris object and laser are set to encounter each other much sooner than this, so that the end of the simulation time will never be reached. To start, a bodymap is created containing all the bodies, celestial or artificial, that are present in the environment. Per body it includes

the properties that are necessary for calculating the accelerations during propagation such as mass, area and aerodynamic coefficient. First, the central bodies that will cause gravitational attraction are added to the map. The Sun, the Earth and the Moon are created as gravitational attractors. The perturbations of other planets like Venus, Mars or Jupiter will have a negligible effect on the debris object's position and are not included in the bodymap.

Since the debris object and the laser will orbit in LEO and will experience effects from atmospheric breaking, information has to be added on the Earth's atmosphere. While the NRLMSISE-00 model gives an accurate description of Earth's atmospheric density and is available in Tudat, it requires a long computation time. Eventually the laser will have to target a complete debris population, so a long computation time per interaction is undesirable. This is why an exponential atmosphere is created that returns approximately the same values for the density at LEO altitudes. An exponential atmosphere takes an initial density value at a specified reference altitude and assumes the density decreases exponentially with altitude (Equation 5.1).

$$\rho(h) = \rho_0 e^{-\frac{h}{H}} \quad (5.1)$$

in which ρ_0 is the initial density, H is the atmospheric scale height and h is the altitude measured from the altitude at which ρ_0 is defined. Instead of defining ρ_0 at sea-level, it will be more accurate to set this value at an altitude of 200 km. In this way the model has to extrapolate over a smaller distance to LEO than from sea level, which will improve the approximation of the density. The scale height is defined as the altitude where the density has dropped by a factor e and will be chosen such that the model densities correspond to the true densities at LEO altitudes. The results are shown in Table 5.1. The values from the U.S. standard atmosphere are estimated using an average solar activity [49]. The Sun has 11-year cycles in intensity, but the effects of the laser are noticeable at longer time lengths [29]. A debris that will spiral into the atmosphere within 25 years will experience multiple solar cycles, which justifies the assumption of an average solar activity for the density. The reference density ρ_0 at 200 km in this model is $2.91 \cdot 10^{-10}$ kg/m³.

Table 5.1: Densities from exponential model versus densities from U.S. standard atmosphere true model [49].

Altitude [km]	True Density [kg/m ³]	Exp. model density [kg/m ³]	Error [%]
200	$2.91 \cdot 10^{-10}$	$2.91 \cdot 10^{-10}$	0
400	$2.42 \cdot 10^{-12}$	$2.22 \cdot 10^{-12}$	-9.0
600	$1.75 \cdot 10^{-13}$	$1.93 \cdot 10^{-13}$	+10.2
800	$1.55 \cdot 10^{-14}$	$1.69 \cdot 10^{-14}$	+9.1
1 000	$1.59 \cdot 10^{-15}$	$1.47 \cdot 10^{-15}$	-7.5

The scale height corresponding to this model is $H = 82.0$ km. The values are correct to around $\pm 10\%$. Since the average density values of the U.S. atmosphere themselves have a large standard deviation resulting from the fluctuations of solar activity, the 10% error of the exponential is a sufficiently accurate estimation. The implementation of the atmosphere concludes the set-up of the celestial bodies. What remains is the creation of the laser and debris object. An estimated mass of 5000 kg will be used for the laser system [10]. The debris

mass, area, aerodynamic coefficient and radiation coefficient all correspond to the parameters listed in Table 3.2. Earth is declared an 'occluding body', implying that any radiation from the Sun will not influence the laser or debris when the Earth is positioned in between the Sun and the object. With these properties included in the body map, the creation of the bodies can be finalized by initiating all bodies at the same initial time and defining the frame of origin in which the bodies are defined. The global frame of origin is set to the Solar System Barycenter (SSB) and the initial time is set to J2000 (January 1st 2000).

Adding accelerations

Now that the bodies are created, the accelerations experienced by the laser and debris object can be implemented. These accelerations will be integrated at every timestep during the propagation and will define the trajectory of the propagated objects. When considering the accelerations to include on an orbiting body, it is important to keep the desired accuracy of the orbit in mind. Just like discarding other planets from the body map since the effects will be negligible, some accelerations can be ignored as well. The laser will observe the debris object from a large distance ~ 800 km, so making the debris orbit accurate to ~ 1 cm would be redundant and would ask a significant amount of computation time. This is undesirable since the program will have to simulate thousands of objects simultaneously in the end. The laser on the other hand is only one object and knowing where it is positioned will be detrimental for the outcome of the simulation. More perturbations will therefore be included to the laser than to the debris objects. The following accelerations are added to the laser body:

- Earth's gravity, corresponding to a spherical harmonics model up to the 5th order.
- Third-body perturbations from the Sun's gravitational influence.
- Third-body perturbations from the Moon's gravitational influence.
- Solar Radiation Pressure (SRP).
- Aerodynamic effects from Earth's atmosphere.

In both the third-body perturbations from the Sun and the Moon, the central bodies are assumed to be point masses. The uneven distribution of mass in these bodies actually cause objects orbiting around them to be accelerated more at some points than at others, but because the Sun and the Moon are both located far away, the point-mass assumption is validated. However, the laser is orbiting Earth relatively nearby, so a point-mass assumption would in this case be too inaccurate. Rather, a spherical harmonics acceleration model is included to estimate Earth's gravitational influence. This means the acceleration experienced from Earth's gravitational field will be irregular throughout the orbit, which is the case for LEO objects in real-life. Finally, the effects from SRP and the aerodynamic acceleration from interactions with the atmosphere are included as well. The debris object will be given the following accelerations:

- Earth's gravity, corresponding to a spherical harmonics model up to the 5th order.
- Effects from SRP.
- Aerodynamic effects from Earth's atmosphere.

Just like the laser, the debris object will experience Earth's gravity as a spherical harmonics model. The third-body perturbations from the Sun and the Moon are left out for the propagation of the debris object. Effects from SRP and atmospheric interactions should not be left

out, since these are of great importance for objects with high AMR such as small LEO debris fragments.

Initial system state

Now that the accelerations have been added to the objects, the only setting that remains before the propagation can be initiated is the initial state of the system. The orbital elements of the laser system should be chosen such that it can target most of the objects in LEO. The spatial distribution of debris objects was shown in Figure 3.8 in terms of perigee altitude and inclination. Most of the debris fragments are located between a perigee altitude $600 \text{ km} < r_p < 1000 \text{ km}$ and between an inclination $70^\circ < i < 100^\circ$. The results of this chapter will give an indication of the range of the laser system, so the initial chosen laser orbit could still be altered. For now, the initial state of the laser is set as follows:

Table 5.2: Initial state of Sun-Synchronous laser orbit.

Orbital parameter	Symbol	Description
Semi-major axis [km]	a	$h + R_{Earth}$ with $h = 800 \text{ km}$
Eccentricity	e	0.0
Inclination [$^\circ$]	i	98.0°
Argument of periapsis [$^\circ$]	ω	0°
RAAN [$^\circ$]	Ω	0°
True anomaly [$^\circ$]	ν	340°

The laser is placed at 800 km altitude, in the middle of the LEO region. The inclination is set so that the laser orbits in a Sun Synchronous Orbit (SSO). Next to the fact that this is an orbit densely populated with debris objects, the laser can also be configured in a 'dawn/dusk-orbit'. As briefly mentioned in Section 3.3, objects in this orbit have a fixed orientation with respect to the Sun so that the solar panels experience maximal sunlight illumination. For sake of simplicity, the initial state of the debris object will be set to encounter the laser within one revolution. This means the debris object will move in a direction 'opposite' to the laser. This can be configured by setting the inclination to $i_{debris} = 180^\circ - i_{laser}$, the argument of periapsis to $\omega_{debris} = 180^\circ - \omega_{laser}$ and the Right Ascension of the Ascending Node (RAAN) to $\Omega_{debris} - \Omega_{laser} = 180^\circ$ [29]. The altitude and inclination will be altered so that the laser can be tested in that particular geometry. The initial state of the debris becomes the following:

Table 5.3: Initial state of debris object.

Orbital parameter	Symbol	Description
Semi-major axis [km]	a	$h + R_{Earth}$ with $600 \text{ km} < h < 800 \text{ km}$
Eccentricity	e	0.0
Inclination [$^\circ$]	i	$82.0^\circ + \Delta\phi$ with $\Delta\phi$ azimuth angle
Argument of periapsis [$^\circ$]	ω	180°
RAAN [$^\circ$]	Ω	180°
True anomaly [$^\circ$]	ν	340°

The laser and debris object are configured so that they both cross the equator at $\nu = 0^\circ$ in opposite directions. By setting both true anomalies at $\nu = 340^\circ$, the objects will be propagated over $\Delta\nu = 20^\circ$ before they encounter each other. The equator is chosen as a crossing point so that any difference in inclination angle equals the difference in azimuth angle $\Delta\phi$. In this way many interactions with different altitude and azimuth angles can easily be initialized and tested. The initial states of both objects will be added to the system initial state which can then be numerically integrated.

5.1.2. Propagation of laser and debris orbit until encounter

The environment and all objects that will be propagated are created, as well as the relevant accelerations on the objects and the system initial state. The simulation of the dynamics of both objects requires three entries: the body map containing all the bodies, settings for the integration, and settings for the propagation. The first of these has been discussed in the previous subsection. The settings for integration and propagation will be discussed below.

Integration of the equations of motion

The equations of motion of orbiting objects can be integrated in multiple ways. The only options supported by Tudat currently are Euler integration and Runge-Kutta 4 (RK4) integration [48]. Where the Euler method takes much less computation time, the RK4 method is far more accurate. The linear difference in the position of a laser with initial state given in Table 5.2 is plotted below, see Figure 5.1.

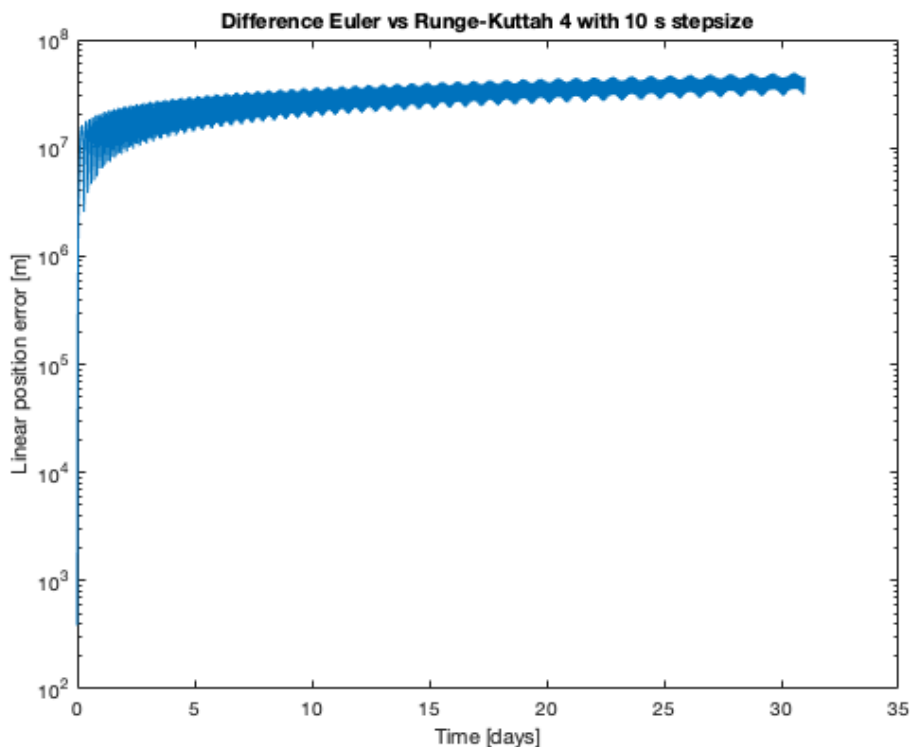


Figure 5.1: Difference Euler integrator w.r.t. RK4 method.

The computation time for the Euler method was only 6 seconds, while the RK4 method took 23 seconds. However, this factor 4 in computation time does not weigh up against the large difference in position. After 1 day the error is already in the order of 10 000 km, which is not acceptable when the laser will have to detect debris from ~ 800 km. Despite the longer

computation time, the RK4 method is chosen as integrator.

Stepsize

When choosing the stepsize for the scenario where a laser and debris are orbiting Earth until they are within a certain reach of each other, three considerations have to be kept in mind.

- A larger stepsize will result in a less accurate position determination than a smaller stepsize.
- A smaller stepsize will result in a longer computation time.
- The stepsize determines the distance between the integration intervals. Since the detection limit for the debris object is set at 800 km and the ablation threshold was calculated to be at 500 km, this puts an upper limit on the distance interval of $\Delta L_{int} = 300$ km. Knowing that the maximum relative velocity of an interaction is $v_{rel} = 15$ km/s (head-on), this put an upper limit on the stepsize of $t_{step} = 20$ s.

The difference in linear position accuracy of a stepsize of $t = 5$ s, $t = 10$ s and $t = 20$ s compared to a $t = 1$ s stepsize integration have been plotted for an RK4 integrator (Figure 5.2).

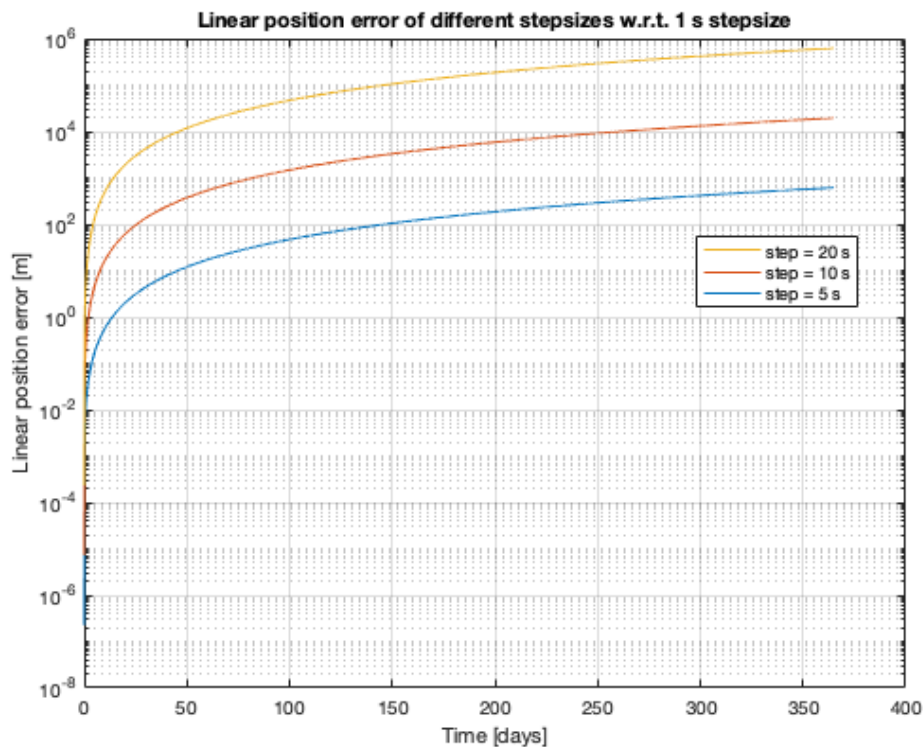


Figure 5.2: Linear position error of larger stepsize w.r.t. 1 s stepsize for 1 year simulation.

The simulation is run for 1 year, which is not representative for the interaction with the laser and one debris object, but will be representative for the interaction with a debris population that will run for a much longer period of time. The results show that using a stepsize of 20 seconds will result in an error of almost 1 000 km. Following the same reasoning as before, this error is too large and not acceptable. A stepsize of 10 seconds results in an error of 10 km, which is acceptable. A stepsize of 5 seconds results in an error of only 1 km, but due to the excessive computation time this stepsize is less optimal than the 10 second timestep. An

stepsize of 10 seconds will be selected for the integration of the laser and debris object until they have encountered each other.

Termination conditions

With the mode of integration defined, only the settings for the propagation remain for the simulation of the dynamics. The propagator setting requires the following information: the bodies from the body map that need to be propagated, the central bodies around which the propagated bodies revolve, the acceleration map containing the accelerations on the bodies during propagation and lastly the termination conditions. The first four entries have already been discussed. The last point should be discussed in some detail, as the termination conditions are a critical part of the simulation. They function as a list of requirements that a potential target debris should adhere to before a green light is given and the target debris gets ablated. The following conditions define when the first propagation of the laser and the debris should be terminated.

- Is the debris object within 800 km of the laser?** The first condition that should terminate the propagation is when the relative distance of the laser and the debris objects drops below the detection limit of 800 km. The relative distance is computed at every integration timestep and the propagation is stopped at the first timestep where the distance threshold is passed. There are, however, interactions imaginable where the debris is within 800 km of the laser but the geometry would still lead to an increase in velocity if ablation would be initiated. Therefore a second condition is implemented that should be met before the propagation is stopped.
- Is the debris object moving towards the laser?** Figure 5.3 shows two possible interactions where the debris object is within targeting range. However, the laser should not ablate the debris object in the encounter on the right, since this geometry would only lead to an increase in velocity of the debris object. As a solution, the inner product of the relative distance and the relative velocity of the debris object with respect to the laser is being monitored during the propagation. The propagation is only stopped when the relative distance is below 800 km and the calculated inner product is negative to ensure that the object gets decelerated.

When the debris and laser do not meet the listed termination conditions, the position of both objects are propagated forward over 10 seconds. This will keep happening until a debris object satisfies both conditions after which the propagation will be terminated and the ablation process of the debris object can be initiated.

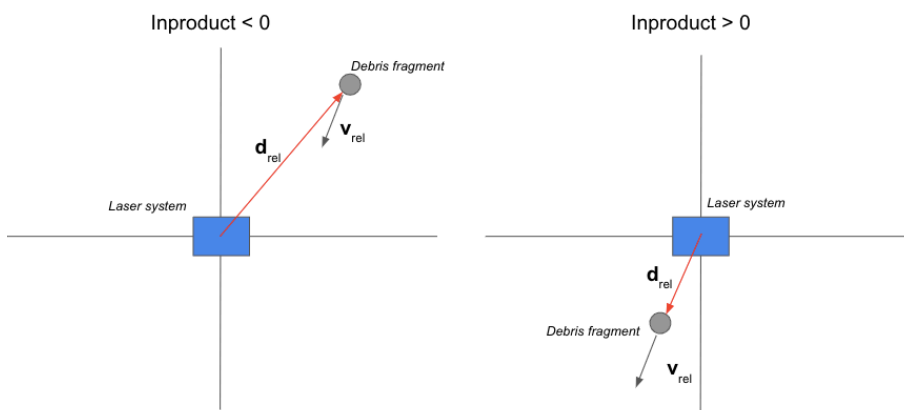


Figure 5.3: Scenario where the debris fragment (grey circle) is moving **(a.)** towards the laser (blue box) (left) and **(b.)** away from each other (right).

5.1.3. Propagation of the laser and debris interaction

When the propagation with the 10 second stepsize is stopped, a second propagation is started with other settings to more accurately simulate the interaction of the debris fragment with the laser beam. The same considerations have to be made for the interaction as for the previous propagation. The optimal stepsize for the interaction and what set of termination conditions should stop the propagation will be discussed.

Stepsize

With the parameters chosen in Section 4.4, objects can be ablated from a distance of $L_{abl} = 500$ km, which is only 300 km after the object is encountered. Since (under the right circumstances) more ablation leads to a bigger decrease in orbital velocity, the time that the debris fragment gets ablated should be maximized. This is why the stepsize will have to be small enough to accurately know when the ablation threshold is passed. Following the same reasoning as for the large stepsize, Figure 5.4 compares the errors in linear position of a laser with initial state listed in Table 5.2 for different integration stepsizes.

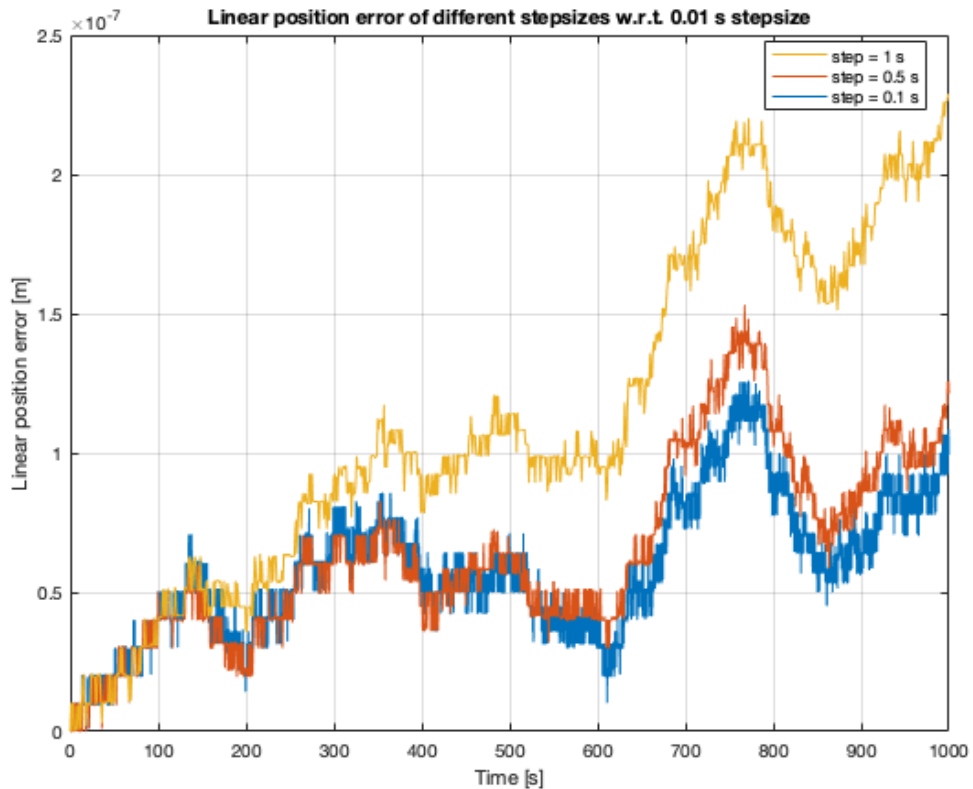


Figure 5.4: Comparing 0.1 s, 0.5 s and 1 s stepsize to a 0.01 s stepsize for laser and debris interaction.

A stepsize t of 0.01 s would produce integration intervals of around $\Delta L = v_{rel} \cdot t \sim 150$ m. This would result in the most accurate results but will also take an unacceptable computation time. A stepsize of 0.1, 0.5 s and 1 s are compared to the reference value. The results show that a stepsize of 1 second would only produce an error of $\Delta r \approx \sim 0.2 \mu\text{m}$ after 1 000 seconds which is negligible considering that the diameter of the smallest debris in the population is 1

cm. A 1 second stepsize leads to integration intervals of $\Delta L = 15$ km. In the worst case a 1 second stepsize would result in a 1 second loss of ablation time, which is acceptable.

Termination condition

Since the fluence has an inverse quadratic relation to the targeting distance $\Phi \propto L^{-2}$, the debris target will receive very high energy levels close to the laser. This is why the termination conditions for the propagation of the interaction are of vital importance to create realistic results. One termination condition was already discussed in the case of the large stepsize termination and will be the same for the interaction: the laser should not target the debris when the inner product $\vec{d}_{rel} \cdot \vec{v}_{rel}$ becomes positive. This would mean the debris has passed the laser and any delivered thrust will only increase the lifetime of the debris object. The second condition that will stop the interaction will be determined by the angular rate of the laser satellite. As the laser system tracks the object, at some point the telescope will have to rotate too fast to keep up with the passing debris. The scenario is shown in Figure 5.5. The transversal velocity v_{trans} is defined as the velocity component that is perpendicular to the relative position vector of the debris with respect to the laser. The magnitude of v_{trans} will determine how fast the laser has to rotate to keep its laser beam focused on the target. To get an expression for this angular rate ω in terms of v_{trans} , the angle β is first calculated using the inner product of the relative position vector and the relative velocity vector.

$$\beta = \arccos\left(\frac{\vec{d}_{rel} \cdot \vec{v}_{rel}}{|\vec{d}_{rel}| \cdot |\vec{v}_{rel}|}\right) \quad (5.2)$$

The transversal velocity component is then computed using this angle.

$$v_{trans} = v_{rel} \cdot \sin(\beta) \quad (5.3)$$

The angular rate, expressed in radians, then takes the following form.

$$\omega = \frac{v_{trans}}{L_{rel}} = \frac{v_{rel} \cdot \sin(\beta)}{L_{rel}} \quad (5.4)$$

The state-of-the-art of rotation steering wheels puts a limit on the angular rate in Equation 5.4 of $\omega_{lim} = 2.0^\circ/s = 3.49 \cdot 10^{-2}$ rad/s [10].

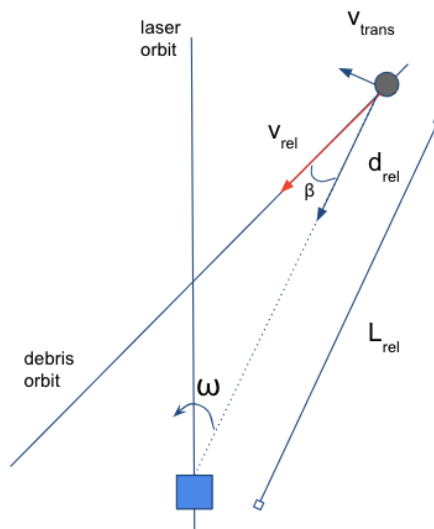


Figure 5.5: Schematic of an interaction between laser and debris. The transverse velocity v_{trans} will determine how fast the laser has to rotate.

With the angular rate limit known, the distance where this threshold is passed can be computed for different geometries, see Figure 5.6. Here, Δr is defined as the difference in altitude between the laser and the debris object in km and the azimuth angle $\Delta\phi$ is defined as the angle at which the laser targets the debris object. In the interaction with $\phi = 0^\circ$ and $\Delta r = 0$ km the laser and debris encounter each other 'head-on'.

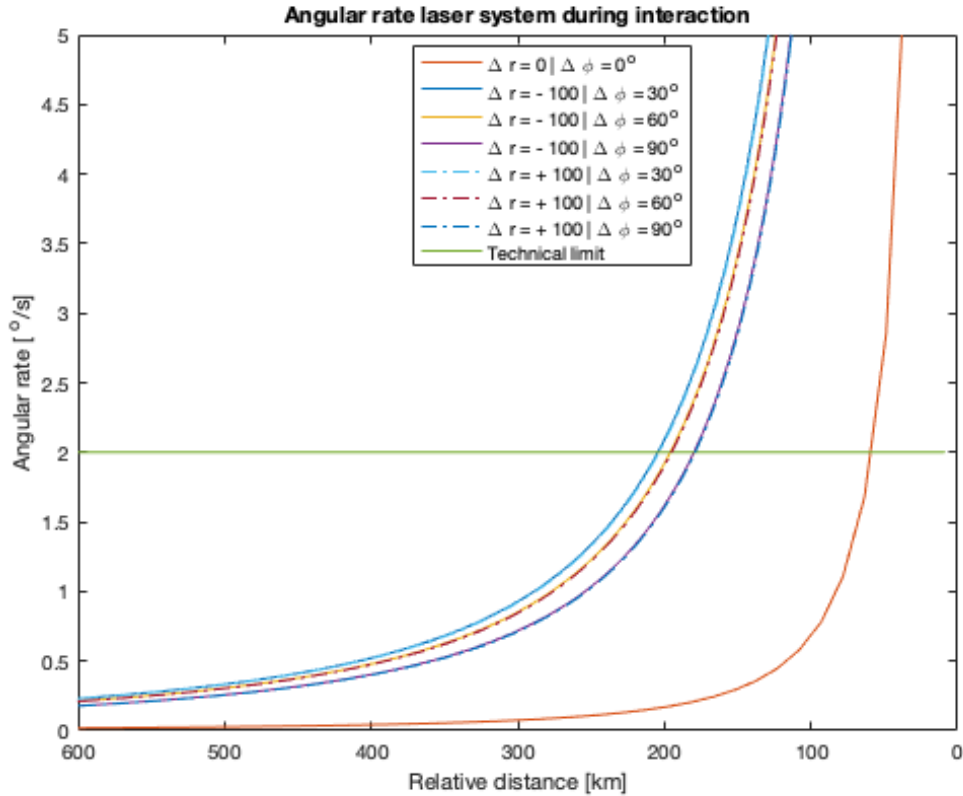


Figure 5.6: Distance where the angular rate limit is passed for different geometries.

The angular rate during the interaction of six possible geometries are plotted, as well as the technical limit (green line). The presented azimuth angles of the interaction are the angles between where the orbits meet, not the angle at which the debris is detected. First, it is noted that the termination occurs at greater relative distance for geometries with lower azimuth angle. The more 'head-on' the interaction is, the earlier the debris will become untrackable. The altitude of the debris object that is targeted does not seem to make a difference to the termination distance. The $\Delta\phi = 30^\circ$ interactions are stopped at $L_{term} = 204$ km, the $\Delta\phi = 60^\circ$ at $L_{term} = 198$ km and the $\Delta\phi = 90^\circ$ at $L_{term} = 178$ km. This can be explained by noting that debris objects that are encountered at larger azimuth angle have lower relative velocities than objects encountered at lower azimuth, which also results in a lower transversal velocity. Equation 5.4 shows that the lower the transversal velocity, the lower the relative distance at which the angular rate limit is exceeded.

Whenever one of the termination conditions is satisfied, the propagation of the interaction is stopped. The results are printed so that the effects of ablation can be compared for different interactions. See flowchart of the complete program below (Figure 5.7).

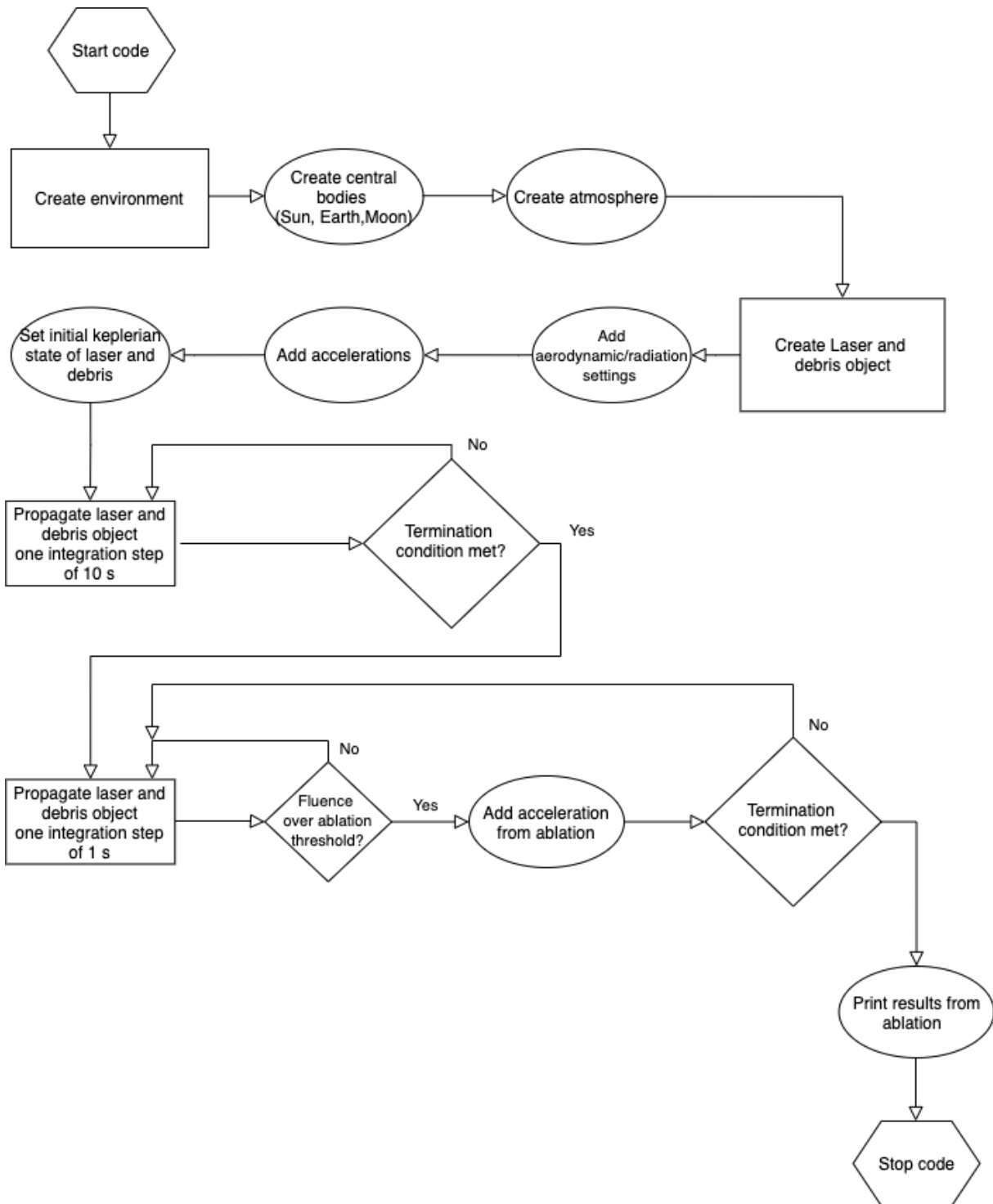


Figure 5.7: Flowchart for interaction of laser with one debris object.

5.2. Coplanar interactions

The coplanar interactions will first be discussed as it covers the most straightforward physics. Coplanar orbits lie in the same orbital plane, meaning that the azimuth angle between the orbits $\Delta\phi$ is 0° . The examples that will be discussed are the head-on interaction where the debris object is also orbiting at the same altitude as the laser, and the interactions where there is an altitude difference between the two objects. The initial state of the laser is given in Table 5.2 and the initial state of the debris in Table 5.3 with inclination $i = 82^\circ$. The results of the orbit propagation up to the point of detection are shown in Figure 5.8. In this illustration, the debris object and laser both start at true anomaly $\nu = 180^\circ$ instead of $\nu = 340^\circ$ to show the orbits. They encounter each other after half a revolution at $z = 0$ km, verifying that they indeed meet at the equator.

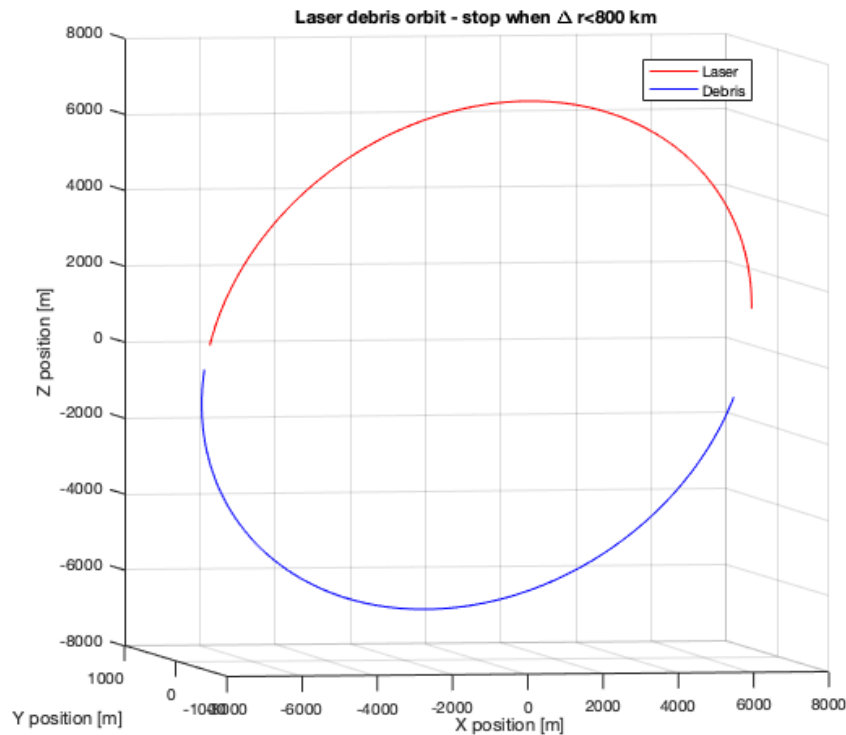


Figure 5.8: Propagation of laser and debris orbit up to the encounter. Both objects start at the right part of the illustration.

At the point of the encounter, the second propagation is initiated. The results for the ablation of three objects are plotted below, see Figure 5.9. The interactions start at a relative distance of around 700 km from the laser. This is because the large stepsize propagation is stopped at the first timestep where the termination condition is met. When the laser fluence exceeds the ablation threshold at about 500 km distance, the deceleration of the debris object will start.

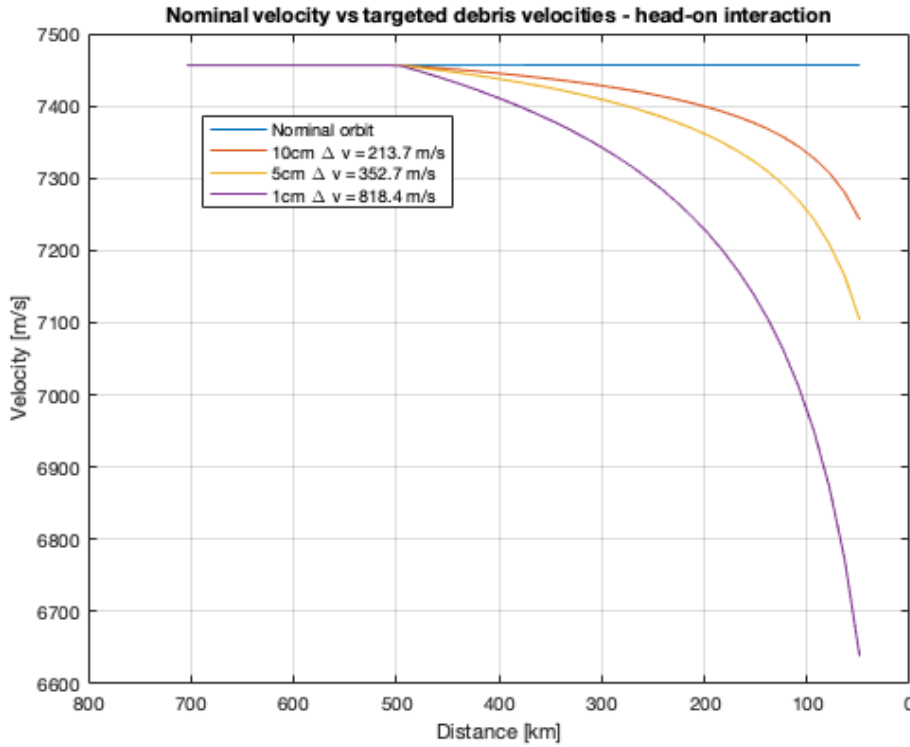


Figure 5.9: Δv from ablation in head-on interaction on 1 cm, 5 cm and 10 cm objects.

The laser system is able to produce a high velocity change of $\Delta v = 213.7$ m/s, even on the 10 cm object that has the lowest AMR. The velocity of the 1 cm object is even slowed down by a total of $\Delta v = 818.4$ m/s. The required Δv to de-orbit debris objects in LEO was plotted in Figure 4.2 in Section 4.1 and showed that an object at 800 km altitude only requires $\Delta v = 170$ m/s to be de-orbited within half a revolution. This means that the laser is able to instantly de-orbit any debris object if it is encountered in an exact head-on geometry. Although these results look very promising, they do not completely represent values that will be achieved in a random encounter since the precise head-on interaction has a slim chance of occurring. This is verified by Figure 5.10, that shows the flux of impact angles of debris objects onto a spacecraft that orbits in SSO with $i = 98.6^\circ$ and $h = 789$ km, which is comparable to the laser orbit. Debris objects from different sources are taken into account, such as explosions (EXPL), collisions (COLL) and Solid Rocket Motor Slag (SRMS). Impact azimuth angles between $\phi = -30^\circ$ and $\phi = 30^\circ$ occur most frequently, but fewer impacts are head-on interaction. The impact angle and the altitude both affect the distance where the angular rate limit is exceeded and where the propagation is terminated. The head-on interaction reaches this limit close to the laser as was shown in Figure 5.5. This means much higher Δv 's are achieved because the fluence is much higher closer to the laser. Moreover, the results from the head-on interaction show that if a substantial Δv is produced on the 10 cm object, the same geometry will return an even higher Δv for the 1 cm object. Keeping this in mind, the next geometry examples will only test whether the laser produces successful results on the 10 cm object.

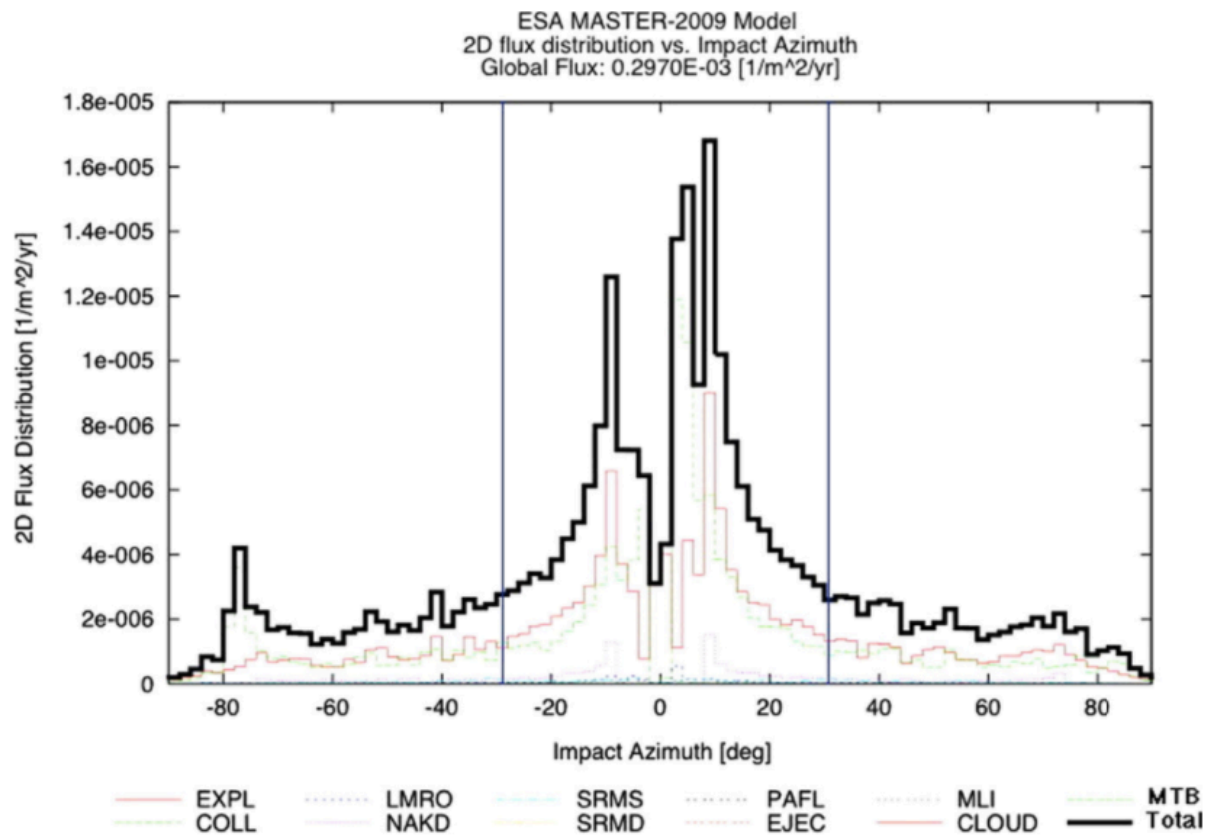


Figure 5.10: The impact azimuth of debris objects for a spacecraft in SSO with $i = 98.6^\circ$ and $h = 789$ km [10].

Different altitude

The region where the majority of the debris in LEO resides is between 600 and 1 000 km. Since the laser system is placed at an altitude of 800 km, it will be important to test the performance of the laser on debris objects that are orbiting at higher or lower altitudes. A geometry where the debris objects orbit at a different altitude than the laser system will produce a radial Δv_r , as well as a tangential Δv_θ . Figure 5.11 shows the acceleration components of the laser in the radial, normal and along-track (tangential) direction during a coplanar interaction where the debris object orbits 100 km above the laser. When the ablation threshold is exceeded at around 500 km, the accelerations on the debris object start to increase. The cross-component of the acceleration is zero during the interaction, which is expected in a scenario where $\phi = 0^\circ$. The radial component increases rapidly near the end of the interaction and reaches a maximum at the point where the laser targets the object exactly from below at a distance of 100 km. The tangential component increases up to a distance of around 130 km after which it decreases rapidly as the object is almost above the laser.

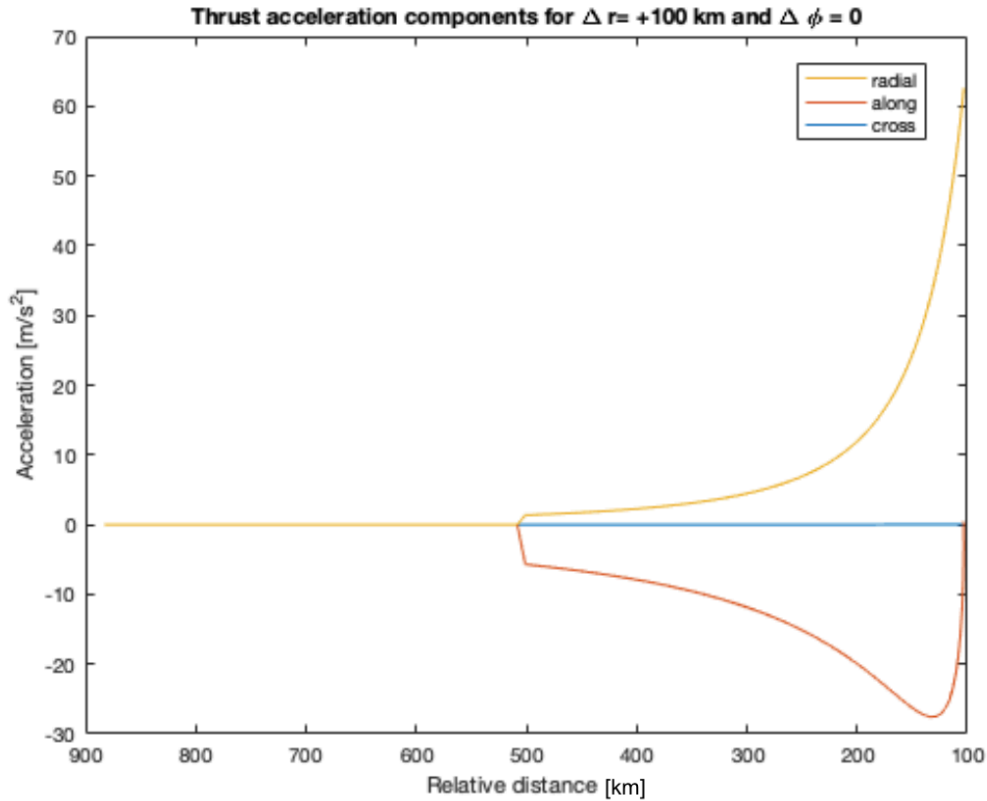


Figure 5.11: Acceleration components during a coplanar interaction.

After a relative distance of 100 km, the object will have passed the laser and the propagation is stopped. In reality the propagation will be stopped even sooner because the angular rate limit will be violated. As briefly mentioned in Section 4.2, the acceleration in the tangential direction mostly determines the reduction of the lifetime of the targeted debris object. The effect of the radial component depends on the specific geometry of the interaction. Up to a distance of around 150 km, the tangential component dominates the radial component in magnitude.

Figure 5.12 shows the results of the laser interaction with a 10 cm debris object from 6 different coplanar geometries. The performance is tested for a debris object orbiting at 1 000, 900, 850, 750, 700 and 600 km. All interactions start at the first integration step where the large stepsize propagation was terminated, which is different for each geometry. This difference in the start time of the interaction does not influence the results since ablation effects are only added from a distance of 500 km from the laser. All debris objects have different orbital velocities due to their different orbital altitude. The results show that debris objects at higher or lower altitudes get decelerated much less than debris objects at the same altitude as the laser, which was expected. Debris objects at 50 km higher and 50 km lower than the laser still get a $\Delta v = 92.3$ m/s and $\Delta v = 93.5$ m/s respectively, which is a factor of ~ 2 less than for the head-on interaction in Figure 5.9.

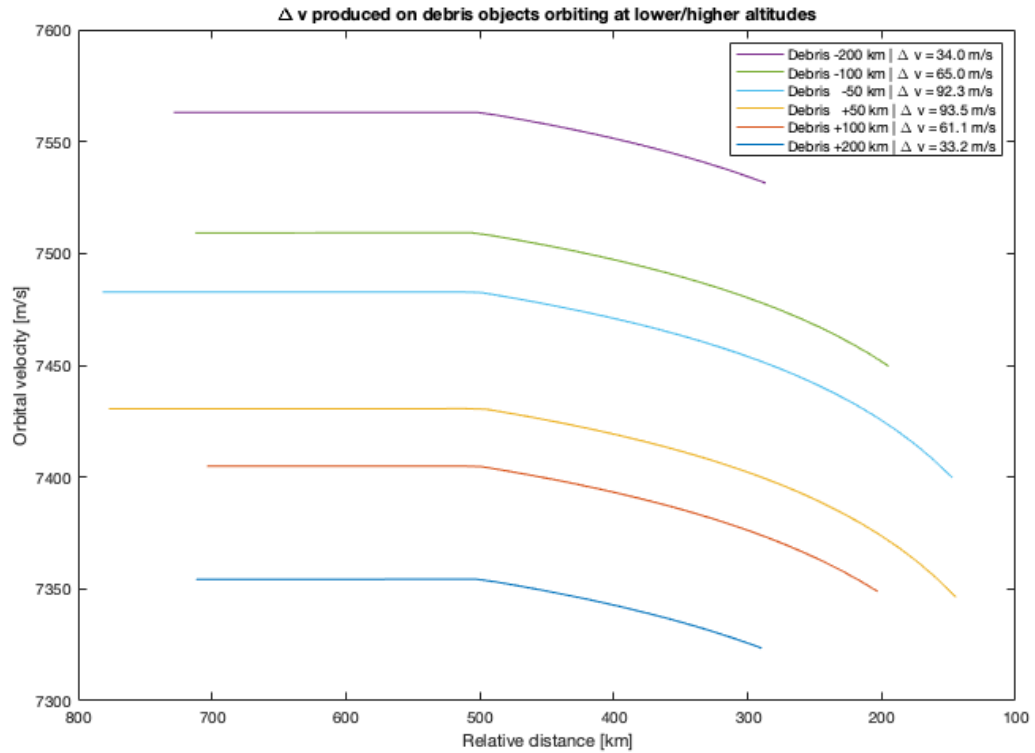


Figure 5.12: Generated velocity change on debris objects orbiting at higher/lower altitudes with $\phi = 0^\circ$.

The slight difference in outcome between the Δv 's from higher and lower altitudes is explained by a difference in termination timestep. Just like the termination of the large stepsize propagation, the propagation of the interaction is stopped at the first timestep where the termination condition is met, which can differ a maximum of one second per interaction. The Δv on debris objects 100 km higher or lower get decelerated a factor ~ 3 less than the head-on interaction and debris objects at 200 km altitude difference a factor ~ 7 . This difference arises from a combination of a shorter interaction time and a less optimal geometry for orbital velocity deceleration. To test whether the laser was successful, the produced decrease in lifetime is compared (Table 5.4).

Table 5.4: Lifetime of 10 cm debris object before and after laser interaction.

Debris altitude [km]	Δv [m/s]	Lifetime before int [yrs]	Lifetime after int [yrs]
600	34.0	3.3	1.4
700	65.0	11.3	1.5
750	92.3	20.7	0.9
850	93.5	69.7	2.8
900	61.1	127.8	17.7
1 000	33.2	429.7	163.5

For every altitude except for 1 000 km, the orbital lifetime of the 10 cm object is lowered below the 25 year guideline. The natural lifetime of the debris fragments in orbits up to 750 km will naturally adhere to the 25 year guideline. This does not imply that the targeting of these objects is unnecessary. On the contrary, any lifetime decrease of a debris fragment should be seen as a form of success. The lower the amount of time a fragment orbits in LEO, the lower the probability of it colliding with an active spacecraft. The same can be said for the 10 cm object at 1 000 km. Its natural lifetime is 429.7 years, which is brought back to 163.5 years after the interaction. Although this interaction would not be classified as successful, this particular object could still be targeted a second time by the laser after which the lifetime could very well be brought below 25 years.

5.3. Non-coplanar interactions

The next set of geometries that will have to be discussed are the non-coplanar interactions, typically defined by a situation where the laser has a non-zero azimuth angle ϕ with respect to the debris. This section will first discuss the technical limits regarding the interaction azimuth angle to find out for what angles the system could not function. Then the results will be shown of the non-zero azimuth interactions where the debris objects orbit at the same altitude as the laser. Next, the effects of both azimuth angle and altitude difference will be taken into account. The latter will give an accurate representation of the abilities of the laser system.

Azimuth angle limit

The laser will not be able to target debris from any given azimuth angle due to the limits of the Field-Of-View (FOV) of the telescope. Figure 5.13 shows a schematic of an encounter with a debris object. The FOV of the laser determines the cone in which objects can be detected and thus determines the maximally allowed azimuth angle. Assuming that the debris would impact the laser exactly at point O , the FOV relates to ϕ_{impact} as follows:

$$180^\circ - \phi_{\text{impact}} = 180^\circ - 2 \cdot \phi_{\text{detect}} \quad (5.5)$$

$$\phi_{\text{detect}} = \frac{\phi_{\text{impact}}}{2} \quad (5.6)$$

$$\text{FOV} = 2 \cdot \phi_{\text{detect}} = \phi_{\text{impact}} \quad (5.7)$$

This relation implies that to target a debris object with azimuth angle $\phi_{\text{impact}} = 90^\circ$, a telescope is required with a $\text{FOV} = 90^\circ$. However, the technical state-of-the-art for a telescope lies at $\text{FOV}_{\text{limit}} = 60^\circ$, resulting in a maximally allowed azimuth angle of $\phi_{\text{max}} = 60^\circ$ [10]. Figure 5.10 showed that the majority of debris objects have an impact azimuth between $-30^\circ < \phi < 30^\circ$, so the $\text{FOV}_{\text{limit}}$ will not negatively affect the laser performance.

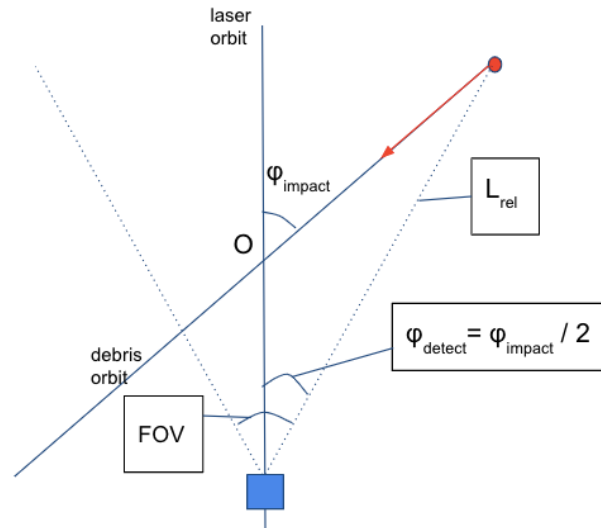


Figure 5.13: Debris detection in Field-of-View of telescope.

Different azimuth angle at same altitude

The interactions with debris objects impacting from an angle will induce a normal Δv_n next to a tangential Δv_θ . As discussed in Section 4.2, this normal component will not affect the lifetime of the debris object. Figure 5.14 shows the propagation of six different geometries up until the encounter of the debris objects. The debris orbits that are plotted have azimuth angles $\phi = 10^\circ, 20^\circ, 30^\circ, 40^\circ, 50^\circ, 60^\circ$ with respect to the laser orbit.

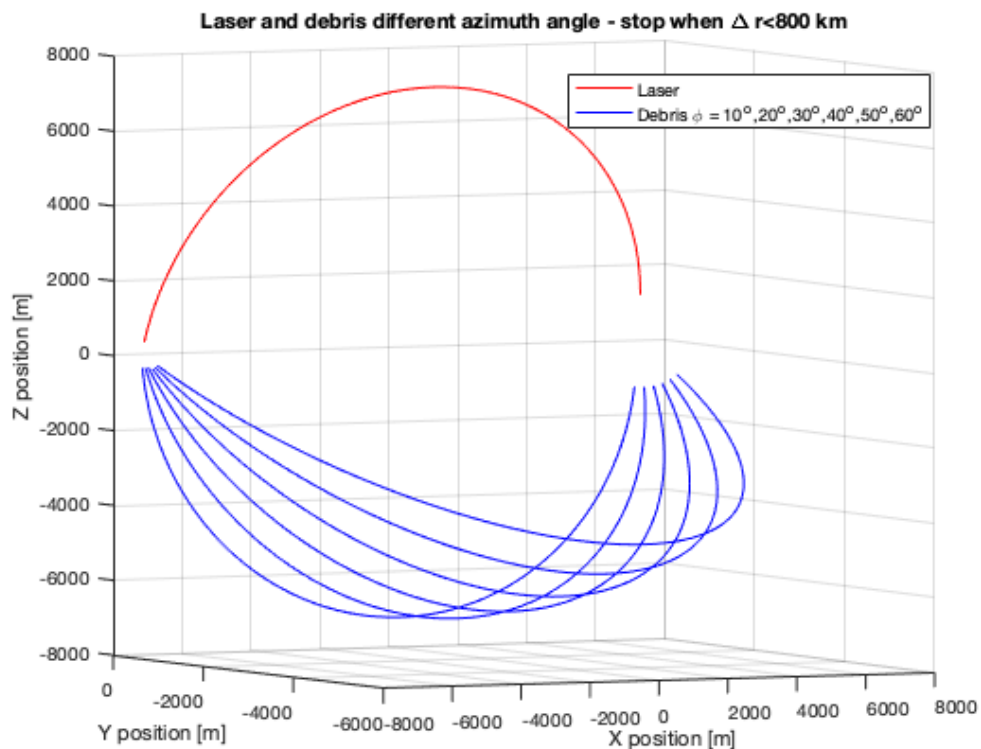


Figure 5.14: Laser and debris orbits with different azimuth angle up until encounter.

The generated Δv on the 10 cm debris objects with the laser system from all geometries are plotted in Figure 5.15. Interactions at an azimuth angle are less efficient than a head-on interaction due to two effects: a fraction of the imparted Δv will be in the normal direction that does not affect lifetime and the laser has to rotate faster to keep track of the debris which results in a faster termination of the interaction.

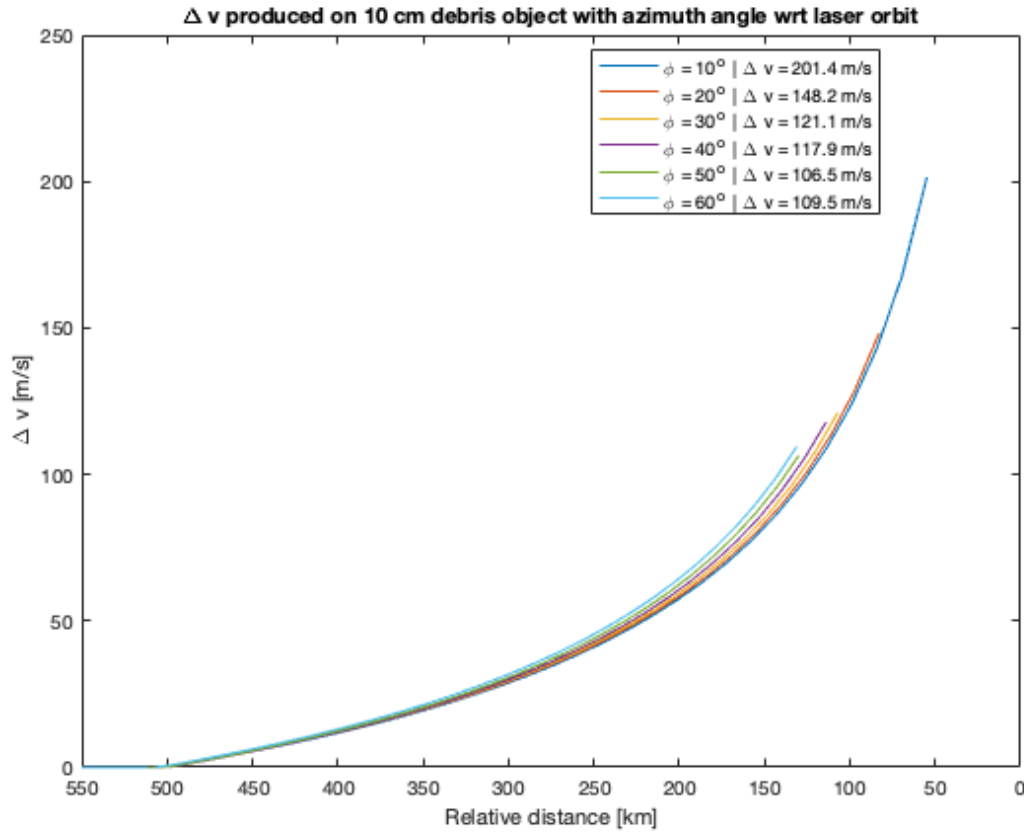


Figure 5.15: Generated Δv on debris object with azimuth angle ϕ w.r.t. laser orbit.

The debris object with $\phi = 10^\circ$ was decelerated a total of $\Delta v = 201.4$ m/s, which is only slightly lower than the Δv of the head-on interaction. At $\phi = 20^\circ$ the loss is already more significant, resulting in a $\Delta v = 148.2$ m/s. However, at azimuth angles higher than $\phi = 20^\circ$ something interesting happens: the Δv does not seem to drop as much as it did from $\phi = 10^\circ$ to $\phi = 20^\circ$. The generated Δv for $\phi = 60^\circ$ is even higher than the one for $\phi = 50^\circ$. This is explained by the fact that the relative velocity of the debris object with respect to the laser is lower for interactions with high azimuth angles. Lower relative velocities result in a longer interaction time which means the debris object gets targeted for a longer time. The relative velocities, interaction time and corresponding lifetime decrease of the 6 geometries are shown in Table 5.5.

Table 5.5: Relative velocities and resulting interaction time of geometries with different azimuth angles.

Azimuth [$^{\circ}$]	v_{rel} [km/s]	t_{int} [s]	Δv [m/s]	T_{life} before [yrs]	T_{life} after [yrs]
10	14.84	31	201.4	38	0.002
20	14.67	28	148.2	38	0.18
30	14.38	27	121.1	38	0.55
40	13.99	28	117.9	38	0.62
50	13.50	28	106.5	38	0.97
60	12.90	29	109.5	38	0.86

The longer interaction time of geometries at high azimuth angle compensate for the shorter interaction distance. The natural lifetime of a 10 cm object would be around 38 years at 800 km. The laser interaction lowers the lifetime of the objects below 1 year for all geometries and de-orbits the debris object with $\phi = 10^{\circ}$ within a day.

Different azimuth angle and altitude

The geometry that the laser will encounter most frequently while orbiting in LEO is where the laser targets a debris object orbiting at another altitude and at an azimuth angle. Laser ablation resulting from a geometry like this will be less efficient due to non-zero components in all three directions: a radial Δv_r , a tangential Δv_{θ} and a normal Δv_n . A schematic of such an interaction is presented in Figure 5.16.

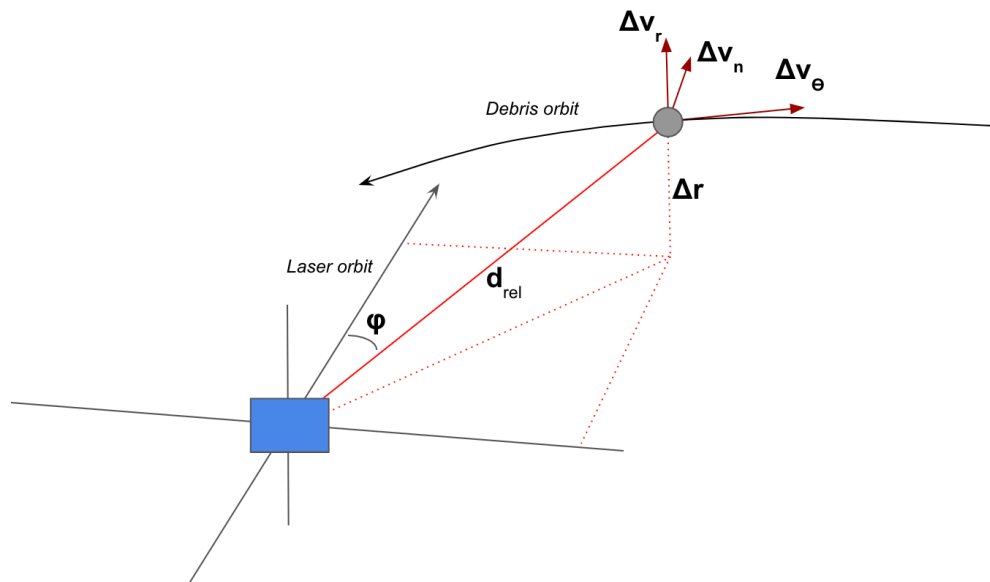


Figure 5.16: Schematic of non-coplanar interaction where debris experiences Δv in three directions. Before showing the results it will be insightful to check the evolution of the separate accel-

eration components during the interaction. Figure 5.17 shows the three components during a non-coplanar interaction where the debris object orbits 100 km above the laser and the azimuth angle is $\phi = 60^\circ$.

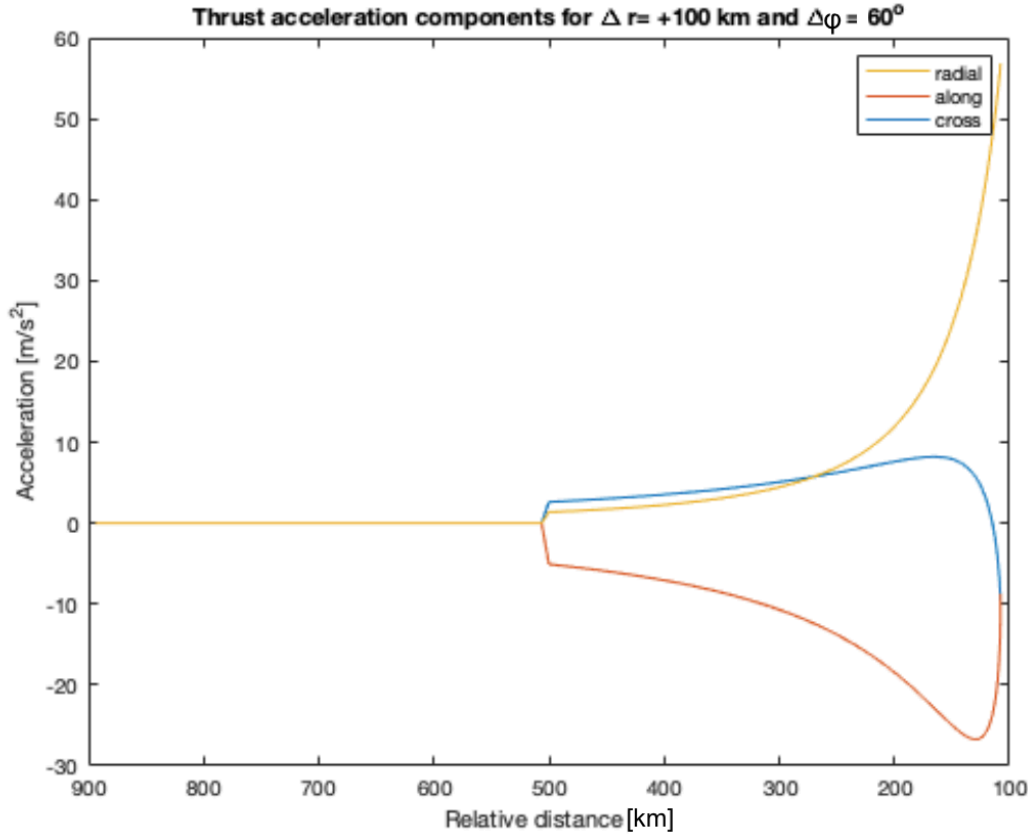


Figure 5.17: Acceleration components during non-coplanar interaction.

Figure 5.17 shows the accelerations up to a relative distance of 100 km, which is equal to the altitude difference. The radial component increases as the target gets more and more above the laser. Whereas the cross-component was zero in the coplanar geometry, the component increases for the $\phi = 60^\circ$ geometry which was expected. The cross-component reaches its maximum at around $L \sim 150$ km after which it decreases and even becomes negative while the tangential component is still negative. This means that the laser has traveled underneath the orbit of the debris object but is still producing a thrust in the anti-velocity direction. Shortly after this moment, the propagation is stopped as the dot-product of the relative position and velocity of the two objects becomes positive. Just as in the coplanar interaction, the propagation will already be stopped sooner due to the angular limit condition. Although the non-coplanar interaction is less efficient in achieving a high Δv , the relative velocities in these geometries are much lower than for a head-on interaction. The longer interaction time will compensate for some of the efficiency losses. The results for the non-coplanar interactions with altitude differences are shown in Figure 5.18.

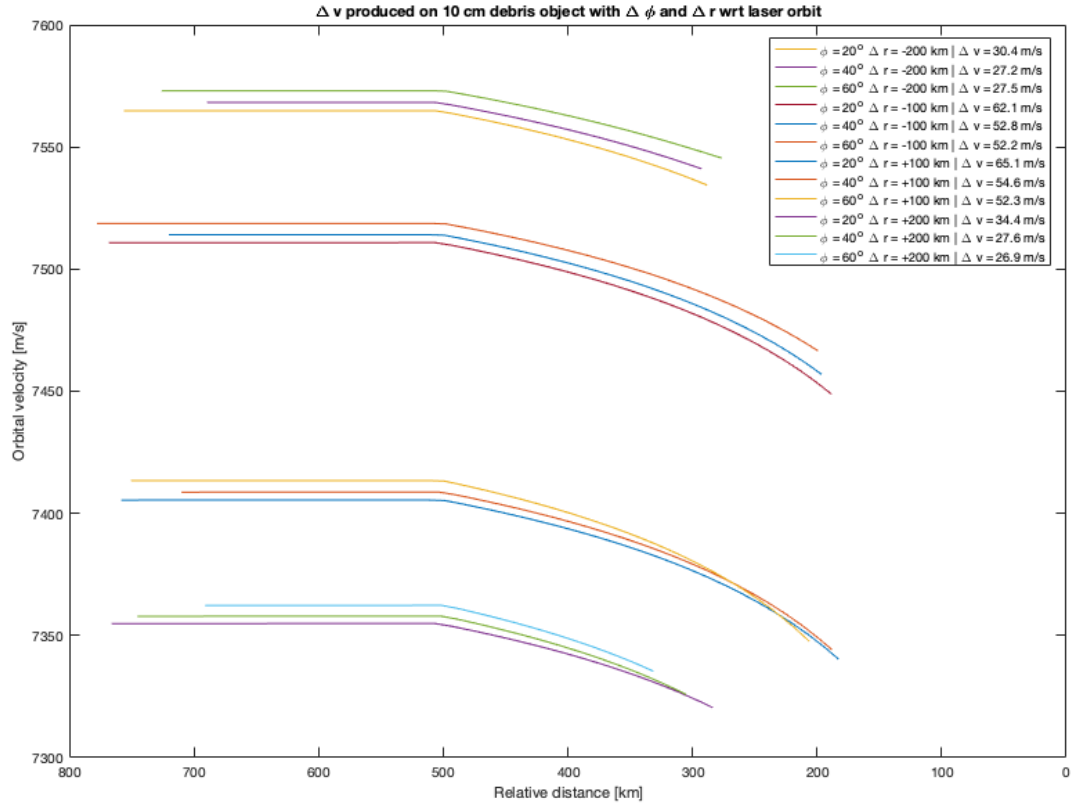


Figure 5.18: Orbital velocity change due laser ablation on 12 different non-coplanar geometries.

The laser was tested on debris objects at altitudes $h = \{600 \text{ km}, 700 \text{ km}, 900 \text{ km}, 1000 \text{ km}\}$ and for impact azimuth angles $\phi = \{20^\circ, 40^\circ, 60^\circ\}$. Important to note for these geometries is that the probability of having a full interaction time is slim in comparison to a head-on interaction. This means that the initial true anomaly of the debris and the laser in the head-on geometry is less deterministic for the interaction: the two objects will encounter each other anyway somewhere along the orbit. However, for the non-coplanar geometries, the initial true anomalies should be set in a very specific manner for an encounter to take place, let alone an encounter with optimal interaction time. The debris objects at $\Delta r = \pm 200 \text{ km}$ were given an initial true anomaly difference of $\Delta \nu = \pm 4^\circ$ and the objects at $\Delta r = \pm 100 \text{ km}$ were given a difference of $\Delta \nu = 2^\circ$ w.r.t. the laser, after which the encounter took place half an orbit later.

The propagation of the interactions are stopped at around $L = 200 \text{ km}$ for the objects at $\Delta r = \pm 100 \text{ km}$ and at around $L = 300 \text{ km}$ for the objects at $\Delta r = \pm 200 \text{ km}$ due to exceeding the angular rate limit of the laser system. At these relative distances, Figure 5.17 shows that the tangential component of the acceleration is the main contributor of the deceleration. The corresponding decrease in lifetime of the interactions is shown in Table 5.6. The results show that the lifetime of objects up to 900 km get lowered to below 25 years. At altitudes 600 km and 1 000 km a velocity change of about 30 m/s is achieved for all objects. For the objects at 600 km this is sufficient since the lifetime of the objects was already quite low, but the objects at 1000 km only get their lifetime halved and still take longer than 25 years to spiral into the atmosphere. Although the lifetime reduction is significant, the objects will have to be targeted a second time. Furthermore it can be noted that geometries with azimuth $\phi = 40^\circ$ perform worse than with azimuth $\phi = 20^\circ$, which was expected. However, the results from

geometries at $\phi = 60^\circ$ are similar to the geometries with $\phi = 40^\circ$. This is due to the lower relative velocities at higher azimuth.

Table 5.6: Results from non-coplanar interactions with altitude difference.

Altitude [km]	Azimuth [$^\circ$]	Δv [m/s]	T_{life} before [yrs]	T_{life} after [yrs]
600	20	30.4	3.36	1.38
600	40	27.2	3.36	1.75
600	60	27.5	3.36	1.73
700	20	62.1	11.28	1.69
700	40	52.8	11.28	2.36
700	60	52.2	11.28	2.41
900	20	65.1	127.79	15.1
900	40	54.6	127.79	22.69
900	60	52.3	127.79	24.75
1 000	20	34.4	429.74	156.47
1 000	40	27.6	429.74	200.56
1 000	60	26.9	429.74	205.66

This chapter has presented the range of geometries from which the lifetime of LEO debris objects can get substantially lowered. The most important result is that the laser can still cause significant effects to debris fragments that orbit 200 km higher or lower. Even if some interactions did not lower the lifetime below 25 years within one interaction, a second interaction will most likely achieve the desired result. Next to that, the results that were presented were for a 10 cm object, which will only be a fraction of the complete debris population. Since lifetime is inversely proportional to the AMR, the interactions on debris objects with higher AMR will result in even lower lifetimes. It is therefore concluded that objects at 1 000 km should certainly be included in the debris population.

6

Laser simulation with debris population

Now that the laser parameters have been carefully chosen and the performance on individual debris particles for all possible geometries has been shown, the laser can be tested on a larger debris population. This chapter will first show the methodology of the simulation, which is largely similar to the one presented in the previous chapter but contains some small adaptations. Next, the characteristics of the randomly generated debris distribution are presented. Finally the results of the laser simulation on the debris population are given.

6.1. Methodology

The flowchart for the simulation with multiple consecutive debris interactions is shown in Figure 6.2. Only the adaptations to the code will be explained in this section, as the choices for integration method and propagation technique are the same as for the simulation with a single debris object and will not be discussed again. In summary, the program starts by creating the central bodies, the laser object and a large number of different debris objects each with randomly generated characteristics. Then the laser and all the debris objects are propagated until a certain termination condition is met. This termination condition will consist of more verification tests than was the case for the single debris object interaction since the laser will now encounter multiple objects and has to choose a good candidate for ablation. During the ablation process, only the laser and the debris candidate are propagated using a small stepsize integration after which the rest of the debris population is propagated using a larger stepsize still, to reduce computation time. This second propagation is likely to overshoot the final timestep at which the ablation interaction of the debris object was terminated, so the targeted debris is then propagated to the timestep of the rest of the population. At this point, all objects should be at the same timestep. Again, a last propagation of the laser and the complete debris population is executed which will act as the period in real-life in which the laser would cool down from the interaction and steer the telescope back to the default orientation. The simulation will continue to run until the final simulation time has been reached. The summary above states that one interaction loop contains 5 different propagations. These will be discussed in detail below.

6.1.1. Creating the debris population

The debris population should be a good representation of the distribution of the true debris fragments in LEO that the laser would target. The program loops over the creation of a single debris body until the desired number of fragments is reached. To create a diverse debris population, the orbital parameters of the debris particles will be assigned a randomly chosen value (Table 6.1). First, a random diameter of the debris object is generated between 1 and 10 cm. From this, the debris cross-sectional area is calculated. Next, a random AMR is generated corresponding to the values presented in Table 6.1. From the generated area and AMR, the mass of the debris object is calculated. The same radiation coefficient $C_r = 1.1$ and aerodynamic coefficient $C_d = 2.2$ is assigned to every debris object. With these values, the aerodynamic and radiation settings can be constructed.

Table 6.1: Range of debris parameters that will make up the debris test population.

Parameter	Lower limit	Upper limit
Diameter [m]	0.01	0.1
AMR [m ² /kg]	0.04	0.16
Altitude [km]	600	1 000
Inclination [°]	70	110
RAAN [°]	0	360
True anomaly [°]	0	360

The eccentricity is not chosen randomly but set to $e = 0.000001$, which will result in a near-circular orbit. The initial argument of periapsis is set to a value of $\omega = 0^\circ$. Initializing the debris population as near-circular orbits is justified for two reasons. First of all, most of the debris objects in LEO have near-circular orbits and second of all the orbits will become elliptical once the debris objects are targeted by the laser [29]. In this way, the laser performance is naturally tested on elliptical orbits as it encounters debris objects a second time. Next, the accelerations that the debris object will experience throughout its orbit are added, which are the same as in Section 5.1.1. Then the initial state of the debris object is constructed by generating random values for the orbital parameters within the limits of Table 6.1. Every random generation of a value assumes a constant distribution function, making sure that every value has an equal probability of arising. The random generator requires the input of a seed number. For a constant seed number, the generator will return the same value every time. For the creation of each debris object, a seed number is used equal to the number of that object. In this way, the generated parameters of a specific debris object can always be retrieved after the propagation.

6.1.2. Propagating the laser and the debris population

When the debris population has been created, the propagation follows the same mechanics as that for a single debris interaction. The integration method is RK4 and the stepsize is set at $t_{step} = 10$ s. An example of a propagation of the laser system and 5 debris objects is shown in Figure 6.1.

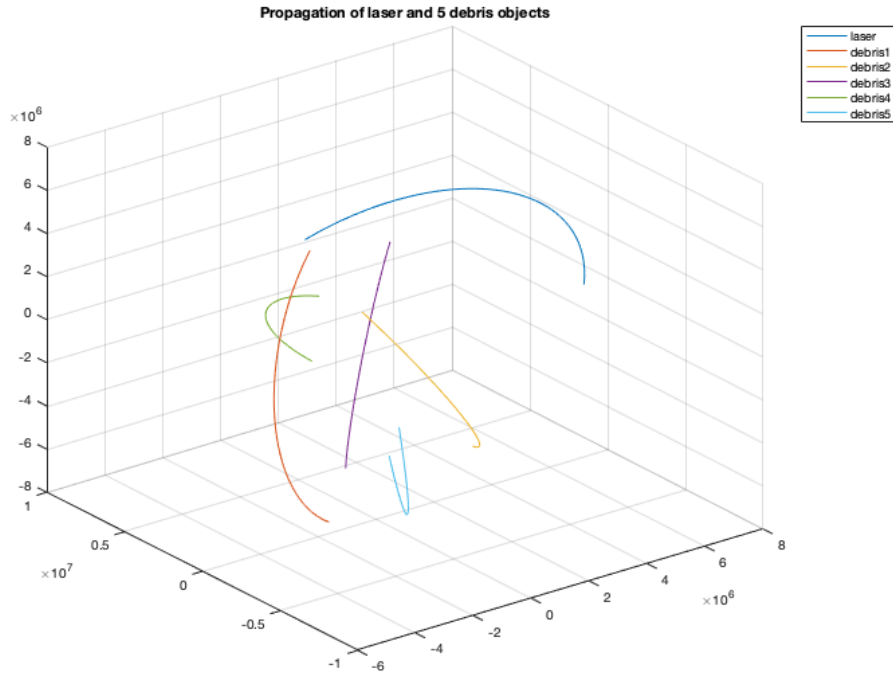


Figure 6.1: Orbits of laser and debris objects.

Termination condition

The laser orbit in Figure 6.1 is depicted in the blue line. At every timestep all orbits are propagated 10 seconds ahead in time until the termination conditions are violated. In this scenario, the propagation was stopped when the laser came within 800 km of 'debris1'. However, contrary to the simulation with 1 single debris object, the termination condition for the debris population should go through some more tests to verify that the interaction with the object will result in a Δv in the right direction. The candidate debris object will have to satisfy the following demands before an interaction is started:

- $L_{rel} < 800$ km. The relative distance of the debris and the laser should be below 800 km for the target to be detected.
- $L_{rel} > 300$ km. The laser interaction with the debris object gets terminated at a certain distance to the laser due to exceeding the angular rate limit. If a debris is detected within 300 km, the interaction will immediately be terminated which makes it a bad candidate.
- $|\phi_{encounter}| < 30^\circ$. As explained in Section 5.3, the FOV of the laser system will maximally allow an azimuth angle at the encounter of $\pm 30^\circ$. This condition also ensures that only objects that are in front of the laser are targeted.
- $d_{rel} \cdot v_{rel} < 0$. Even when a debris is detected between 300 and 800 km and within the required azimuth range, the debris can still move away from the laser making the geometry not suitable for decreasing the velocity. The dot-product of the relative position and the relative velocity ensures that the debris object moves towards the laser as was explained in more detail in Section 5.1.1.

Only if a debris object meets all four termination conditions, the propagation of the laser and the debris population will be stopped and the second propagation will be started to simulate the ablation process.

6.1.3. Propagating the interaction of the laser and debris target

When the right debris object has been selected, the interaction of the laser is simulated. It would be redundant and ask too much computation time to propagate the complete debris population with a stepsize of 1 s, so the initial state of the propagation is only made up of the state of the laser and the target debris at the timestep where the previous propagation was terminated. Now the scenario is the same as that of the laser interaction with a single debris object as described in Section 5.1.3. The ablation acceleration is added to the target debris dynamics when the fluence threshold is exceeded. One extra termination condition is added to ensure that the velocity of the debris does not get increased:

$$\vec{v}_{orb,debris} \cdot \hat{F}_{thrust} < 0 \quad (6.1)$$

By demanding that the direction of the velocity of the debris object should never point in the same direction as the direction of the thrust vector, the propagation is terminated immediately when the velocity gets increased. This termination condition is necessary since the geometry of the interaction can still change between the detection point and the ablation start point. Since the interactions with individual debris objects described in Chapter 5 were initialised in such a way that the geometry remained mostly the same between detection and ablation, this demand was not necessary and was not included.

Propagating all objects to the same timestep and implement cool-down time

Now that the candidate debris has been targeted and its lifetime has hopefully been decreased substantially, the rest of the debris population should get propagated to the same timestep as the targeted object. This propagation is performed using a larger stepsize of $t_{step} = 10$ s. The initial state is given by the final state of every debris object at the end of the first propagation, before the laser interaction began. As is shown in Figure 6.2, the debris population gets propagated 10 seconds in time up to the integration step where $t_{objects} > t_{debris}$. At this point the debris population is propagated to a timestep no further than 10 seconds beyond the targeted debris object. Now the debris object is propagated with a 1 second stepsize until the point where $t_{debris} = t_{objects}$ so that all objects are found at the same timestep again. After replacing the state of the targeted debris with the corresponding debris state in the population, the system state now contains the correct state of every object at the same time. Before starting the loop again and letting the laser scan a new target, a final propagation is implemented with the final system state as initial state. The complete population will be propagated for a total duration time of $t_{cool-down} = 120$ s. A stepsize of $t_{step} = 20$ s for this propagation is used to reduce computation time, which is still validated knowing that a larger stepsize will only result in large errors at long time scales. This period of time is implemented to make the results more realistic. In real life, the laser can not target another object immediately after an interaction is finished. In the cool-down period the attitude control subsystem will point the laser back to its default orientation and the laser will cool-down from the most recent interaction. When the cool-down time is reached the propagation of the complete population starts again, with 10 s stepsize initially. This will happen until the simulation arrives at the simulation end epoch.

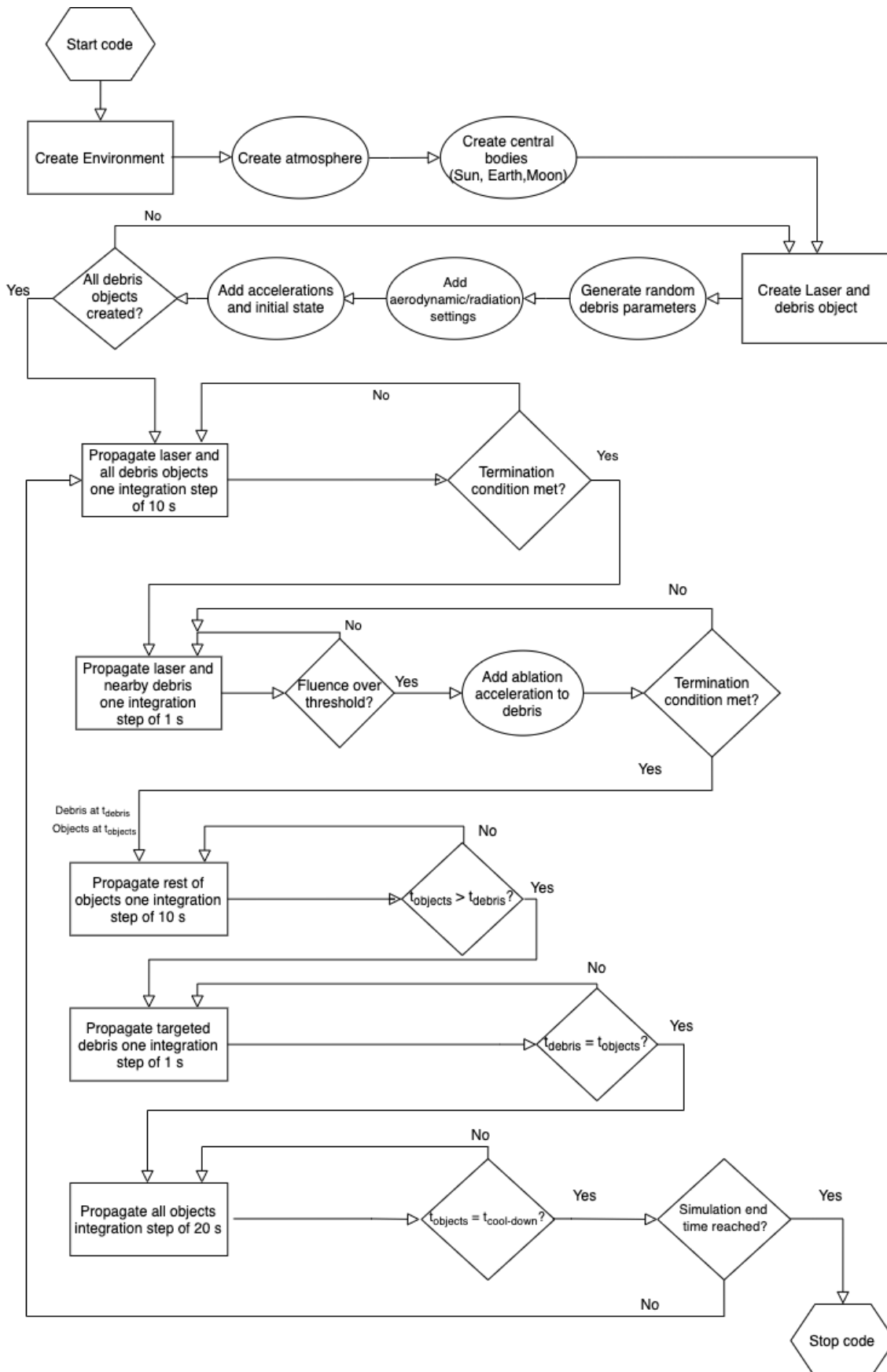


Figure 6.2: Flowchart of laser simulation with debris population.

6.2. Debris population distribution

In Chapter 3 it was stated that an estimated 900 000 debris objects greater than 1 cm are orbiting in space, of which 500 000 in LEO. The most realistic test for the laser performance would have been to run a simulation on a population with this size, but propagating 500 000 objects simultaneously would have taken too much computation time clearly. Rather, the performance of the laser on a much smaller dummy population of 5 000 objects was simulated for a period of 3 weeks, which already took 7 days of computation time. The results of the total decrease of lifetime will be presented after different points in time to check the evolution of the laser performance. After every interaction, the program saves the results and stores them in a map. An example of the parameters that are saved is given in Table 6.2.

Table 6.2: Example of results of simulation

N_{int}	N_{deb}	t	t_{int}	h_{peri}	h_{apo}	i	Δv	AMR	ϕ	T_1	T_2
		[s]	[s]	[km]	[km]	[$^\circ$]	[m/s]	[m ² /kg]	[$^\circ$]	[yr]	[yr]
1	326	10	38	941.06	942.06	88.89	118.31	0.13	18.98	59.25	1.27
2	881	170	33	828.6	829.4	81.46	27.12	0.048	14.26	44.46	22.51
...
100	998	37630	32	635.57	909.14	96.04	27.15	0.093	23.88	5.27	1.93

The first interaction is with debris object '326' occurs after 10 seconds and lasts for 38 seconds. The debris object initially orbits at 942 km altitude and has a 88.89° orbital inclination, an AMR of $0.13 \text{ m}^2/\text{kg}$ and is encountered at an azimuth angle of $\phi = 18.98^\circ$. The total imparted $\Delta v = 118.31 \text{ m/s}$ causes the lifetime of the object to be lowered from 59 years to only 1.27 years, which makes this interaction quite successful. Parameters like inclination, AMR and encounter azimuth are stored to know how the laser operates for different geometries. The perigee and apogee are both saved to check when an object orbits in an elliptical orbit such as for debris '998' at interaction 100. This means that this object has been targeted before and was brought from a near-circular orbit to the listed elliptical one. Before analyzing the results it will be insightful to show the distribution of the debris objects in the dummy population of 5 000 objects.

Parameter distribution

The apogee, AMR, inclination and RAAN are generated randomly following a uniform distribution function (Table 6.1); so all values should occur with equal probability. Figures 6.3 - 6.6 show the parameter distribution of the 5 000 objects in the population. Earth's radius is subtracted from the apogee to get the apogee altitude for ease of interpretation. The apogee altitude of all objects lies between 600 and 1000 km. Figure 6.4 shows the distribution of the AMR of the population, which follows a uniform distribution with values between $0.04 < \text{AMR} < 0.16$. Finally, the inclinations and the RAAN of the orbits are shown in Figure 6.5 and Figure 6.6. Since all randomly generated values are uniformly distributed and satisfy the boundaries given in Table 6.1, the dummy population is successfully generated.

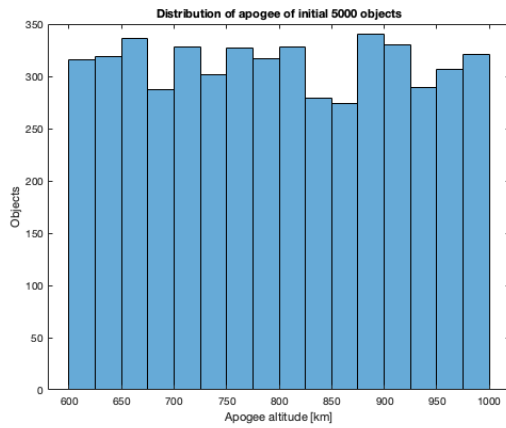


Figure 6.3: Distribution of apogee of population.

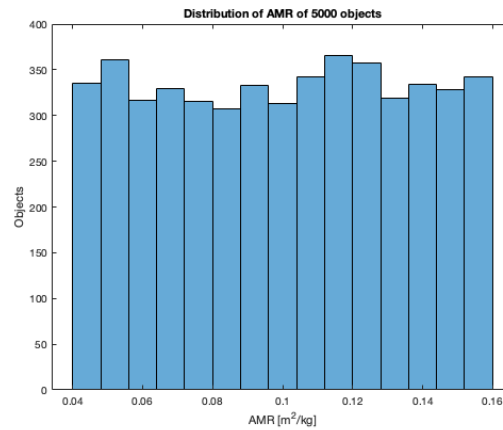


Figure 6.4: Distribution of AMR of population.

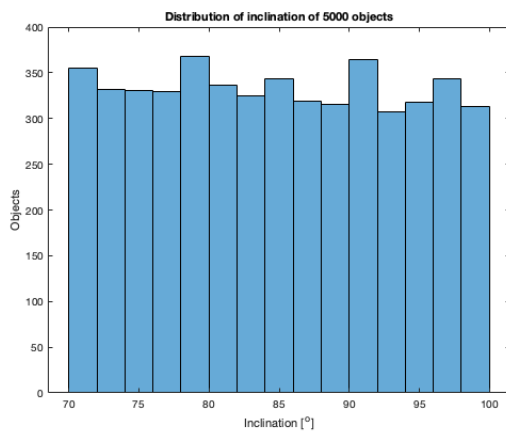


Figure 6.5: Distribution of inclination.

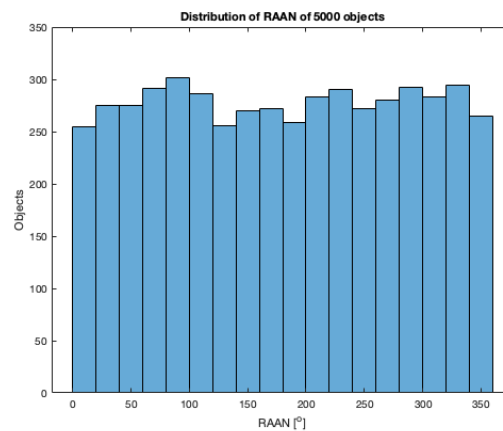


Figure 6.6: Distribution of RAAN of population.

6.3. Simulation result on debris population

After the creation of the population, the simulation will start to propagate the interactions between the laser and the debris objects it encounters. This section will show the results of every single interaction. The simulation was run for a total number of 6000 encounters which took place over 19 days. First the performance of the laser over time is discussed after which the lifetime reduction is plotted separately against the parameters of the objects.

6.3.1. Laser performance over time

The lifetime reduction per interaction gives the most accurate representation of the success of the laser system as it directly shows the impact of the laser ablation process. Figure 6.7 shows the lifetime of the debris object before the laser encounter plotted against the lifetime after the encounter. The yellow dots represent the interactions up to 5 days, the red dots the interactions from day 5 to day 10, the blue dots from day 10 to day 15 and the green dots from day 15 to day 19. The horizontal and vertical red lines show the 25 year limit. Although the plot is densely populated due to 6000 data points, the figure shows a shift from the upper right where the yellow dots are concentrated to the lower left where the green dots are concentrated, which means that the laser system lowers the lifetime of the population over time. Figure 6.8 shows this more clearly. The lifetime reduction of every interaction is plotted after 5, 10, 15 and 19 days.

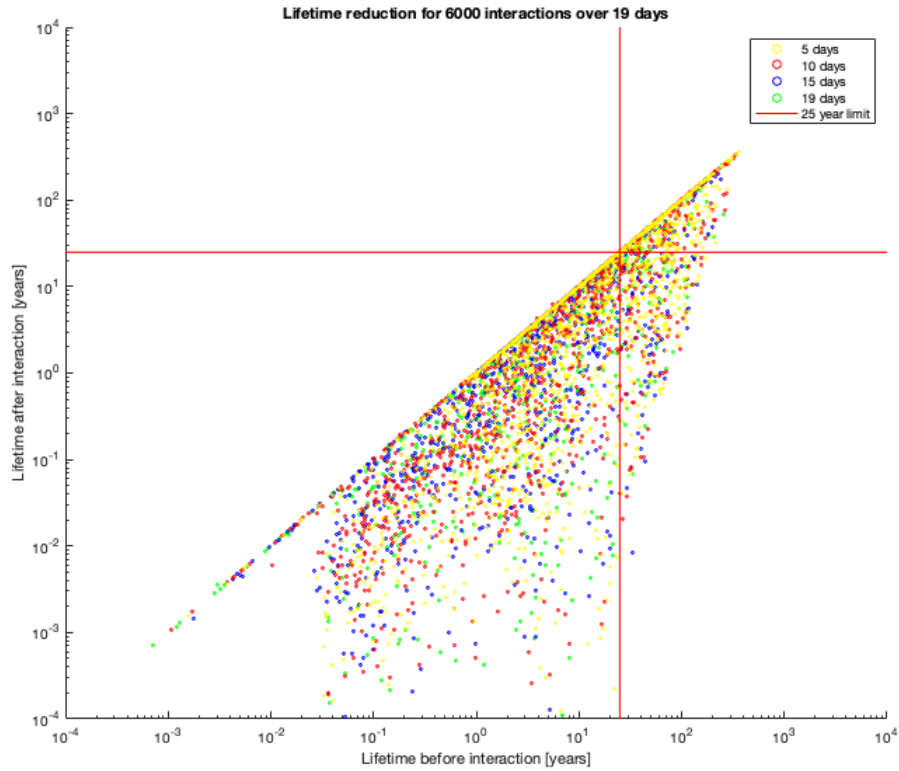


Figure 6.7: Lifetime reduction for all 6 000 interactions over time.

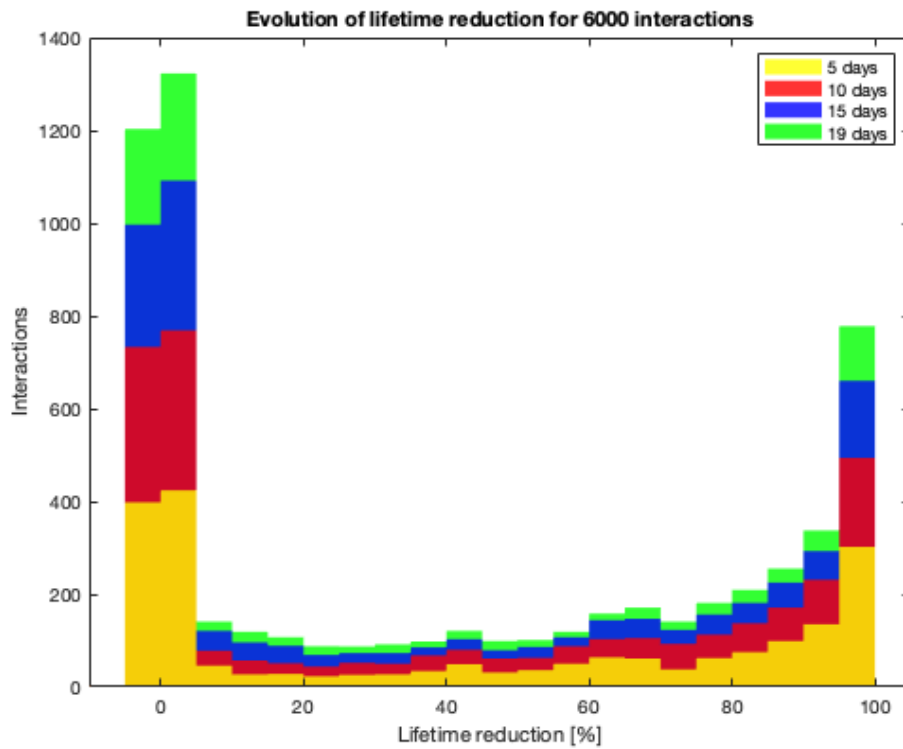


Figure 6.8: Lifetime reduction for all 6 000 interactions.

Figure 6.8 shows that the lifetime reduction increases over time. The color coding is the same as in Figure 6.7. After 19 days, a total of 1579 interactions resulted in a decrease of more than 80%. There are also 1207 interactions that result in a lifetime increase. However, these are never above 5 % and are likely to be objects targeted a second time again. The gradual shift of the data points to the bottom left in Figure 6.7 is explained by the fact that in the 19 days of simulation time, the laser does not encounter every debris object. Rather, it encounters the same debris objects more than once. The 6000 interactions that the laser has had, were only with 2422 different objects, meaning that 48% of the population was encountered. Although this effect will be less in real life due to the much larger number of debris objects, it is still likely to happen that the laser encounters the same debris object twice or even more often. This is because debris fragments that get a low Δv during a first interaction are likely to keep orbiting in the same region as the laser. Next to that, debris objects from 1000 km that get a moderate Δv might have their apogee lowered to the operational altitude of the laser, making a second encounter more likely. The distribution of apogee and inclination of the 6000 encounters are shown in Figures 6.9 and 6.10. The apogee distribution shows that after multiple interactions with the same objects, the population still orbits in vicinity of the laser altitude. In general, the perigee of the debris orbit will be lowered more than the apogee, which reinforces that double interactions in real life are not completely unlikely. The distribution of inclination of the encountered objects shows that the laser encounters more objects with lower inclination.

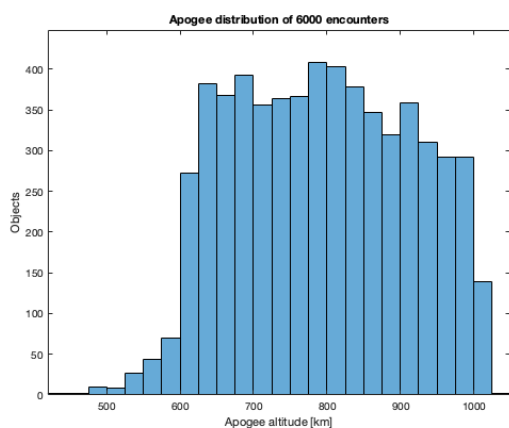


Figure 6.9: Distribution of apogee altitude of encounters.

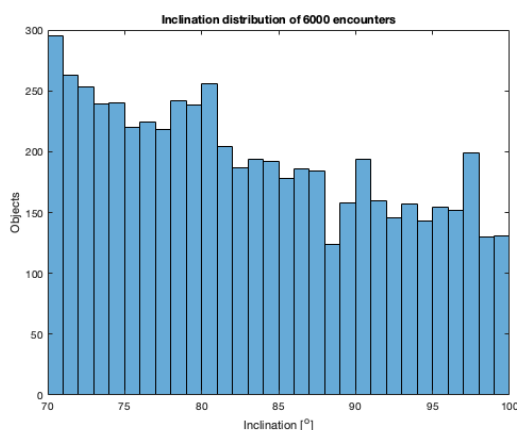


Figure 6.10: Distribution of inclination of encounters.

It will also be interesting to see only the effect on the encountered 2422 objects. Figure 6.11 shows the lifetime of the object before it encounters it the first time plotted against the lifetime of this debris object after the last encounter. The red cross depicts the 25 year limit. Out of the 2422 encountered different objects, there were 1479 objects with a lifetime below 25 years before the laser interaction. After the simulation, this number was increased to 1895 objects, which means that 416 objects were effectively lowered below the guideline. These objects are represented by the blue dots in the bottom right of the red cross of Figure 6.11. The blue dots in the top right of the cross represent the 489 objects that still have a lifetime of 25 years after the laser simulation has ended. Next to checking how many objects are lowered below a lifetime of 25 years, it would also be interesting to see how many objects are lowered even more than this.

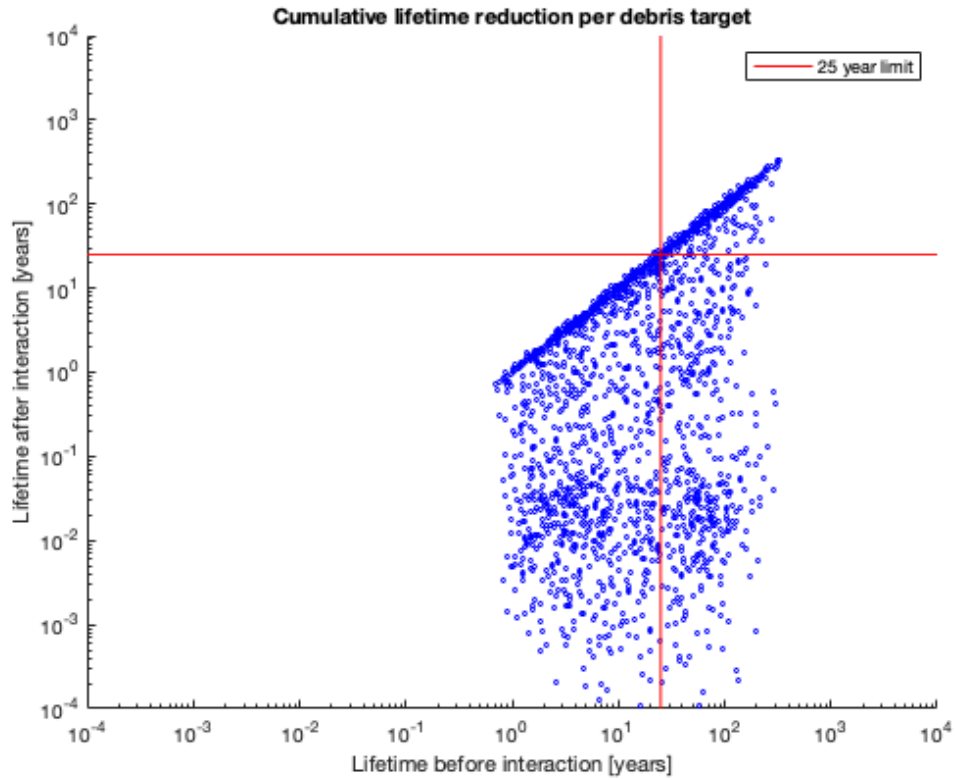


Figure 6.11: Cumulative decrease in lifetime on the 2422 different objects.

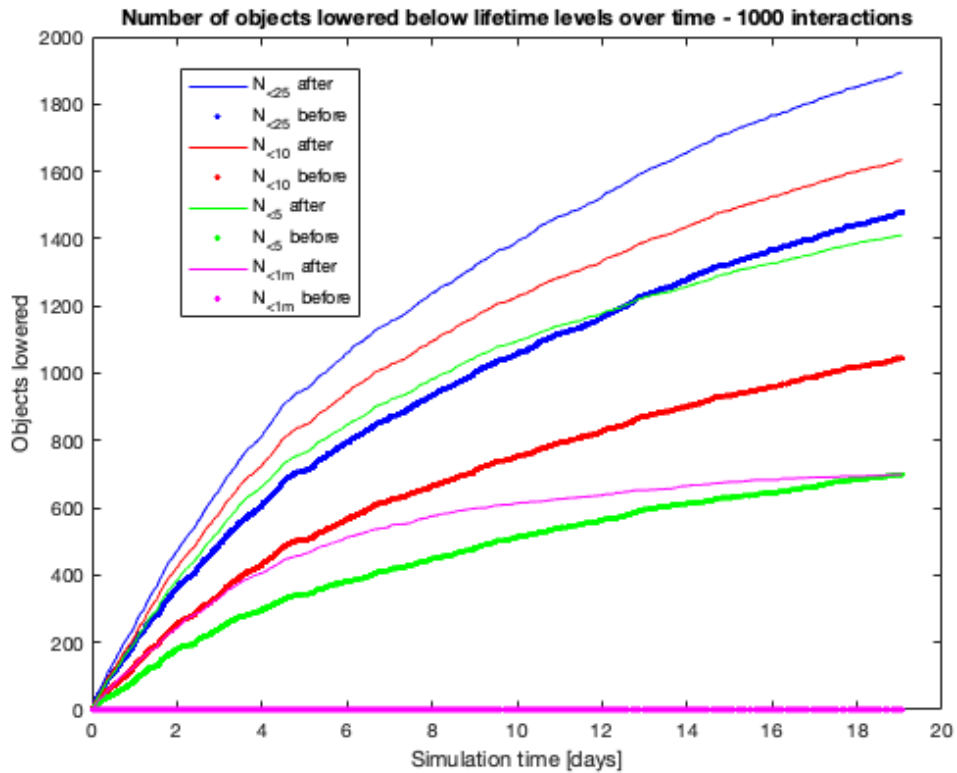


Figure 6.12: Objects lowered below lifetime values over time

Figure 6.12 shows the evolution of the number of objects with lifetime $T_{life} = \{25\text{yrs}, 10\text{yrs}, 5\text{yrs}, 1\text{month}\}$ before and after the laser interaction. The longer the simulation runs, the more objects get their lifetime decreased. An object may only be called effectively lowered below a certain lifetime if its nominal lifetime was above this value. The largest increase of effectively lowered objects is found for a lifetime below 1 month (magenta line), which is due to the fact that before the interaction there were no objects with such a low lifetime. The total number of objects with lifetime below 25 years is the largest after 19 days (blue line), but the number of effectively lowered objects below 25 years is the lowest ($N_{<25,after} - N_{<25,before}$). Table 6.3 shows the number of lowered objects after 5, 10, 15 and 19 days. After 5 days the laser has had 2037 interactions with 1148 different objects. Out of these 1148 debris fragments the laser has already effectively lowered 464 objects below a lifetime of 1 month and 241 objects below 25 years. After 10 days this has increased to 614 objects below 1 month and 334 below 25 years, which are incredible results after such a small time period. After completion of the simulation, 416 objects are brought below 25 years and 699 below 1 month. Important to note is that Figure 6.12 and Table 6.3 shows the number of all targeted objects and not the number of interactions and thus takes double encounters into account.

Table 6.3: Results of lowered lifetime of objects over time.

Objects lowered after:	5 days	10 days	15 days	19 days
$N_{interaction}$	2037	3662	5043	6000
$N_{objects}$	1148	1771	2181	2422
$N_{<25yrs}$ nominal	710	1058	1324	1479
$N_{<25yrs}$ targeted	951	1392	1713	1895
Effectively lowered	241	334	391	416
$N_{<10yrs}$ nominal	505	753	933	1045
$N_{<10yrs}$ targeted	846	1228	1483	1634
Effectively lowered	341	475	550	589
$N_{<5yrs}$ nominal	343	513	630	699
$N_{<5yrs}$ targeted	764	1096	1296	1410
Effectively lowered	421	583	666	711
$N_{<1m}$ nominal	0	0	0	0
$N_{<1m}$ targeted	464	614	677	699

6.3.2. Atmospheric sensitivity

When inspecting Table 6.3, it is important to note that the density of the atmosphere has a strong influence on the objects lifetime and thus on the performance of the laser system. The simulation was run with $\rho_0 = 2.91 \cdot 10^{-10}$ and $H = 82$ km. The errors of the exponential model with respect to the true reference atmospheric densities were presented in Table 3.1. Here, the reference values corresponded to the atmospheric density assuming average solar activity. This was justified since many debris objects have a lifetime longer than one 11-year

solar cycle. However, Figure 6.13 shows that there exists an upwards trend in the maximum number of sun spots per solar cycle. The performance of the laser should thus also be plotted for higher atmospheric densities.

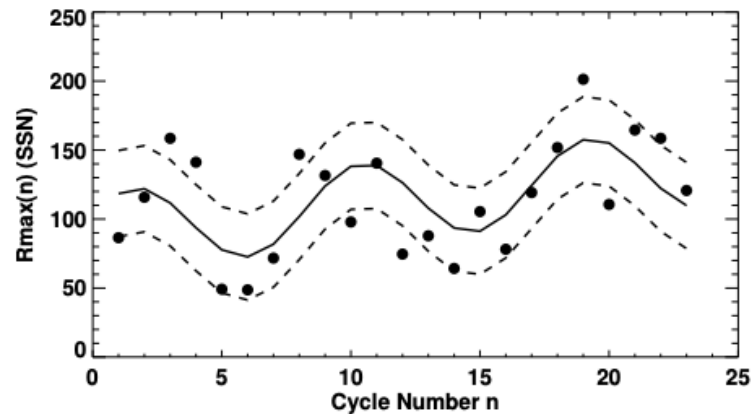


Figure 6.13: The maximum number of sunspots per cycle for last 22 solar cycles [50].

The sensitivity of the laser performance to the atmospheric density is plotted in Figure 6.14. The red dots assume $\rho = 0.9 \cdot \rho_0$ and the blue dots assume $\rho = 1.1 \cdot \rho_0$. The red dots are clearly shifted more to the right than the blue dots, meaning that a lower atmospheric density results in higher orbital lifetime. This coincides with the inversely proportional relation shown in Equation 4.8. The bottom right part of the red cross again depicts the debris fragments that have their lifetime effectively lowered below 25 years. For the nominal atmosphere this region counted 416 objects. For a less dense atmosphere (red dots), this number reduces to 390 objects, but for a denser atmosphere (blue dots), the number is increased to 444 objects. A denser atmosphere clearly results in a more effective laser performance.

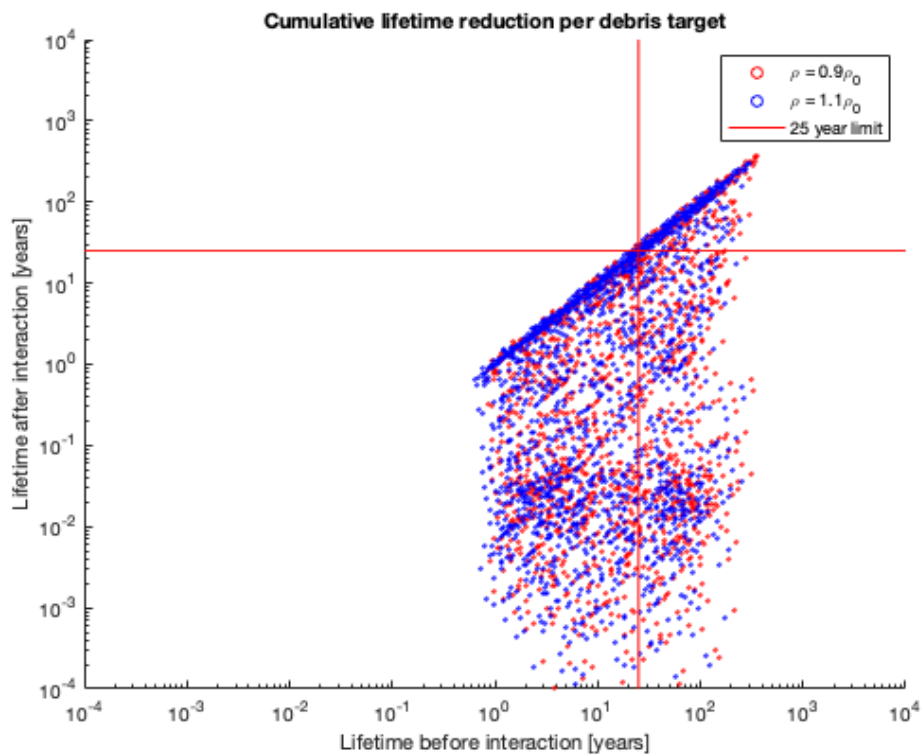


Figure 6.14: Number of objects lowered below 25 year limit assuming different atmospheric densities.

6.3.3. Evolution of total debris population

The results of Table 6.3 have been realised in a simulation time of 19 days. However, some effects of the laser will only be noticeable after 25 years. To show these effects more clearly, the evolution of the complete debris population is plotted for two different scenarios: one where the debris objects are only influenced by atmospheric drag and one where the laser ablation system is introduced next to the atmospheric drag. The results are shown in Figures 6.15 - 6.22.

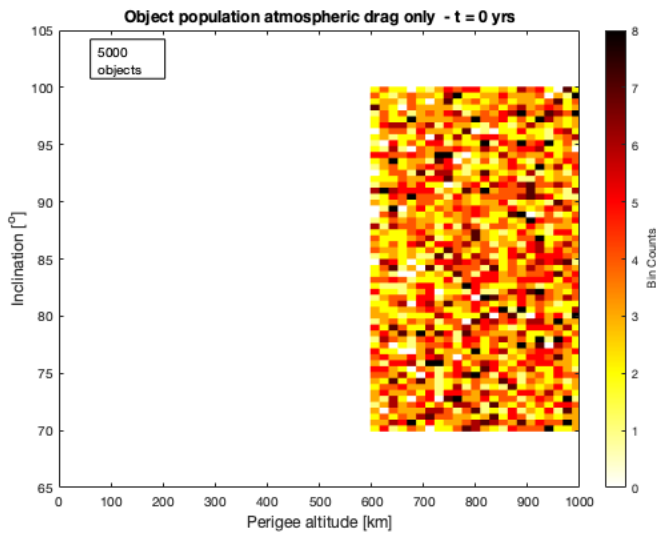


Figure 6.15: Initial population without laser.

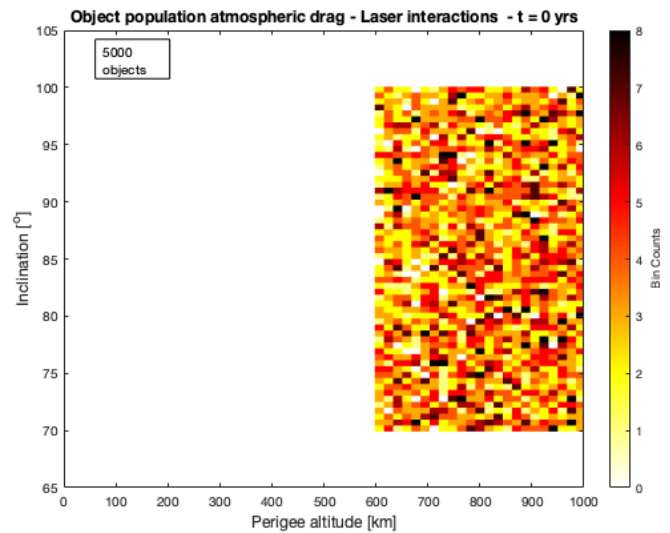


Figure 6.16: Initial population with laser.

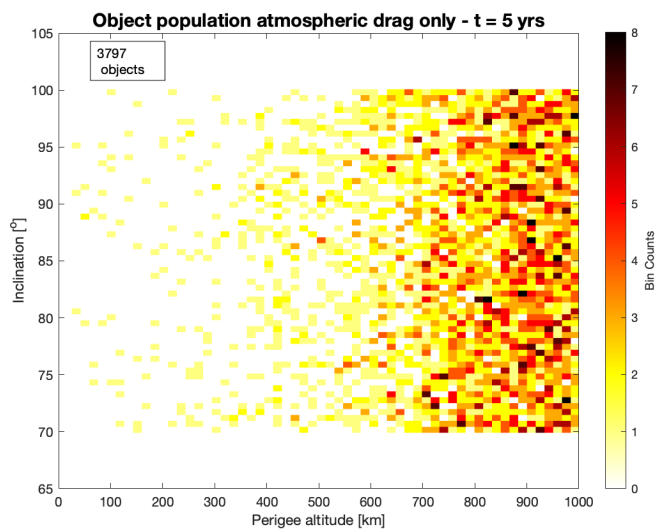


Figure 6.17: Population without laser t = 5 yrs.

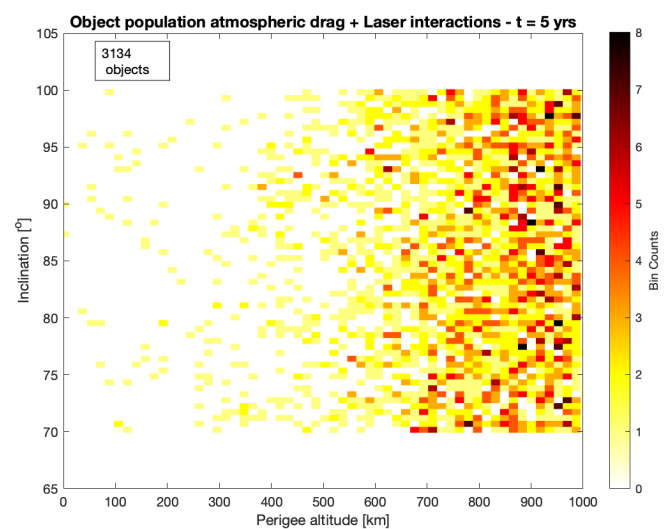


Figure 6.18: Population with laser t = 5 yrs.

The first two plots (Figures 6.15 and Figure 6.16) show the initial distribution of the population of 5000 debris objects, which are clearly equal for both scenarios. The objects are evenly distributed between 70° and 100° and between 600 and 1000 km, as was shown in Figure 6.5 and 6.3. The plots also show the total number of objects that are still orbiting above Earth's

surface. The reduction in perigee of every debris object is computed using the reduction in semi-major axis per revolution Δa_{rev} in Equation 4.8. The reduction in perigee altitude of all 5 000 objects is computed after every year. This causes the number of removed objects to be slightly lower than in Table 6.3. After 5 years there is already a difference visible between the two scenarios: there are less dark colored bins in Figure 6.18 than in Figure 6.17 and the total number of objects in orbit has dropped from 3797 to 3134 objects, a decrease of 663 objects.

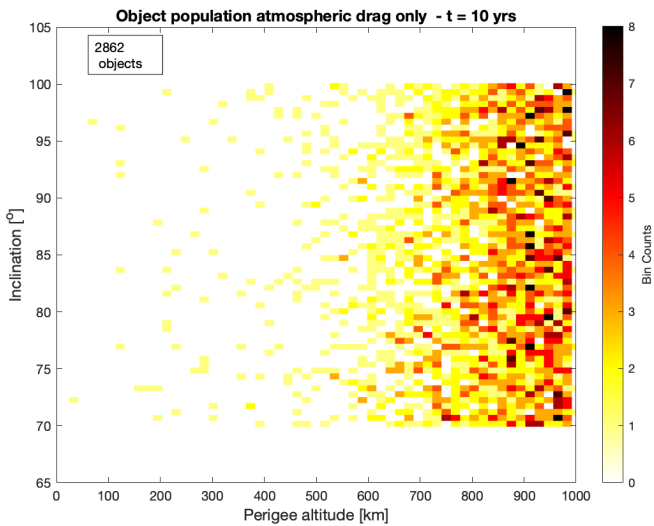


Figure 6.19: Population without laser $t = 10$ yrs.

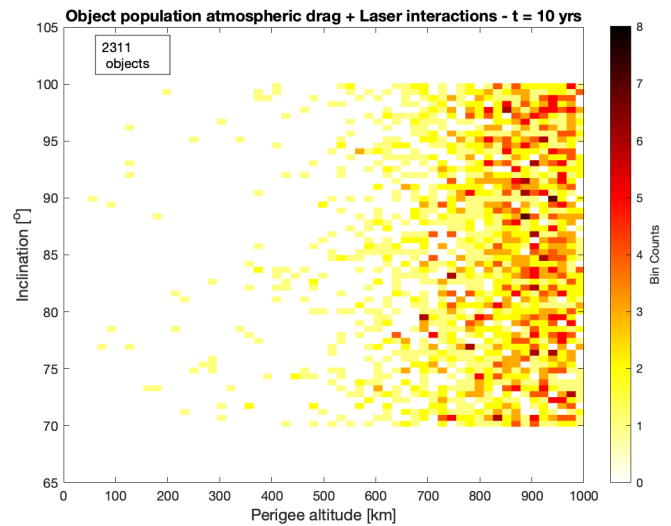


Figure 6.20: Population with laser $t = 10$ yrs.

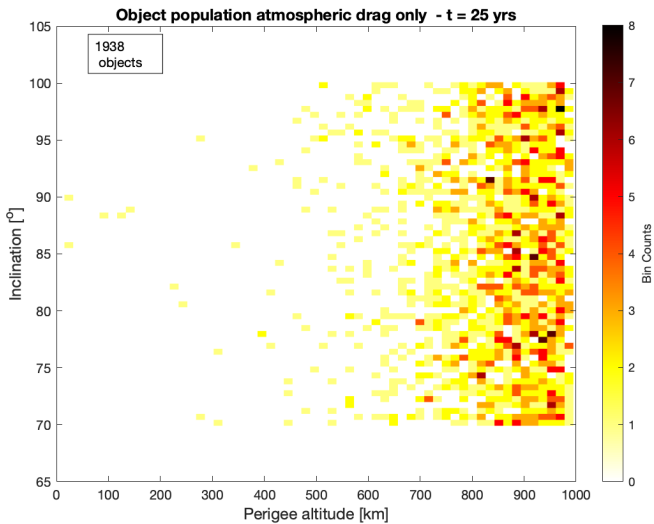


Figure 6.21: Population without laser $t = 25$ yrs.

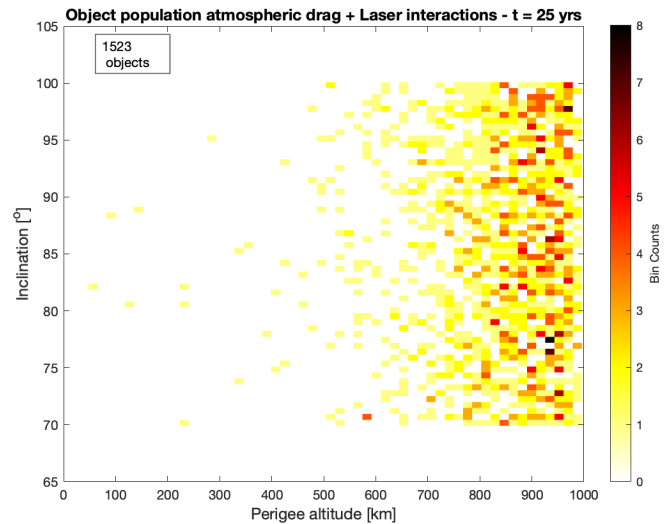


Figure 6.22: Population with laser $t = 25$ yrs.

After 10 years (Figure 6.19 and Figure 6.20), there are barely dark spots left for the scenario where the laser is active and the total number of objects is reduced from 2862 to 2311. After 25 years (Figure 6.21 and 6.22), there are only 1523 remaining in orbit, which is 415 objects less compared to the situation without laser. Seen the fact that the laser has only been active for 19 days, this is a promising reduction.

6.3.4. Predicting results on longer time scale

It would be interesting to extrapolate these values to predict the performance of the laser on a longer time scale than 19 days. Since the evolution of the effectively lowered objects is not linear over time, but seems to stagnate after about one week, it is important to choose a representative reference value to extrapolate from. The number of lowered objects is compared to a simulation with only 1000 interactions (Figure 6.23). For this simulation, a population of 1000 objects is constructed. The laser has 1000 interactions in which it encounters 382 different debris objects in 6 days. Figure 6.23 shows that the number of effectively lowered objects below 1 month also stagnates over time. After 3 days, 147 objects are effectively lowered below 1 month. Extrapolating this to 10 days would give 490 objects. However, Table 6.3 shows that after 10 days already 614 objects are lowered below 1 month in the 5 000 objects population, so another reference value should be chosen to extrapolate from.

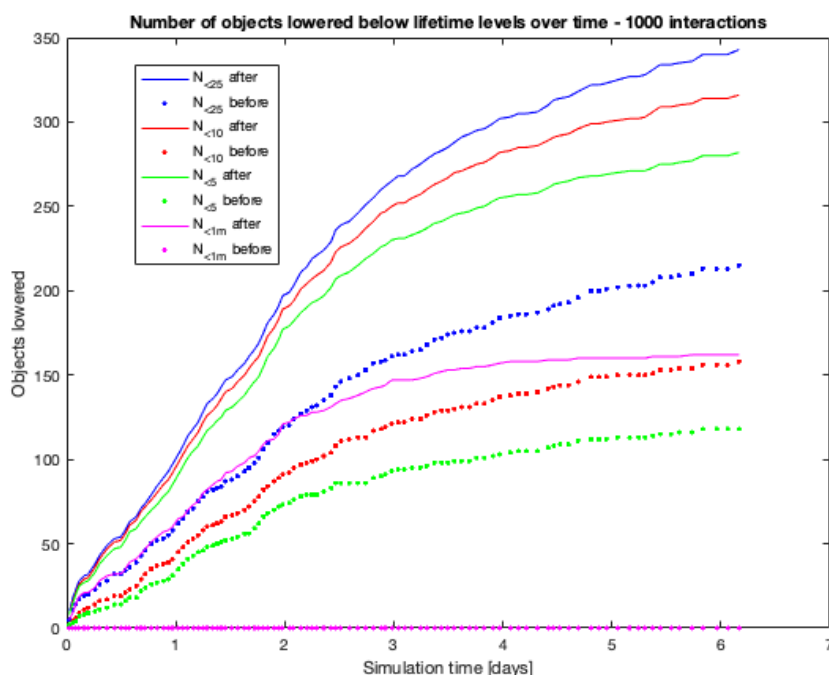


Figure 6.23: Evolution of number of objects lowered below lifetime values.

After 2 days a total of 122 objects get lowered below 1 month. Extrapolating this to 10 days would give 610 objects, which matches up much better with the results of the 5 000 objects simulation. The stagnation only occurs if there are no candidate debris objects left in the population to lower below a certain lifetime. For a 500 000 debris population, this stagnation effect will occur after a very long time as there would be virtually always a potential candidate to target. This implies that an extrapolation value should be used from the near-linear growth at the beginning of Figures 6.12 and 6.23. Next to this, another factor comes into play. The time between successive encounters depends on the size of the debris population. For a larger number of objects, this time will be very short as there is always a candidate to target. The time difference is plotted for the duration of the simulation for the 1000 and 5 000 object populations (Figures 6.24 and 6.25). Both plots have a minimum of 120 seconds, which was added as a cool-down period for the laser. The 1000 object simulation shows large time periods between the encounters: within a day the laser already has to orbit for over 1500 seconds before a new debris object is encountered which is very undesirable. The 5 000 object simulation shows more realistic time periods in the beginning of the simulation: up

to 4 days the time between encounters remains near around 300 seconds, which is a more realistic value. A reference extrapolation value is taken at 4 days. In this time period, the laser effectively lowers 405 debris objects below a lifetime of 1 month (Figure 6.12). With this removal rate, a yearly number of 36 865 objects could be removed from orbit which would be an impressive achievement. Following the same reasoning, the laser could yearly effectively lower the lifetime of 18 797 objects below 25 years that did not adhere to this rule before the simulation. These results suggest that a laser ablation system could function very efficiently as a small-scale debris removal method.

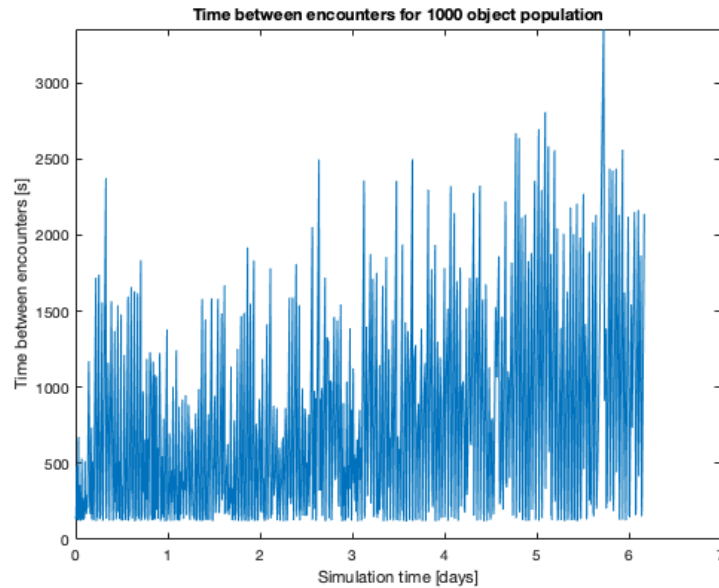


Figure 6.24: Time between encounters 1000 objects.

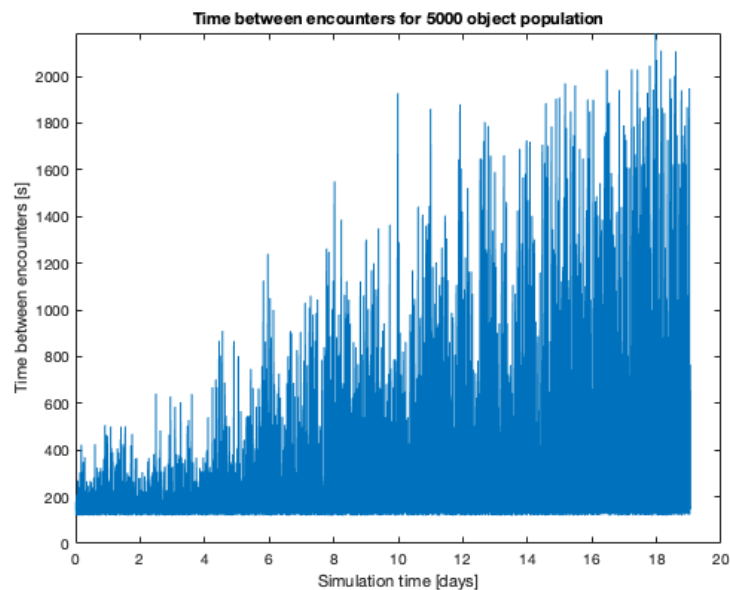


Figure 6.25: Time between encounters 5 000 objects.

6.3.5. Laser performance per debris parameter

With the results of the complete population presented, a closer look will be given into the laser performance as a function of different debris parameters.

AMR

Figure 6.26 shows the generated Δv of the first encounter with each of the 2422 encountered objects. The laser produces higher Δv 's on objects with higher AMR, as was explained in Section 4.1: the acceleration from the laser on an object has a linear relation with the AMR. Since the objects orbit in different geometries, the Δv are still spread out, but Figure 6.26 clearly shows that the maximum achieved Δv increases with AMR value.

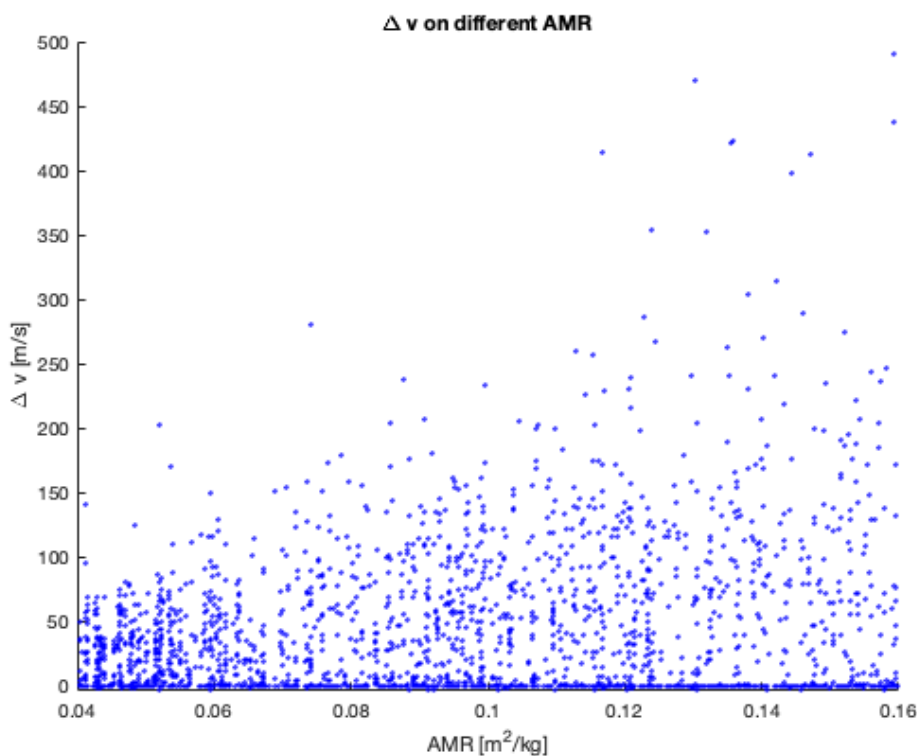


Figure 6.26: Generated Δv on first encounter with 2422 objects.

Figure 6.27 shows the lifetime before (blue dots) and after (red dots) the interaction resulting from these Δv 's. Section 4.1 also showed that the orbital lifetime has an inverse relation with the AMR value. This can be seen in Figure 6.27 where the blue dots (nominal lifetimes) are found at lower values for higher AMR values. After interaction, the lifetime of high AMR objects is decreased to lower values than high AMR. However, since objects with low AMR have such a high lifetime before the interaction, the reduction in lifetime is still significant. Figure 6.28 shows that the lifetime reduction is evenly spread for all AMR values. Only lifetime reductions over 95% occur more frequently above $AMR > 0.07 \text{ m}^2/\text{kg}$. The results suggest that laser ablation is able to significantly reduce the lifetime of objects over the complete AMR range.

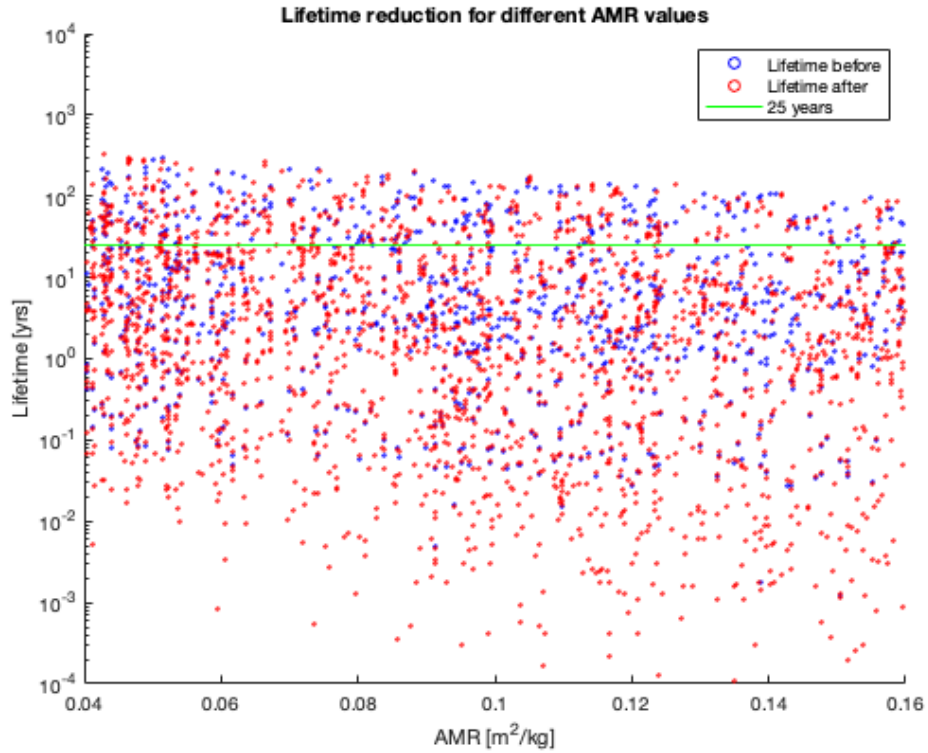


Figure 6.27: Lifetime of different AMR objects before and after interaction.

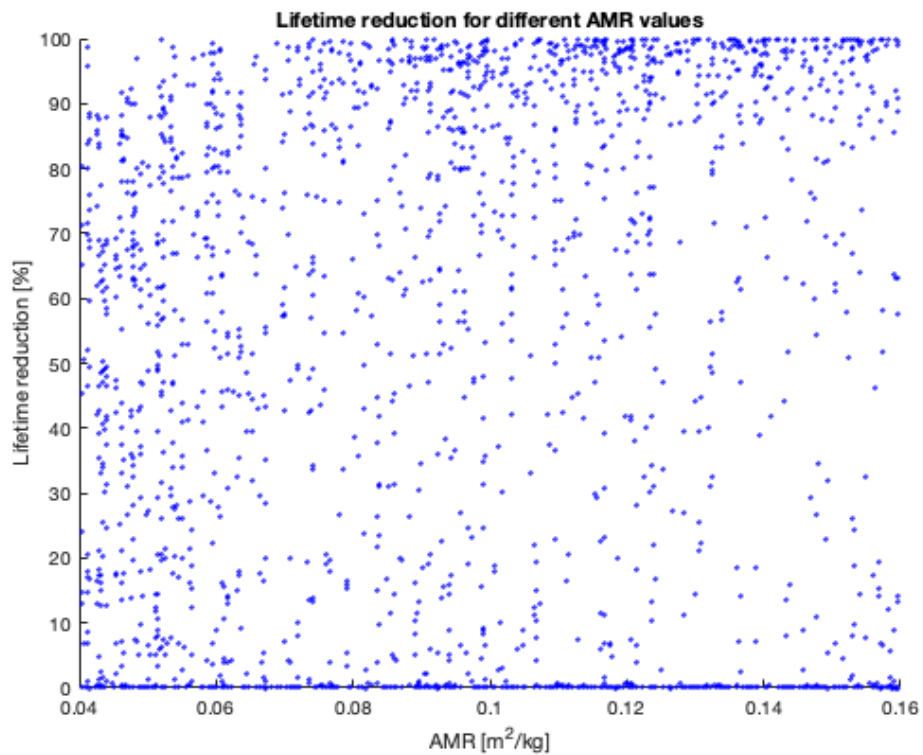


Figure 6.28: Lifetime reduction of different AMR objects.

Azimuth

Figure 6.29 shows the lifetime before (blue dots) and after interaction (red dots) for different azimuth values. The 25 year limit is plotted as the green line. Since the effects of the laser interaction is identical for negative and for positive azimuth angles, the absolute value of the azimuth is shown. The red dots clearly dominate the lower part of the figure, which demonstrates the success of the laser.

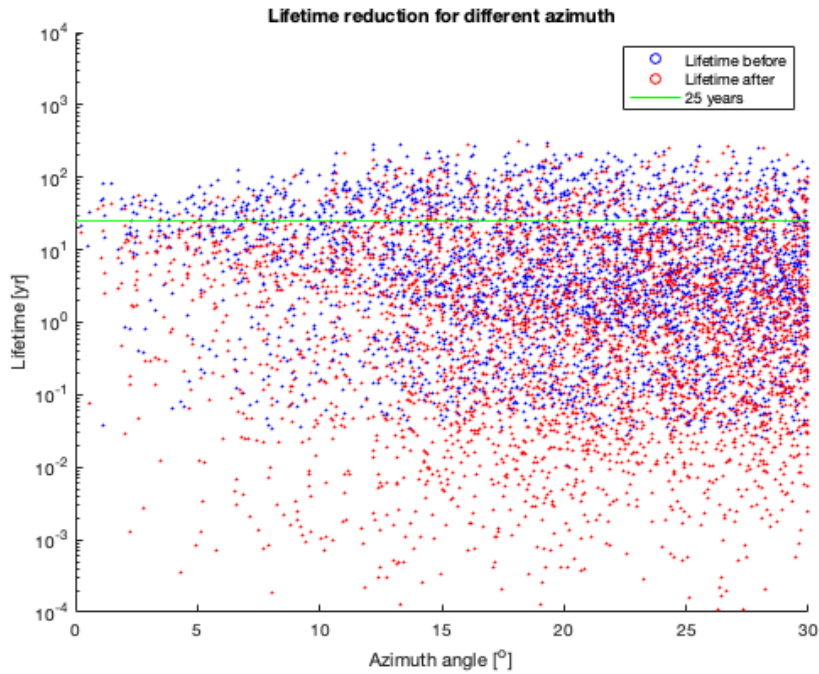


Figure 6.29: Lifetime before and after interaction for different azimuth.

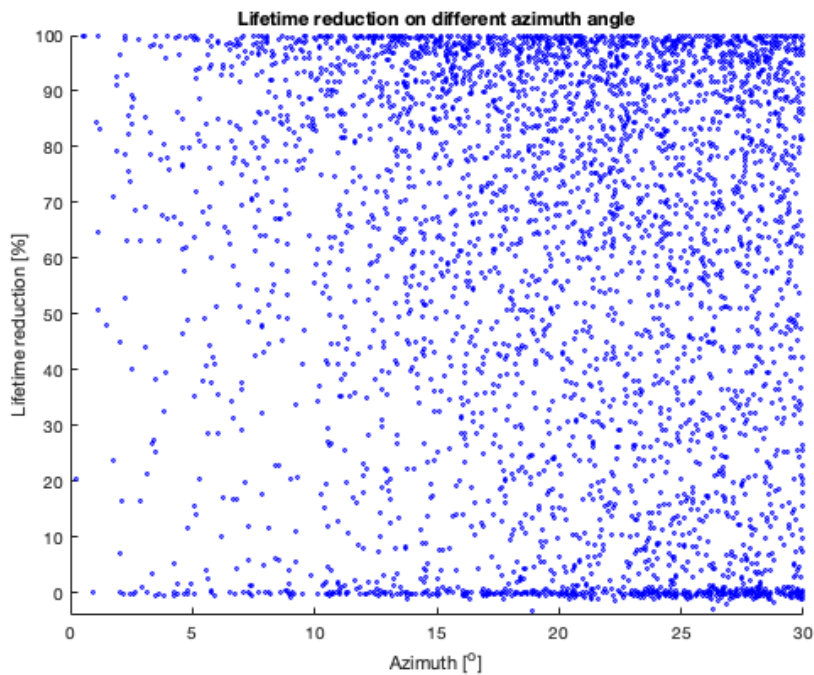


Figure 6.30: Lifetime reduction per interaction for different azimuth.

Figure 6.30 shows the lifetime reduction for different azimuth values. Clearly, the laser encounters more debris objects at higher azimuth angles. This was expected since the probability of a head-on interaction is small as was shown in Section 5.1.1 (Figure 5.8).

Apogee

Figure 6.31 shows the generated Δv 's on debris objects with different apogee altitude. At 800 km, the operational altitude of the laser, a gap in data points can be seen since exact head-on interactions are rare. From this altitude, the magnitude of the Δv 's decrease for higher and lower debris altitude as the geometries get less and less optimal. For debris objects at $h_{apo} = 600$ km and $h_{apo} = 1000$ km, still significant velocity change are generated of about 100 m/s. These encounters correspond to objects with high AMR values. Figure 6.32 shows the lifetime of the objects before and after the interaction at different apogee altitude. The plot shows that from about 800 km, objects have a lifetime above 25 years. Figure 6.33 shows that the lifetime reduction are slightly higher at lower apogee altitude, but the data points are still quite evenly distributed. The results suggests that the laser performs well over the full altitude range.

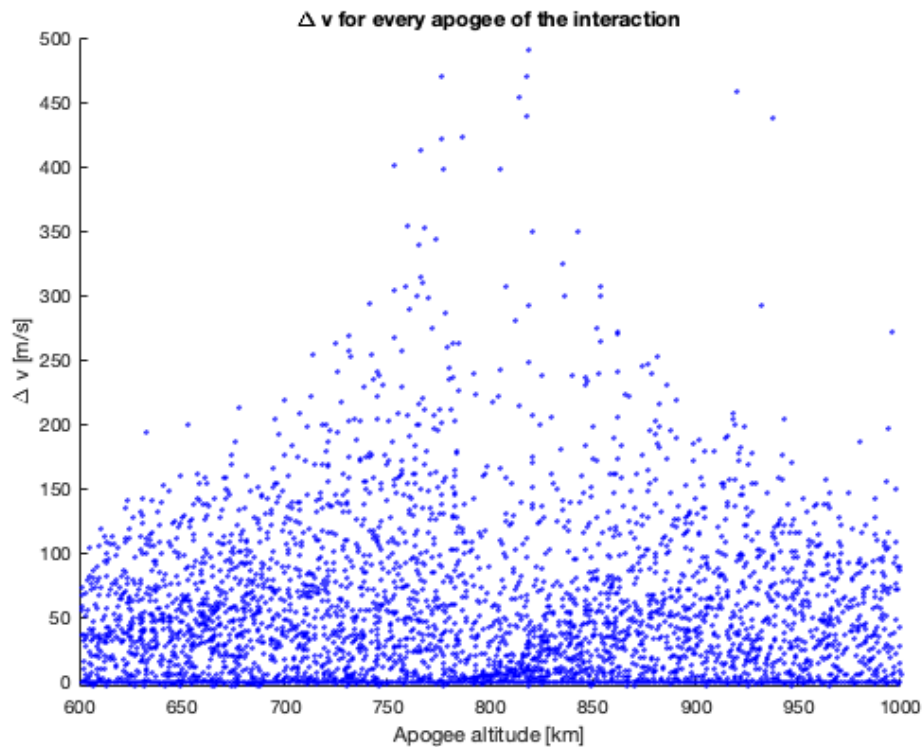


Figure 6.31: Generated Δv on debris objects with different apogee altitude.

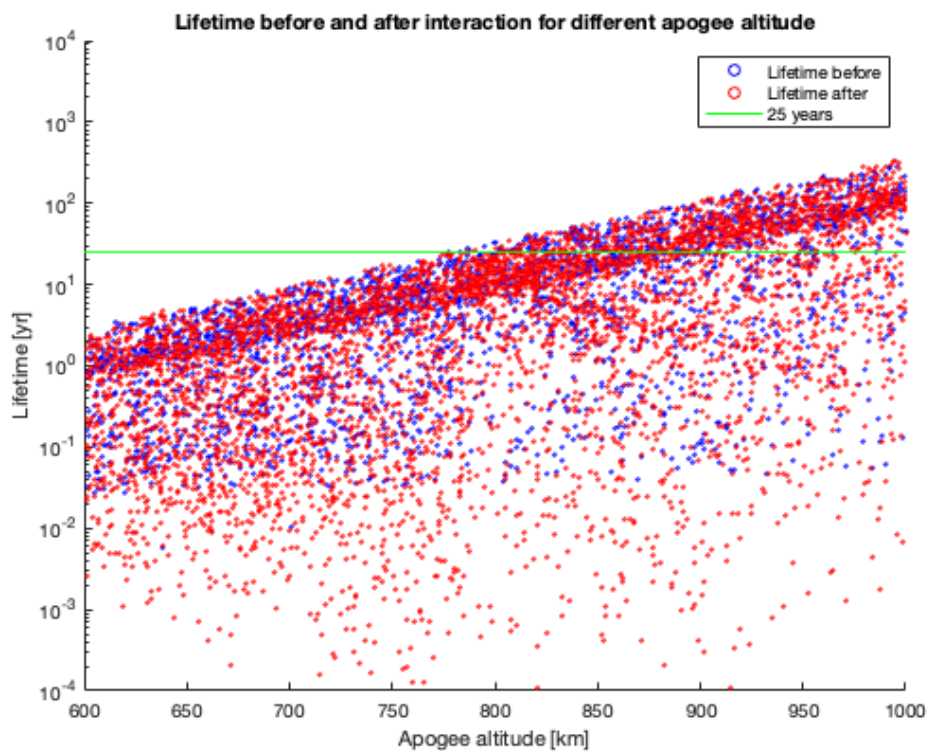


Figure 6.32: Lifetime before and after interaction of objects with different apogee.

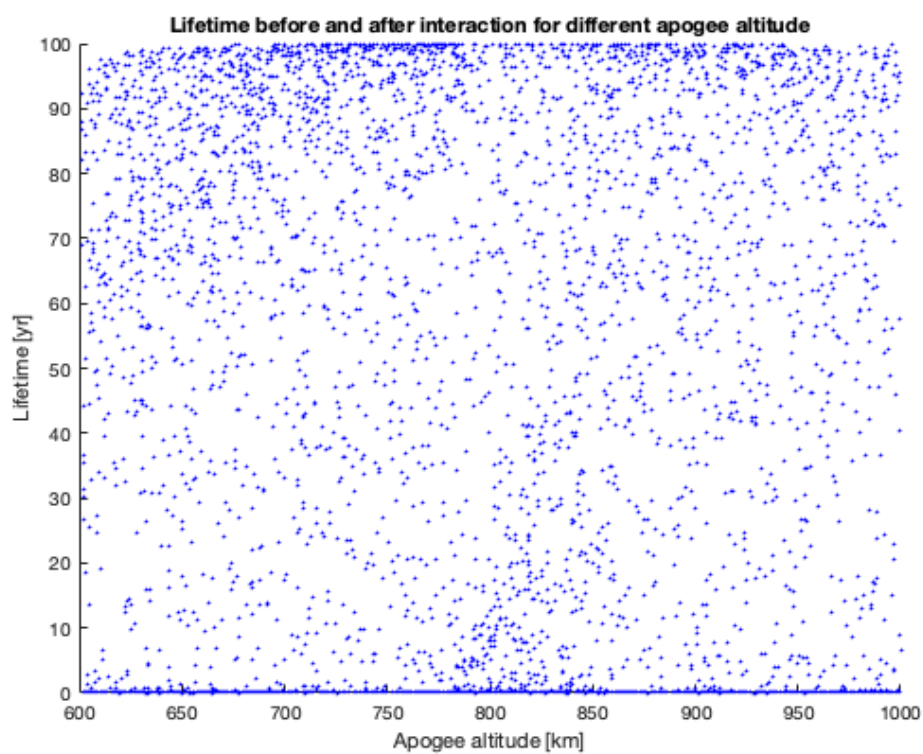


Figure 6.33: Lifetime reduction of objects with different apogee.

Perigee

One interesting aspect is not yet covered. The laser interaction will mostly lower the perigee instead of the apogee, so the change in perigee should be plotted for each interaction. Figure 6.34 shows the perigee altitude of the 2422 different debris objects before and after the interaction with the laser. The green line depicts the de-orbit altitude at 200 km. After the simulation of 19 days, 352 objects are lowered below 200 km and are removed from orbit. The few points that increase the perigee result from an unsuccessful interaction, but these are negligible to the total decrease in perigee of the object population.

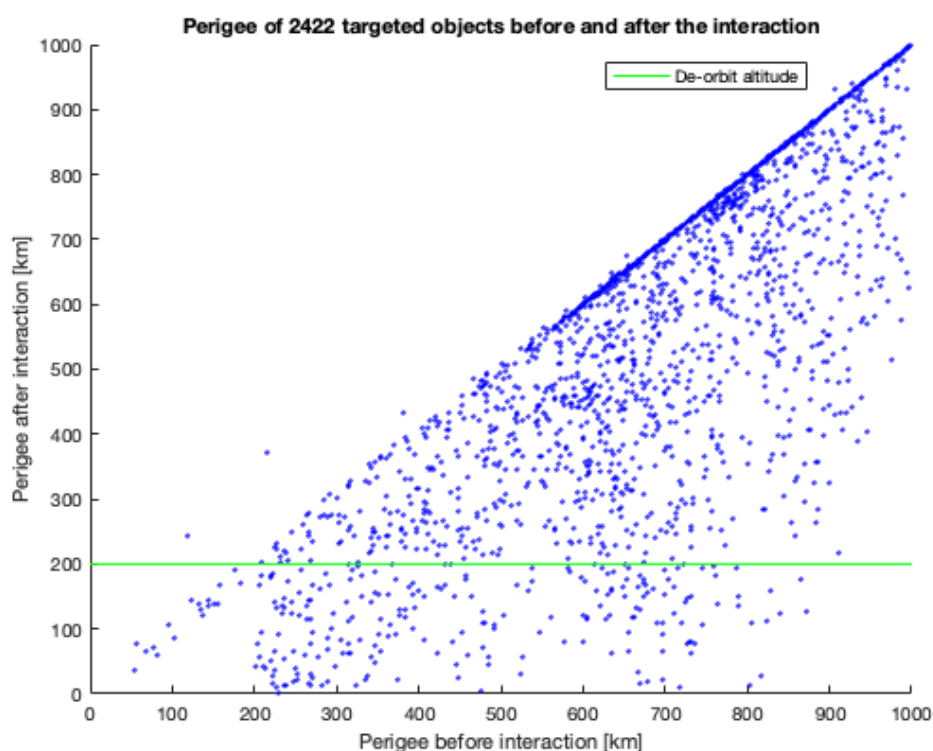


Figure 6.34: Perigee before and after for all 6000 interactions.

Summary

This chapter has presented many plots to extract all information from the population dataset. A summary of the most important results are given below.

- A 19 day simulation was run containing 5 000 objects. The laser had 6000 interactions in which 2422 different objects were targeted, implying the laser had multiple double encounters.
- After the simulation, 699 objects were lowered below a lifetime of 1 month and 416 below a lifetime of 25 years.
- Low inclinations were encountered more frequently than high inclinations and the majority of encounters were at azimuth between $10^\circ < \phi < 30^\circ$.
- The laser causes slightly larger lifetime reductions for objects with high AMR values.
- The laser causes slightly larger lifetime reductions for objects at low apogee.
- Extrapolating the performance to a real-life situation with a 500 000 debris population,

the laser will encounter debris targets non-stop and an estimated 36 865 objects could yearly be lowered below 1 month, 18 797 objects below 25 years.

7

Validation and verification

As the concept of ADR by laser ablation has only been extensively studied since several years ago, available material to validate the results of this report is limited. Although there have been studies that show how much energy a laser could provide, there have been no reports published that simulate the interactions of a laser ablation system with a randomly generated debris population for multiple weeks. This chapter will first compare the presented results with the few researches on laser ablation and verify that the integrator of the program returns accurate results.

External validation

A paper by Phipps [10] shows the performance of a laser 21 kW laser that shoots $E_{pulse} = 380$ J at frequency $f = 56$ Hz. Only 'head-on' interactions are assumed. The laser would de-orbit fifteen objects per hour on average. This would extrapolate to 131 400 objects per year. However, the 100 000 objects are all assumed to have $AMR = 1$ m²/kg, which is a very inaccurate assumption and has far-reaching results. First, assuming such a high AMR the report concludes that every object it encounters is de-orbited within half a revolution. This required de-orbit Δv might not have been reached for a 10 cm target with $AMR=0.04$ m²/kg, which would return a lower result by a factor of 25 ($a_{las} \propto AMR$). Secondly, objects with lower AMR have a longer lifetime ($T_{life} \propto AMR^{-1}$). This means that for the same Δv , an object with $AMR = 1$ m²/kg might have its lifetime reduced below a de-orbit value, but an object with $AMR = 0.04$ m²/kg will not. Besides the fact if the debris population of Phipps [10] is realistic, at least the paper shows that a laser orbiter is capable of targeting many objects and delivering the required energy for ablation. A follow-up research by Phipps and Bonnal [20] alters the laser system to shoot $E_{pulses} = 83$ J with a frequency $f = 120$ Hz. The paper shows that the same assumed population of 100 000 objects with $AMR = 1$ m²/kg could be completely removed within 10 months. Although this paper finds somewhat lower results due to stricter assumptions, the paper by Phipps does show that a laser ablation system has tremendous abilities for lowering debris particles lifetime.

Figure 4.2 showed the required Δv to lower the perigee of LEO debris objects to 200 km. A similar result was obtained by Scharring *et al.* [51], plotting the required Δv to lower debris objects to 200 km and to 50 km (Figure 7.1).

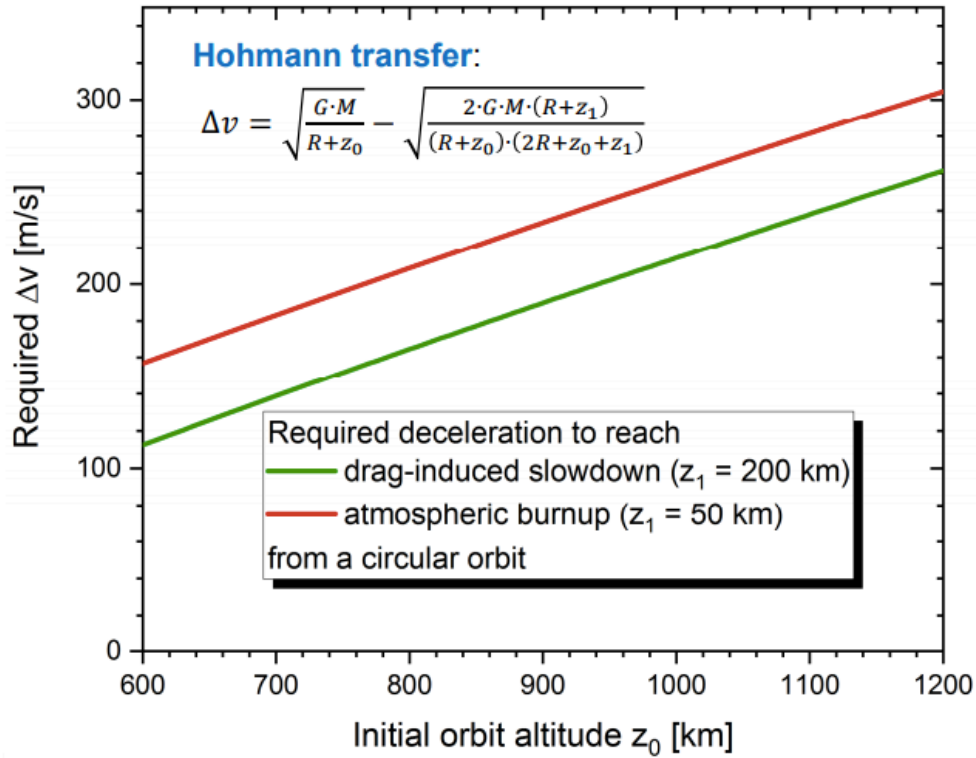


Figure 7.1: Required Δv to lower LEO debris to 200 km (green) and 50 km (red) [51].

Table 7.1 compares the results of Figure 7.1 with Figure 4.2. The results are all accurate to below 5 %. Although these results are not detrimental for the final performance of the laser system, it is still important to verify that the presented plots are correct.

Table 7.1: Comparing Δv 's from Figure 6.34 with data from Figure 7.1 [51].

Altitude [km]	Δv_{report} [m/s]	Δv_{lit} [m/s]	error [%]
600	114.9	112.3	2.2
700	142.6	138.6	2.8
800	169.9	164.3	3.3
900	196.8	189.3	3.8
1000	223.4	213.7	4.3

A plot with more a more direct effect on the laser performance is Figure 4.3 where the nominal lifetime of three LEO debris objects is plotted. The computation of the lifetime is particularly important since it determines how effective the laser system removes objects. Next to that, the lifetime is computed assuming an exponential atmosphere and is thus prone to error. The values are compared to Figure 3.12, in which Phipps *et al.* [22] has plotted the orbital lifetime of a 1, 10 and 100 cm spherical debris fragment with density $\rho = 0.2 \text{ g/cm}^3$ based on the U.S. standard atmosphere. Here, the 1 cm object has an AMR of $0.75 \text{ m}^2/\text{kg}$ and the 10 cm object an AMR of $0.075 \text{ m}^2/\text{kg}$. The 10 cm object in this report has an AMR of $0.16 \text{ m}^2/\text{kg}$, which is a factor 2.13 higher than the value of Phipps *et al.* [22]. Since the AMR is inversely proportional to the lifetime, the values of Figure 4.3 are corrected by a factor

1/2.13 so they can be compared with the data read off from Figure 3.12. For objects at 600, 700 and 800 km, the lifetimes are fairly accurate: the errors in lifetime are below 5%. Larger errors are found at altitudes 400, 500, 900 and 1000 km. Firstly, these errors come from the assumption of an exponential atmosphere. However, the errors in Table 3.1 do not exactly coincide with the errors in lifetime listed below. The method of computing the lifetime also produces discrepancies: following Wertz *et al.* [29], the nominal lifetimes in this report are computed assuming that the debris object experiences a constant atmospheric drag at the initial altitude. It would have been more accurate to integrate Equation 4.8, including the change in atmospheric density and orbital period as the object spirals towards Earth. However, this would have substantially increased the computation time of the simulation. The assumption of a constant atmospheric drag explains the errors listed below (Table 7.2). The atmospheric densities at 600 and 800 km altitude used in this report were about $\sim 10\%$ higher than the true values (Table 3.1). This denser atmosphere compensates for the assumption that the object experiences a constant drag, which makes the errors in lifetime accurate to below 5%. The density at 1000 km arising from the exponential model was $\sim 7.5\%$ lower than the true value. This estimation, together with the assumption that the object experiences constant drag, accumulates to the large error of 32.45% in the nominal lifetime. The most important thing is that the large errors are all positive, meaning that computed lifetimes in this report are higher than the literature values. This suggests that the laser will lower even more objects when a more accurate density model is implemented and the loss in altitude is integrated as the objects spiral into the atmosphere.

Table 7.2: Comparing lifetimes from Figure 4.3 with data from Figure 3.12 [22].

Altitude [km]	T_{life} report (corrected) [yr]	T_{life} literature [yr]	error [%]
400	0.5	~ 0.2	150
500	1.8	~ 1.0	87
600	6.2	~ 6	4.05
700	20.7	~ 20	1.05
800	69.8	~ 70	-0.25
900	234.8	~ 200	17.65
1000	789.5	~ 600	32.45

Internal verification

First the two available integrator techniques in Tudat, Euler and RK4, were compared by plotting the difference in linear position error in Figure 5.1, which verified the choice for an RK4 integrator. Figure 5.2 showed the linear position error of this integrator for different stepsizes. This plot verified the choice of the stepsize of $t_{step} = 10$ s. However, the choice of the propagator has not yet been discussed. Below, all propagator types that are available in Tudat are compared [48]. Figure 7.2 shows the Root Mean Squared (RMS) error of the propagator types compared to an unperturbed Kepler orbit. Figure 7.3 shows the RMS error of the propagator type simulating orbits perturbed by the sun, moon, aerodynamic effects and SRP. Both plots assume an RK4 integrator with a 5 second stepsize and are simulated for a total time of 10 days. The cowell and encke propagator are the only two types that propagate the state in cartesian coordinates. Since the desired output of the system state is in cartesian

coordinates, one of these two propagators is selected. This report propagates perturbed orbits and has aimed to minimize computation time since the final simulation contained about 5000 objects. Figure 7.2 shows that the Encke propagator results in a longer computation time and also gives a larger error, which is why the Cowell propagator was chosen.

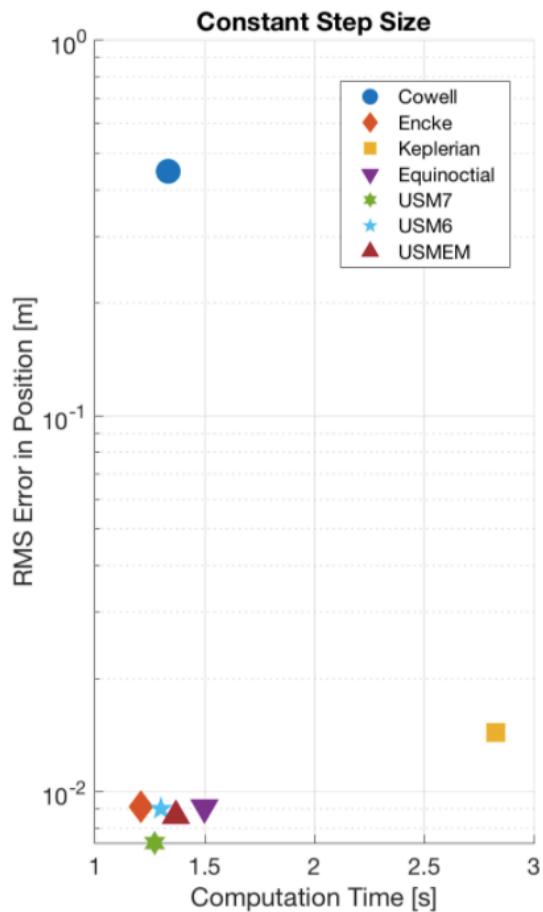


Figure 7.2: Propagator error unperturbed [48]

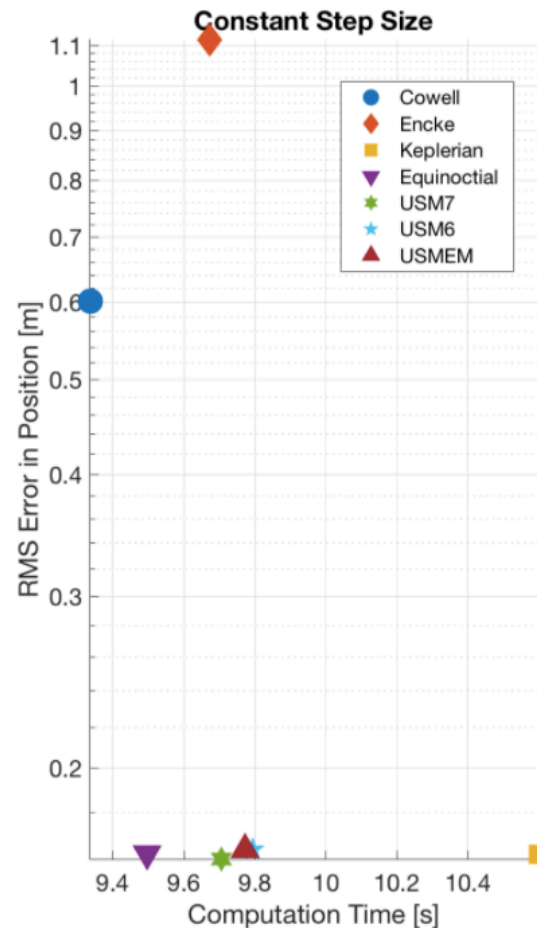


Figure 7.3: Propagator error perturbed [48]

The program should still be tested to see if it returns correct values. Using a cowell propagator and an RK4 integrator with stepsize 5 seconds, the linear position error with respect to an unperturbed Kepler orbit has been plotted (Figure 7.4). After about 10 days, the linear error in position is about 0.5 m. This coincides with the value of the cowell propagator in Figure 7.2, which shows an error of 0.45 m after 10 days. With this, it is verified that the propagator and integrator of the program produce the correct results.

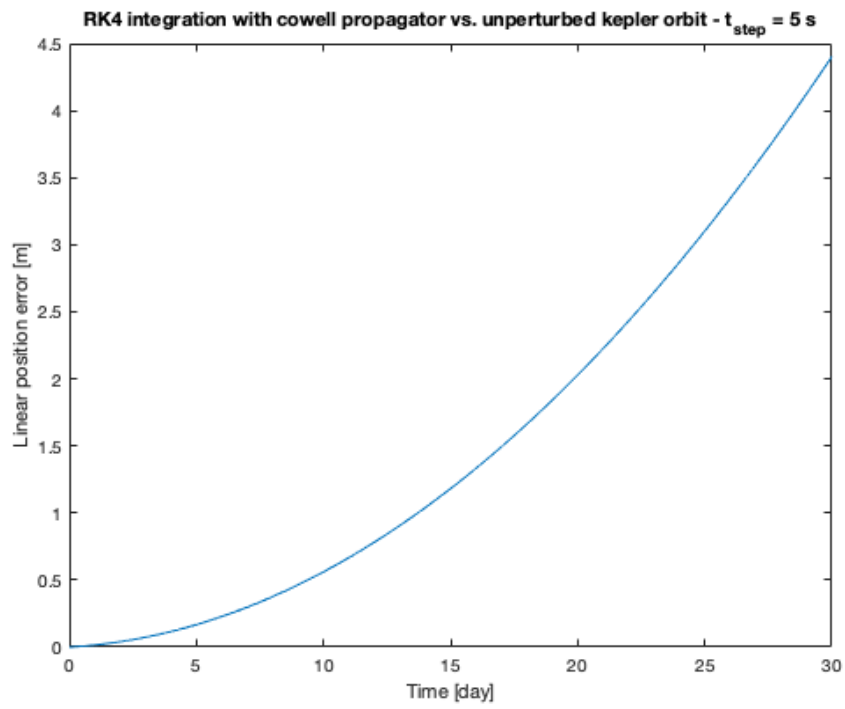


Figure 7.4: Linear position error RK4 integrator cowell propagator w.r.t. unperturbed Kepler orbit.

8

Conclusions and recommendations

This report has researched the performance of a space-based laser system on the removal of space debris fragments between 1 and 10 cm. First, a look into the material density and main sources of debris objects in LEO validated the choice of aluminum spheres as test objects. Experiments from simulated fragmentation events showed that a representative value for the AMR range to assume for these objects was $0.04 \text{ m}^2/\text{kg} < \text{AMR} < 0.16 \text{ m}^2/\text{kg}$. The boundary limits for the different laser parameters were discussed and the final laser system was decided to shoot $\tau = 100 \text{ ps}$ pulses with $E_{\text{pulse}} = 600 \text{ J}$ at a frequency of $f = 33.33 \text{ Hz}$ using a laser wavelength $\lambda = 335 \text{ nm}$ and a $D = 1.5 \text{ m}$ telescope. With these laser settings, the fluence ablation threshold could be passed at a relative distance of $L = 500 \text{ km}$ from the laser. Technical constraints from the optical tracking system gives the telescope $\text{FOV} = 60^\circ$ and the requirement of a black background and optimal lighting of the debris object demands a placing of the laser system in a dusk/dawn SSO with constant illumination.

The procedure of the program was explained in detail and the termination conditions were highlighted. The debris object should never move away from the laser and the telescope should never rotate faster than $\omega = 3.49 \cdot 10^{-2} \text{ rad/s}$ to avoid mechanical failure. The system was tested from all possible geometries at which it might encounter debris objects during a real-time simulation. Results show that all debris objects between 1 and 10 cm will be de-orbited within half a revolution in a 'head-on' interaction. Moreover, results showed that altitude difference with the debris object decreases the efficiency of the laser. The lifetime of the 10 cm object (and thus all test objects) could still be lowered below 25 years from every altitude except for debris objects orbiting at 1000 km altitude. Interactions at the same altitude and with an azimuth angle still produce high $\Delta v \sim 100 - 200 \text{ m/s}$ due to a longer interaction time. Interactions with altitude difference and an azimuth angle showed that only the lifetime of 10 cm objects at 1000 km are not lowered below 25 years. Important to note is that the produced $\Delta v \sim 30 \text{ m/s}$ in both 'unsuccessful' scenarios still lower the lifetime to some extent and might cause the object to be de-orbited after a second encounter.

A dummy population of 5 000 objects was created by randomly generating the parameter values. The objects are concentrated between 600 and 1 000 km altitude and an inclination band between 70° and 100° . A 19 day simulation was run in which the laser had 6 000 encounters with 2422 different objects, which means that 48% of the initial constructed population was encountered during the simulation time. After 10 days the lifetime of a total of 334 objects

with lifetime higher than 25 years are lowered below the 25 years guideline and 614 objects are lowered below 1 month. Extrapolating the values after 4 days of simulation time to a longer time period predicts that annually the laser could lower the lifetime of about 36 000 debris objects below one month and 18 000 debris objects below 25 years. This would imply the active removal of more than 150 000 debris fragments from LEO within 5 years, which would be a tremendous success. These results suggest that a space-based laser system could operate very well as a small-scale debris removal technique and could help ensure the future safety of the space environment.

Recommendations

There are still many aspects of the laser ablation system that need to be researched to optimize the performance. Section 6.3.2 showed a brief sensitivity study on the effects of the atmospheric density on the number of lowered objects by the laser system. Follow-up research should investigate the sensitivity of other parameters such as the laser power, the telescope diameter and the solar panel area, but also the debris parameters such as debris material and density. On top of this, simulations have to be run with the laser system orbiting at a different altitude, which will determine the range of debris objects it can detect. Another interesting concept would be to test the performance of multiple laser ablation systems to remove debris objects, e.g. one at 600 km, one at 800 km and one at 1000 km. The performance will most likely be improved by implementing multiple systems, but the cost of the project will increase as well. A trade-off should be made between the time in which the debris population should be removed and the cost of the laser systems. Two other aspects that require more in-depth research are the influence of irregular shapes and attitude of debris particles on the laser ablation performance. This report has assumed spherical debris objects, which only represents a fraction of the LEO debris population. Another factor that is not included in this report is the mass fraction of the debris that is ablated during the laser interaction. The loss in mass results in a higher AMR of the debris object which will reduce the lifetime even further. Implementing the mass loss per interaction will make the laser performance more realistic. The most important follow-up research will be a simulation of the laser system with a larger debris population for a longer time than was done in this report. In a following research where large computation times will not be an issue, a simulation of 500 000 debris objects for 1 or 2 years should be run. The objects should have randomly generated attitude and shapes. This will give the most accurate representation of the performance of a laser ablation system on the LEO debris population.



Project outline

ADR by laser ablation

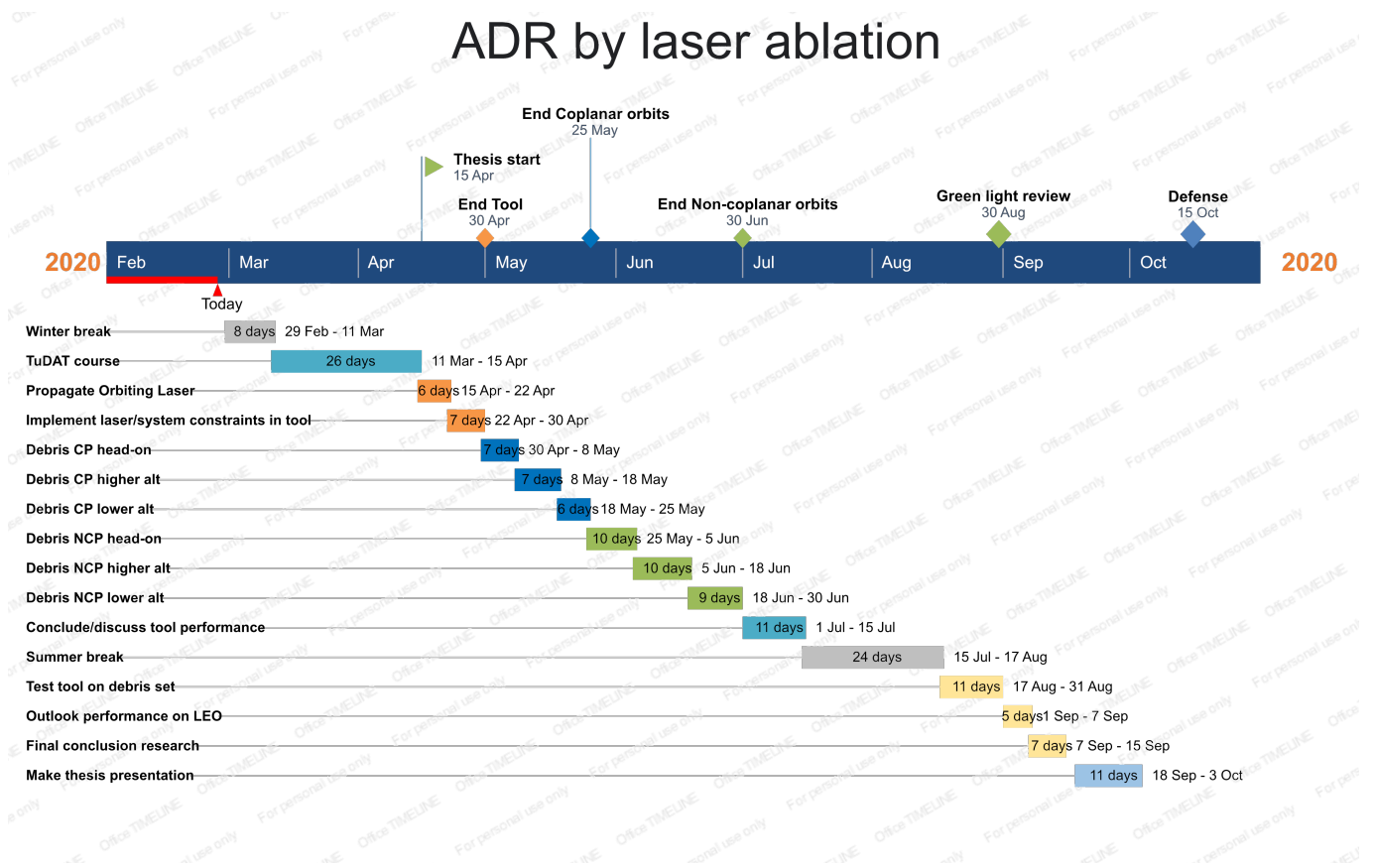


Figure A.1: Original planning for the 7 month research thesis.

Bibliography

- [1] United Nations Office For Outer Space Affairs, *Space debris mitigation guidelines of the committee on the peaceful uses of outer space*, (2010) pp. 1–12.
- [2] H. Klinkrad, *Space debris*, Encyclopedia of Aerospace Engineering (2010).
- [3] H. Klinkrad, *Space debris: models and risk analysis*, Springer-Praxis books in astronomical engineering (Springer; Published in association with Praxis Pub, Berlin; New York; Chichester; UK, 2006).
- [4] H. Klinkrad, J. Alarcon, and N. Sanchez, *Collision avoidance for operational ESA satellites*, in *4th European Conference on Space Debris*, Vol. 587 (2005) p. 509.
- [5] T. Kelso *et al.*, *Analysis of the iridium 33 cosmos 2251 collision*, Center for Space Standards and Innovation (2009).
- [6] D. J. Kessler, N. L. Johnson, J. Liou, and M. Matney, *The Kessler syndrome: implications to future space operations*, *Advances in the Astronautical Sciences* **137**, 2010 (2010).
- [7] C. Bonnal, *Design and operational practices for the passivation of spacecraft and launchers at the end of life*, *Proceedings of the Institution of Mechanical Engineers, Part G: Journal of Aerospace Engineering* **221**, 925 (2007).
- [8] B. B. Virgili and H. Krag, *Analyzing the criteria for a stable environment*, in *AAS/AIAA Astrodynamics Specialist Conference, Girdwood, AK, USA. AAS11*, Vol. 411 (2011).
- [9] M. Shan, J. Guo, and E. Gill, *Review and comparison of active space debris capturing and removal methods*, *Progress in Aerospace Sciences* **80**, 18 (2016).
- [10] C. R. Phipps, *LADROIT, A spaceborne ultraviolet laser system for space debris clearing*, *Acta Astronautica* **104**, 243 (2014).
- [11] H. Krag, *ESA, annual space environment report*, [ESA Space Debris Office](#) (2020).
- [12] C. R. Phipps, K. L. Baker, S. B. Libby, D. A. Liedahl, S. S. Olivier, L. D. Pleasance, A. Rubenchik, J. E. Trebes, E. Victor George, B. Marcovici, J. P. Reilly, and M. T. Valley, *Removing orbital debris with lasers*, [Advances in Space Research](#) **49**, 1283 (2012).
- [13] U. N. C. on the Peaceful Uses of Outer Space, *Technical report on space debris*, UNITED NATIONS PUBLICATION (1999).
- [14] C. Pardini and L. Anselmo, *Assessment of the consequences of the Fengyun-1C breakup in Low Earth Orbit*, *Advances in Space Research* **44**, 545 (2009).
- [15] C. R. Phipps, *A laser-optical system to re-enter or lower low Earth orbit space debris*, *Acta Astronautica* **93**, 418 (2014).
- [16] J. L. Forshaw, G. S. Aglietti, N. Navarathinam, H. Kadhem, T. Salmon, A. Pisseloup, E. Joffre, T. Chabot, I. Retat, R. Axthelm, *et al.*, *Removedebris: An in-orbit active debris removal demonstration mission*, *Acta Astronautica* **127**, 448 (2016).

- [17] H. Hakima and M. R. Emami, *Assessment of active methods for removal of LEO debris*, *Acta Astronautica* **144**, 225 (2018).
- [18] D. Mehrholz, L. Leushacke, W. Flury, R. Jehn, H. Klinkrad, and M. Landgraf, *Detecting, Tracking and Imaging Space Debris*, *ESA Bulletin*(0376-4265) , 128 (2002).
- [19] J. S. Kang, *Orbital debris mitigation using high density plasma*, (2013).
- [20] C. R. Phipps and C. Bonnal, *A spaceborne, pulsed UV laser system for re-entering or nudging LEO debris, and re-orbiting GEO debris*, *Acta Astronautica* **118**, 224 (2016).
- [21] W. O. Schall, *Orbital debris removal by laser radiation*, *Acta Astronautica* **24**, 343 (1991).
- [22] C. Phipps, G. Albrecht, H. Friedman, D. Gavel, E. George, J. Murray, C. Ho, W. Priedhorsky, M. Michaelis, and J. Reilly, *Orion: Clearing near-earth space debris using a 20-kw, 530-nm, earth-based, repetitively pulsed laser*, *Laser and Particle Beams* **14**, 1 (1996).
- [23] R. Soulard, M. N. Quinn, T. Tajima, and G. Mourou, *ICAN: A novel laser architecture for space debris removal*, *Acta Astronautica* **105**, 192 (2014).
- [24] L. Anselmo and C. Pardini, *Analysis of the consequences in low earth orbit of the collision between Cosmos 2251 and Iridium 33*, in *Proceedings of the 21st International Symposium on Space Flight Dynamics* (Centre Nationale d'Etudes Spatiales Paris, France, 2009) pp. 1–15.
- [25] H. Klinkrad, *The current space debris environment and its sources*, in *Space Debris* (Springer, 2006) pp. 5–58.
- [26] G. W. Ojakangas, B. J. Anderson, and P. D. Anz-Meador, *Solid-rocket-motor contribution to large-particle orbital debris population*, *Journal of Spacecraft and Rockets* **33**, 513 (1996).
- [27] S. Stabroth, M. Homeister, M. Oswald, C. Wiedemann, H. Klinkrad, and P. Vörsmann, *The influence of solid rocket motor retro-burns on the space debris environment*, *Advances in Space Research* **41**, 1054 (2008).
- [28] C. Wiedemann, E. Gamper, A. Horstmann, V. Braun, and E. Stoll, *The contribution of NaK droplets to the space debris environment*, in *Proceedings of the 7th European Conference on Space Debris, Darmstadt, Germany* (2017) pp. 18–21.
- [29] J. R. Wertz, D. F. Everett, and J. J. Puschell, *Space mission engineering: the new SMAD* (Microcosm Press, 2011).
- [30] C. Phipps, J. Luke, D. Funk, D. Moore, J. Glowonia, and T. Lippert, *Laser impulse coupling at 130 fs*, *Applied Surface Science* **252**, 4838 (2006).
- [31] J. P. Loftus, P. D. Anz-Meador, and R. Reynolds, *Orbital debris minimization and mitigation techniques*, *Advances in Space Research* **13**, 263 (1993).
- [32] P. Anz-Meador and A. Potter, *Density and mass distributions of orbital debris*, *Acta Astronautica* **38**, 927 (1996).
- [33] T. Ebisuzaki, M. N. Quinn, S. Wada, L. W. Piotrowski, Y. Takizawa, M. Casolino, M. E. Bertaina, P. Gorodetzky, E. Parizot, T. Tajima, *et al.*, *Demonstration designs for the remediation of space debris from the international space station*, *Acta Astronautica* **112**, 102 (2015).

- [34] K. F. Wakker, *Fundamentals of astrodynamics*, [TU Delft Library](#) (2015).
- [35] D. Liedahl, A. Rubenchik, S. B. Libby, S. Nikolaev, and C. R. Phipps, *Pulsed laser interactions with space debris: target shape effects*, *Advances in Space Research* **52**, 895 (2013).
- [36] R. Panwar and J. Kennewell, *Satellite orbit decay calculations*, [The Australian Space Weather Agency](#) (1999).
- [37] H. Lim, H. Bang, and S. Lee, *Adaptive backstepping control for satellite formation flying with mass uncertainty*, *Journal of Astronomy and Space Sciences* **23**, 405 (2006).
- [38] Q. Wen, L. Yang, S. Zhao, Y. Fang, Y. Wang, and R. Hou, *Impacts of orbital elements of space-based laser station on small scale space debris removal*, *Optik* **154**, 83 (2018).
- [39] S. Hashmi, *Comprehensive materials processing* (Newnes, 2014).
- [40] *Gaussian beam propagation*, *The Laser Optics Resource Guide* (2020).
- [41] J. Mason, J. Stupl, W. Marshall, and C. Levit, *Orbital debris–debris collision avoidance*, *Advances in Space Research* **48**, 1643 (2011).
- [42] J. M. Stupl, N. Faber, C. Foster, F. Yang Yang, and C. Levit, *Lightforce photon-pressure collision avoidance: efficiency assessment on an entire catalogue of space debris*, (2013).
- [43] R. Battiston, W. Burger, A. Cafagna, C. Manea, and B. Spataro, *A systematic study of laser ablation for space debris mitigation*, *Journal of space safety engineering* **4**, 36 (2017).
- [44] B. Nadir, *16.851: Satellite engineering*, Massachusetts Institute of Technology (2003).
- [45] A. Raziei, K. P. Hallinan, and R. J. Brecha, *Cost optimization with solar and conventional energy production, energy storage, and real time pricing*, in *ISGT 2014* (IEEE, 2014) pp. 1–5.
- [46] P. Dubock, F. Spoto, J. Simpson, D. Spencer, E. Schutte, and H. Sontag, *The Envisat satellite and its integration*, *ESA bulletin* **106**, 26 (2001).
- [47] R. Battaglia, F. Pirillo, M. Ferri, F. Sarullo, A. Di Felice, M. Demeo, and G. Tornaghi, *Warden-w-band advanced radar for debris early notification*, in *Space Debris*, Vol. 473 (2001) pp. 139–145.
- [48] D. Dirkx, *TU Delft Astrodynamical Toolbox (Tudat) documentation*, (2020), <https://www.tudat.tudelft.nl/>.
- [49] U.S. National Oceanic and Atmospheric Administration and U.S. Air Force, *US standard atmosphere, 1976*, Vol. 76 (National Oceanic and Atmospheric Administration, 1976).
- [50] D. H. Hathaway, *The solar cycle*, *Living reviews in solar physics* **12**, 4 (2015).
- [51] S. Scharring, R.-A. Lorbeer, J. Kästel, and W. Riede, *Laser-based space debris mitigation in the low earth orbit*, in *Laser Applications Conference* (Optical Society of America, 2019) pp. CM3C–2.